博士論文（要約）

Creation of Nano-sized Valves for Nanofluidic Device

（ナノ流体デバイスに向けたナノサイズバルブの創成）

Hiroki Sano

佐野 大樹

Department of Applied Chemistry
School of Engineering
The University of Tokyo

December 2021

Table of Contents

Chapter 1

Introduction

1.1 Background

1.1.1 Introduction of microfluidics

Origin of microfluidics

Recently, researches integrating chemical processes in a μm space have greatly developed and the technology have been applied to the field of biochemistry, medical, environment.[1–3]Such a small space is achieved by fabricating channels on a substrate with a width and/or a depth of 10^2 μm and enclosing the channel by bonding another substrate on top. In these μm-scaled confined space, chemical processes such as mixing reagents, extraction of substances are carried out. Devices integrated with various chemical processes are often called "microchips" or "microfluidic devices."

The development in this field is similar to the development of computers that arose from 1940s until nowadays. The first computer invented, which is well known as ENIAC, contained several vacuum tubes, resistors, *etc.* This was bigger than a human size and hardly affordable for individual use.[4] As the technology in microelectric systems (Micro Electro-Mechanical Systems: MEMS) used for semiconductor devices rapidly developed, miniaturization of the components used for computers was achieved. These miniaturized components were integrated on a small chip as integrated circuits (IC) and became possible to downscale the size of the computer while possessing the same or more functions. Today, computers are miniaturized, inexpensive, and portable PCs and smartphones have been a part of our daily life. In terms of analytical devices, analyses were conventionally only possible at hospitals or research laboratories that possess large and professional apparatuses. However, thanks to the development of the fabrication technology of MEMS and the concept to utilize the μm space as a field for chemical reaction, the analytical devices have been miniaturized with the same or higher efficiency. Nowadays, various

medical, environmental analyses can be conducted using a portable microchip.

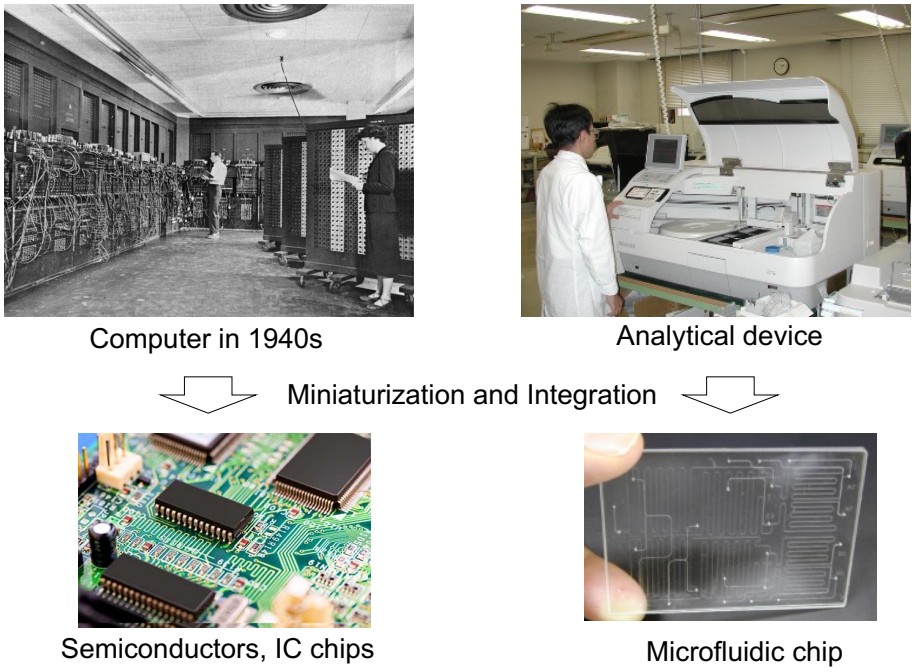

Figure 1-1: Miniaturazation and integration in the case of computers and analytical devices

The first example that realized integration of several chemical processes on a single device is known to be the microscale gas chromatography system by Terry's group.[5] The device consisted of a sample injection valve and a separation capillary column fabricated on a silicon wafer. However, this work did not attract researchers much at that time and the field was not yet cultivated.

In the late 1980s, the fabrication technology in micro electromechanical mechanical systems (MEMS) had rapidly developed for research in the semiconductor industry. This has been one major factor for the development of the field of microfluidics. In 1990, Manz *et al.* integrated a liquid chromatography system on a silicon wafer consisting of a separation column and a detector.[6,7] This research described how reactions in microspace would lead to fast and efficient analysis and showed the potential of microfludic devices.

After this success of integrating chemical systems, Manz *et al.* established a methodology to integrate chemical processes and proposed the concept of "micro-Total Analysis System (μ–TAS)."[8,9]

There are various significant features in microspace such as lower thermal capacity and larger surface-to-volume ratio. The effect of gravity is negligible in microspace so the mass transfer is dominated by molecular diffusion. Accordingly, heating or cooling of the analytical field can be rapidly achieved, and fast, efficient chemical reactions can be carried out while the amount of the sample solution and other reagents can be reduced.

In contrast to this positive features, miniaturization of chemical processes inevitably leads to smaller number of molecules in the detection volume. For example, when a solution with a concentration of 1 nM is confined in a $1\mu\mathrm{m} \times 1\mu\mathrm{m} \times 1\mu\mathrm{m}$ cube, only 0.6 molecules are contained in this cube. That is why a detector with a sensitivity at single molecule level is required. At the time, fluorescence detection was the main detecting method. Laser induced fluorescence (LIF) had the sensitivity to detect single molecules,[10,11] but the target molecules were restricted to fluorescence molecules. There the range of use was greatly limited.

In 1998, Kitamori's group developed a thermal lens microscope (TLM) utilizing photothermal conversion effect.[12] When a molecule absorbs energy from light, fluorescence molecules emit energy as light, but the majority of molecules are non-fluorescence and emit energy as heat. For TLM, a probe laser and an excitation laser are irradiated to the molecules. When a molecule absorbs energy from the excitation laser and generates heat, the refractive index of the solution changes. This is known as thermal lens effect.[13] Due to the change of the refractive index, the intensity of the probe laser detected through a slit behind the channel changes. Because the intensity change is dependent on the change

of the refractive index, which is caused by heat generated from the molecules, the number of molecules that absorbed the light can be detected. In addition to this detection method, Kitamori *et al.* introduced a method to drive the fluid by pressure when electric osmosis flow was the general method of flow control. Electric osmosis flow could only be applied to electrically charged molecules, while pressure-driven flow could be applied to electrically charged and neutral molecules. In this way, mixture of different solutions such as organic solvents and aqueous solvents could also be controlled.

With this technology of detection and flow control for versatile chemical components, various chemical processes were realized as unit operations on a microchip. Kitamori's group proposed a methodology to integrate chemical processes into microspace, so called micro unit operations (MUOs). Figure 1-2 shows some examples of MUOs.[14–16]

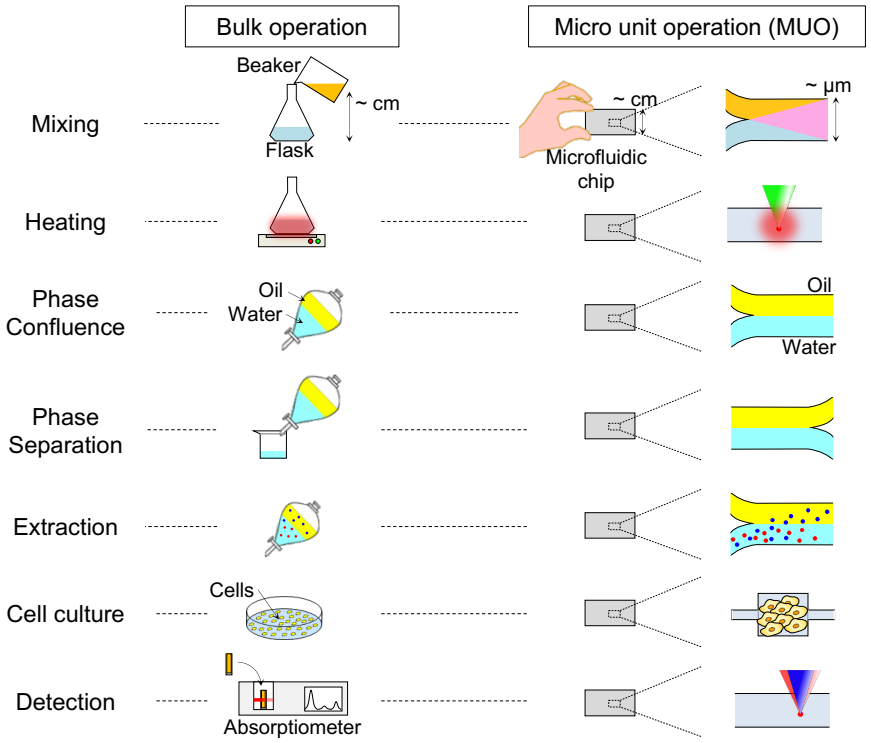

Figure 1-2: Micro Unit Operations (MUOs)

Based on this concept, analyses in a bulk experiment is realized in a microchip as fol-

lows. First, the analysis is divided into chemical processes. Next, the chemical processes are converted into unit operations, and then replaced with corresponding micro unit operations. These MUOs are be combined directly and/or parallelly in a continuous flow realizing an integrated chemical analytical system. Kitamori's group named this continuous flow chemical processing (CFCP) and realized wet analysis of Co^{2+} ions (Figure 1-3).[17]

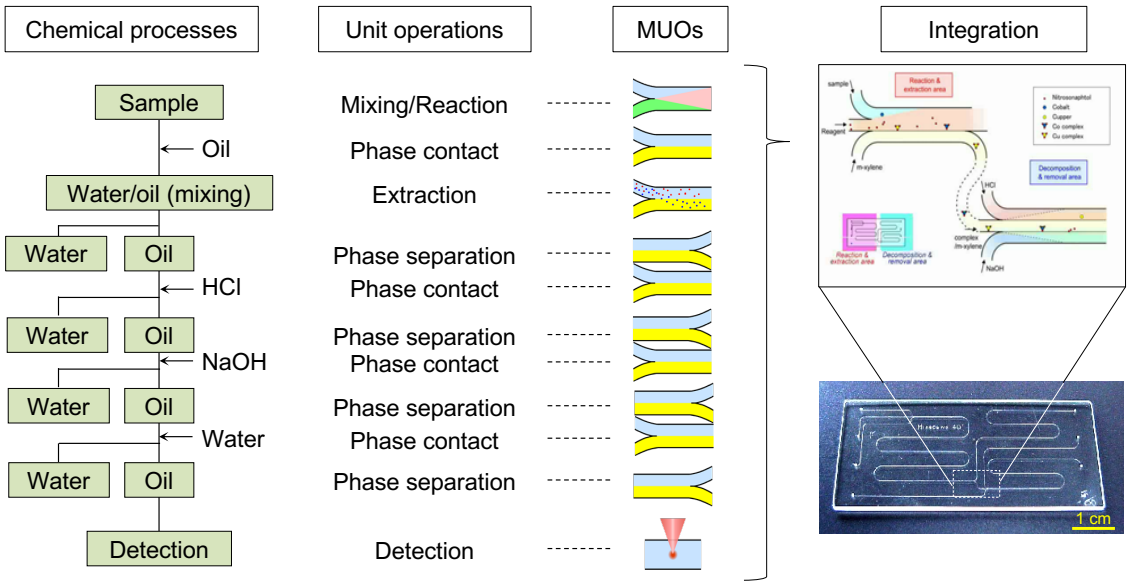

Figure 1-3: Concept of integrating chemical processes into a microchip. The unit operations of the chemical process is converted into MUOs and connected as a continuous flow.

Emergence of new materials for microfluidic devices

As the field has spread widely, the variety of materials used for the devices have also been widening. Compared to inorganic materials such as glass and silicon, polymers are materials that are easily accessible, inexpensive, and does not require a special facility like a clean room for device fabrication. Among several polymers proposed for microfluidic devices such as polymethylmetacrylate (PMMA) , polycarbonate (PC) ,

polyethyleneterephthalate (PET) , *etc.* polydimethylsiloxane (PDMS) is the most popular material used nowadays. PDMS has been introduced by D. C. Duffy in 1998 as a material easy to use.[18] By pouring liquid PDMS to a master mold and cured , micro-scaled channels are easily fabricated. These channels can be sealed with another substrate of PDMS, glass, or other materials by simply making contact. The high elasticity is also a great advantage of PDMS in microfluidics, for deformation of the channel of membrane structures can be utilized to microvalves and micropumps. Quake *et al.* developed an in-line valve using two layer of microchannels; a fluid channel and a control channel to pneumatically pressurize and deform the fluid channel.[19] Since this valve had a small dead volume (~100 pL) and a simple structure, it has greatly contributed to realize complicated flow operations.

Despite the great advantages of using PDMS in terms of the simplicity of the fabrication process as described above, PDMS also possesses innate disadvantages.[20] First, the chemical endurance of the material is low. For example, the material swells when treated with organic solvents such as acetone and toluene. In addition, PDMS is a porous material and allows permeation of gases. This can be considered as a positive character when gases are intended to be provided, for example in a cell cuture system, but at the same time it causes evaporation of water through the channel wall, which will change the concentration of the solution. Therefore, its usage as an analytical system is limited to simple and aqueous analyses. Second, its optical property is a shortage when considering an analytical system for various analytes. It seems to be a transparent material under visual lights, but it greatly absorbs light in the ultraviolet (UV) area.Therefore, it is difficult to be applied for detecting molecules that possess absorbance in the UV region (*e.g.* DNA, protein molecules). Third, the surface is innately hydrophobic, which causes adsorption of

hydrophobic molecules and biomolecules. For this effect, quantitative experiments will be difficult. Many strategies are reported for modifying the surface of PDMS, but still it cannot fully overcome these disadvantages.[21,22] Finally, because the channels cannot be washed by introducing organic solvents or by heating under a severe condition, the devices cannot be reused.

As materials other than PDMS, thermoplastics such as PMMA, PC, PET have also been introduced. Because of their rigidity, the sealing property of the channels is high enough that gases are hardly permeable. Compared to PDMS, the chemical endurance against organic solutions of these materials are slightly higher, but still incompatible with solvents such as ketones and hydrocarbons.

1.1.2 Downscaling to nanofluidics

In contrast to PDMS or other polylmeric materials, glass has a high chemical endurance, optical property, versatility of surface modification, and is possible to repeatably use the device by cleaning the channels with acid, alkali or by heating the device. Due to these advantages, sophisticated and versatile analyses are realized.

Furthermore, the high rigidity of glass allows further downscaling of the analytical field to 10–1000 nm space. Kitamori's group expanded the concept of MUO to this space (*i.e.* nano unit operations: NUOs) and pioneered the field of nanofluidics.[23] Using the technology of electron beam lithography that had been developed in the field of semiconductor manufacturing, they successfully fabricated 10–1000 nm-sized nanochannels on a glass substrate.[24,25] Because it was difficult to realize this size of space either by top-down or bottom-up fabrication, this space area was an unexplored region. They named this area

"Extended-nano space" and pioneered this field between bulk chemistry and molecular chemistry.

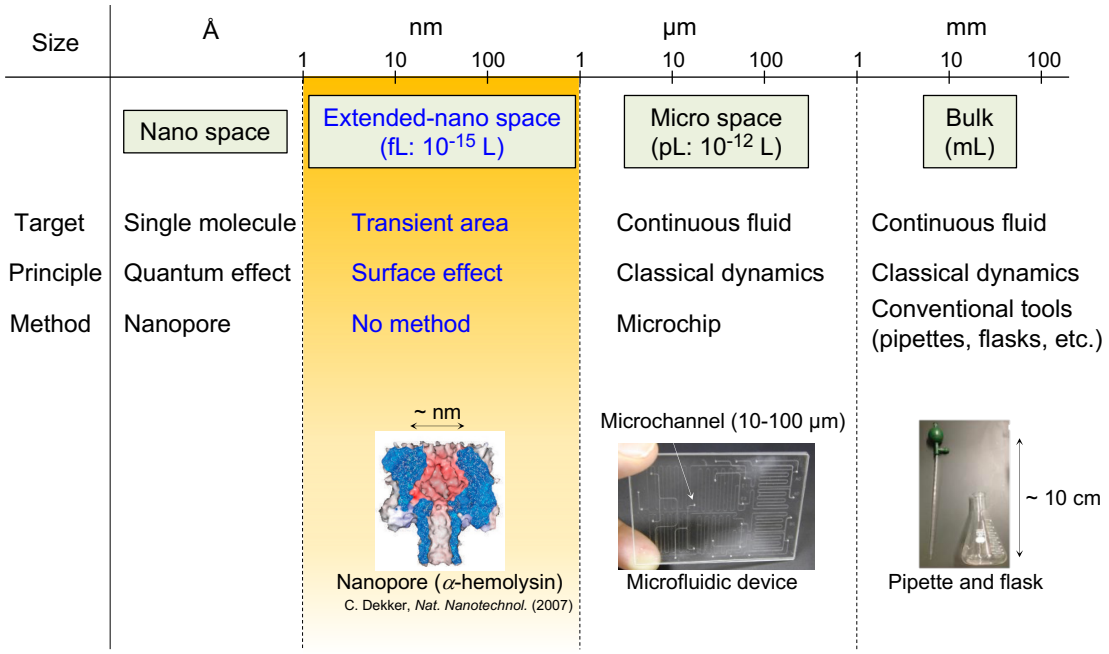

Figure 1-4: The positioning of the research field of extended-nano space. The graphic of α-hemolysin was cited from a review with permission.[26]

To cultivate the field of extended-nano fluidics, they first established a method of fluid control and detection as they have achieved in the field of microfluidics. First, they developed a fluid control method in nanochannels introducing fluid via microchannels and an external capillary tube.[27] Then, as a detection method, they applied the basic idea of utilizing thermal lens effect for molecular detection to extended-nano space, and developed a highly sensitive detection method called differential interference contrast thermal lens microscope (DIC-TLM).[28,29]

Using these fundamental technologies, Kitamori's group revealed that the property of water in extended-nano space is different from that in bulk or in microspace. For example, water in extended-nano space has a four times higher viscosity,[30] lower dielectric constant,[31] and 20 times higher proton mobility.[32,33] In order to explain these phenomena,

Kitamori's group proposed a three-phase model consisting of bulk phase, proton transfer phase, and adsorption phase. Among these, the bulk phase and the adsorption phase were well known, but the proton transfer phase has not been pointed out until this top-down fabrication method was established.

Since the extended-nano space is about 10^3 times smaller than microspace, the surface-to-volume ratio is even larger than that in microspace. This dominant effect of the surface can be actively utilized for chemical processes. For example, using the difference of interaction between the glass channels wall and molecules, the nanochannel can be used as a separation column for chromatography just by flowing the sample in the channel. This nanofluidic liquid chromatography realized separation of a sample volume of ~fL within a few second, having a separation efficiency of 7,100,000 plates/m.[34,35] Another example is a reaction between antigen and antibody immobilized on the wall of the nanochannel. When the target protein is introduced in the region where capture antibodies are immobilized, it is captured with the efficiency of almost 100 %.[36] With this high capture efficiency, analysis of a single protein molecule by integrating the process of enzyme linked-immunosorbent assay (ELISA) in the nanochannel was realized.[36]

Single cell proteomics

Recently, single cell proteomics is desired in the field of biology and medicine. In conventional cell analysis, a group of about 10^6 cells is crushed and analyzed. However, this method cannot be applied to rare samples such as circulating tumor cells (CTCs). In addition, recent studies show that individual cells contain different amount of mRNAs,[37] proteins,[38] and metabolites[39] even for those with identical genomes. Therefore, a method to analyze a single cell, or the proteins that a single cell secretes is desperately desired in

order to understand the cell function and to establish a correct treatment for diseases such as cancer and immune diseases.

The process of single cell protein analysis is shown in Fig. 1-5. The volume of a single cell is only pL and in order to detect the protein molecules in a single cell, the sample volume would be fL. To conduct this analysis, it is necessary to maintain the ultra-small volume and integrate the whole process in a series.

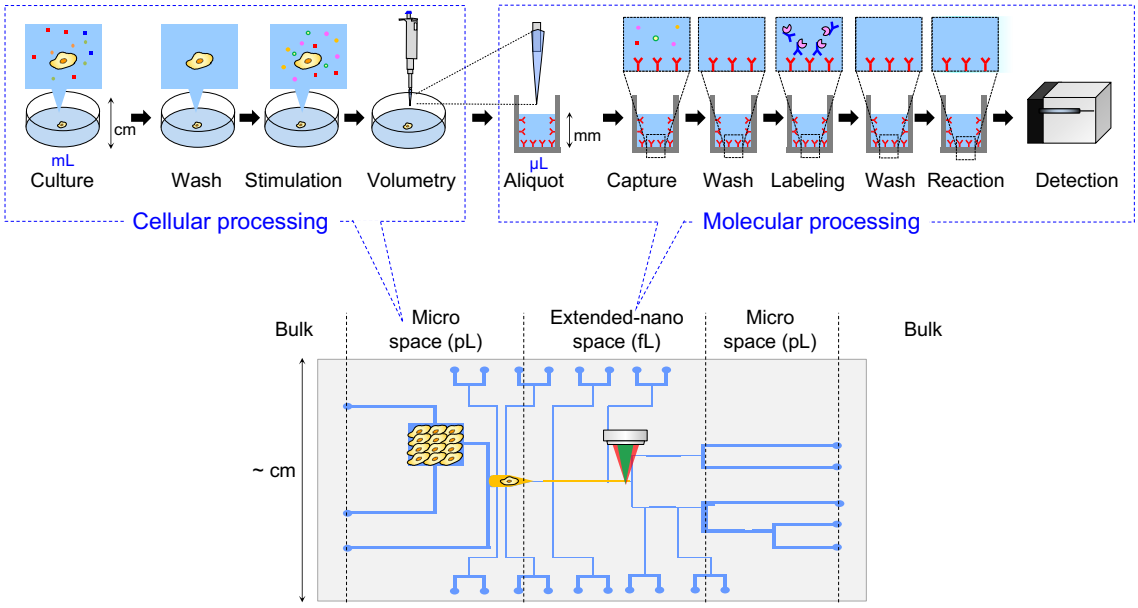

Figure 1-5: Concept of integration cellular processes and molecular processes into a micro/nano integrated fluidic device.

Our group has been tackling this subject using micro/nano integrated fluidic device. The cellular process is integrated into microspace (volume: pL) and the molecular process is integrated into nanospace (volume: fL). In this way, the secreted proteins can be analyzed maintaining its small volume without being diluted and the whole process was integrated. Based on this concept, we succeeded in quantification of a cytokine proteins secreted from a single B cell.[40]

However, in order to control flows of several reagents for such a sophisticated analysis,

several microchannels and nanochannels must be fabricated and connected, which results in channels with numerous branching. Therefore, pressure balance must be maintained at every channel to control the fluid direction of a reagent. In the previous work,[40] the driving pressure was controlled at nine channels for simply flowing a certain reagent into the reaction channel (Fig. 1-6(a)). All nine pressure values differs if the aimed reagent switches, and if the pressure balance collapses, the reagents would be contaminated by unexpectedly mixing with other reagents.

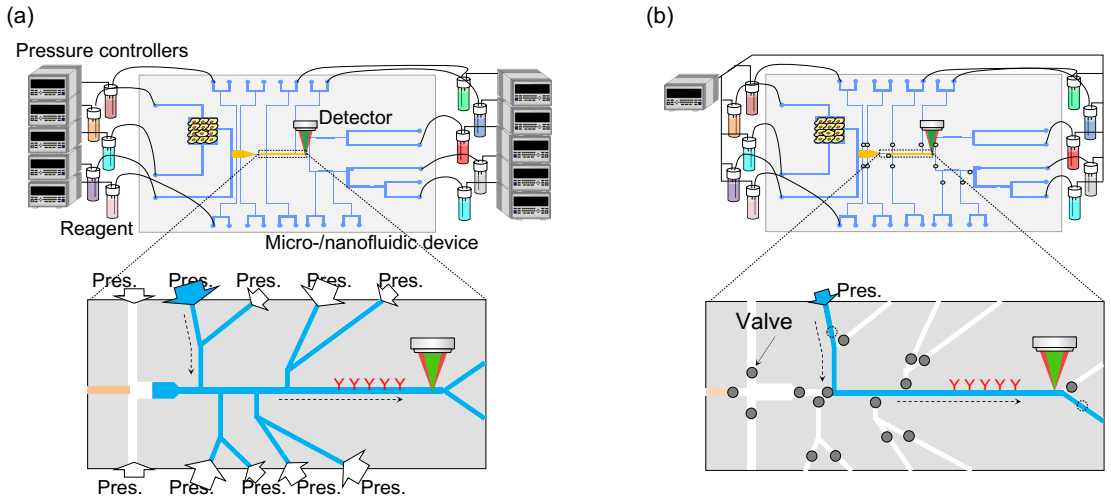

Figure 1-6: Fluid control method in nanofluidics. (a) Current fluid control by maintaining pressure balance at each channel. (b) Fluid control using valves. The flow direction can be controlled by simple opening/closing the valves.

Thus, although micro/nano integrated fluidic devices are a powerful tool to realize ultimate analyses handling single/countable molecules, even the simplest fluid operation requires difficult operation, which can be operated only by highly skilled technicians. This implies that it is difficult to make a further integration of chemical processes. To overcome the problem of the difficulty in fluid control, integration of valves in micro-/nanofluidic devices is a general solution. Because the fluid can be controlled directly at the point of the channels and the flow can be digitally stopped or flowed, there is no need to consider

the pressure balance or even used independent pressure controllers for each reagent (Fig. 1-6(b)).

1.1.3 Valves in micro-/nanofluidics

As valves were already used as a component in the origin of microfluidic devices,[5] a valve is considered as a fundamental tool for analyses, for it plays the role of sample injection, flow rate regulation, sample isolation, *etc.* Valves developed in micro-/nanofluidics nowadays can be classified into active valves and passive valves: Active valves are operated by external actuators or stimuli and passive valves work depending on the flow direction or pressure. Both type of valves include mechanical valves and non-mechanical valve. Mechanical valves are those with moving parts (*e.g.* membranes, deforming channels, wheels, *etc.*) and non-mechanical valves are those without moving parts (*e.g.* phase change valve, burst valves).

Table 1-1: Classification of valves

Active valves	Mechanical valves	Membrane valve
		Diaphragm valve
		In-line valve
	Non-mechanical valves	Hydrogel valve
		Paraffin valve
Passive valves	Mechanical valves	Cantilever valve
		Membrane valve
		Ball valve
		Wheel valve
	Non-mechanical valves	Laplace valve

Mechanical active valves

The origin of mechanical active valves is a membrane-type valve developed by Terry's group.[5] When they developed the gas chromatography system on a silicon substrate, a nickel diaphragm actuated with a magnetic force was integrated as a valve.[5] As the materials for microfluidic devices has changed to PDMS, membranes fabricated by PDMS also became popular.[41,42] This type of valve is predominantly a "normally closed (NC)" valve. That is, the membrane is placed in a way that seals the microchannels and it deforms and opens the channels only when it is actuated. Because it is only the membrane part that functions as a valve, the whole device does not necessarily have to be a deformable material. Grover fabricated a membrane from PDMS and attached it to a glass substrate (Fig. 1-7).[43] In addition to a normal three-layered diaphragm structure, a four-layered structure was proposed to reduce the contact of solvent and the PDMS membrane. The valve is fully opened when the vacuum pressure is -20 kPa, and can stop flow of a pressure up to 80 kPa when the membrane is pressurized with 60 kPa. Furthermore, three valves were placed in series and its performance as a peristaltic pump was verified. The maximum pumping rate was 89 nL/s although this can be tuned by the frequency of valve actuation and the size of the valve chamber.

Because the valve is normally closed, the reagents and PDMS membrane contact only at a small area and a short time, which implies little influence caused by using PDMS, but still there is a restriction of reagents.

Another major mechanical active valve is the in-line valve developed by Quake's group in 2000.[19,44] They introduced an in-line open/close valve using channel deformation and a simple fabrication method of multilayer soft lithography. Two PDMS substrates with microchannels fabricated on each is bonded in a way that the channels crosses each

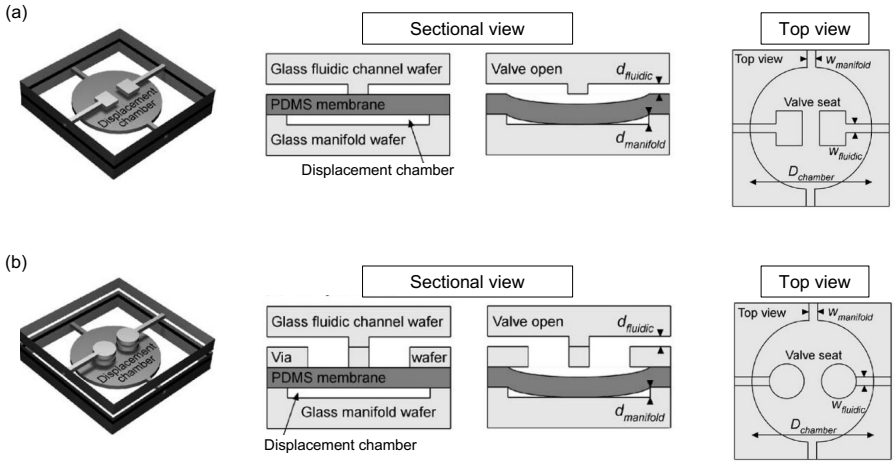

Figure 1-7: PDMS membrane valve incorporated into a glass device. The graphics were cited from an article with permission.[43]

other (Fig. 1-8). The channel below is called the "fluid channel" and the channel above is called the "control channel." A pneumatic pressure is applied through the control channel, which deforms the fluid channel and seals the flow path. The valve had a great advantage for integration because the valve area was only 100 μm × 100 μm and 10 μm in depth with no dead volume, and also the fabrication method of multilayer soft lithography was suitable for mass production. In 2002, the group realized integration of 2056 valves into one device (Fig. 1-8(b)).[45] Because of this simple method for integration, this type of valve (so called "Quake valve") is mostly integrated in recent PDMS microfluidic devices.

Non-mechanical active valves

Molecules or substances that change their volume depending on temperature, pH, light, *etc.* can be applied to valves as a moving part. For example, there are reports of phase transition valves using hydrogel,[46] sol-gel,[47] paraffin,[48,49] ice,[50] *etc.* The first report was a hydrogel valve presented by Beebe's group.[46] They incorporated a hydrogel

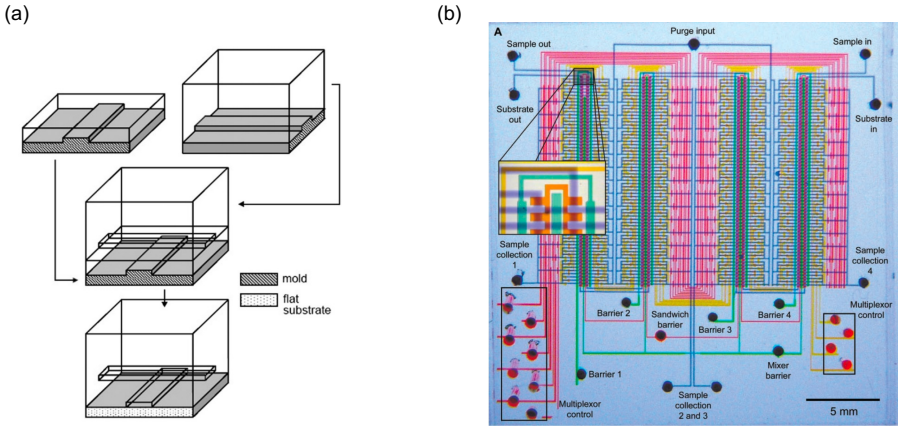

Figure 1-8: (a) A schematic image of the fabrication of Quake valve. The fluidic channel and the control channel were both fabricated by soft lithography and bonded with each other. (b) 2056 valves integrated on one device. The graphic was cited from an article with permission.[45]

block that changes its volume corresponding to different pH values (Fig. 1-9(a)). The volume change of the hydrogel blocks itself can be applied to seal the channels as well as an actuator to deform a membrane. The hydrogel components were fabricated inside the microchannels by irradiating ultraviolet light using a photomask. A microvalve that consists of a flexible PDMS membrane and a hydrogel actuator was designed (Fig. 1-9(b)).[46] The hydrogel swells as the pH 11 solution was flowed into the upper control channel. With the volume change of the hydrogel, the membrane deformed and blocked the orifice with a displacement of up to 185 μm . The response time of the 3D hybrid valve was 19 s.

This principle is also applied to glass-made nanofluidic valves. Xu *et al.* incorporated a brush of poly(N-isopropylacrylamide) (PNIPAM) into a nanochannel.[51] When the channel is heated over 37 °C , PNIPAM shrinks and opens the nanochannel, and when the channels is cooled down to 37 °C , PNIPAM swells and seals the nanochannel. Although this valve has a robust structure and a pressure capacity of 200 kPa, the response time of 37 s and polymers incorporated in the channel limits its application.

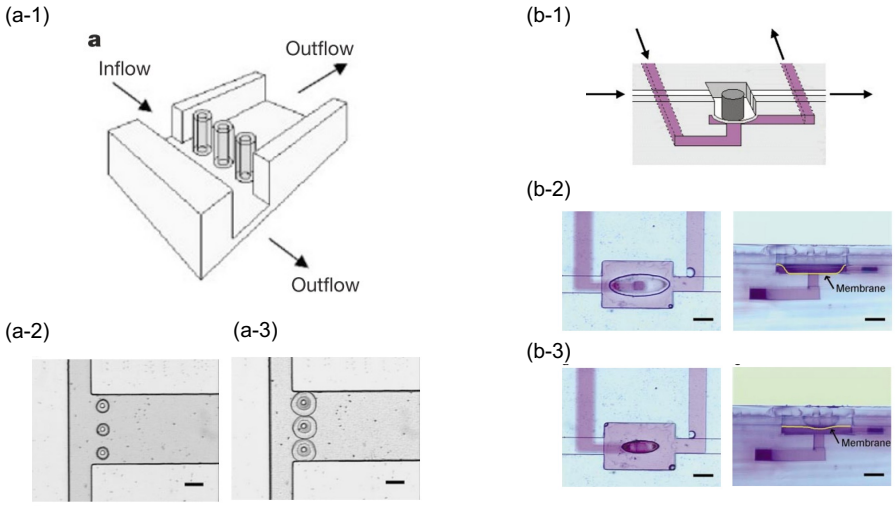

Figure 1-9: (a-1) A schematic view of the hydrogel valves incorporated in the microchannel. (a-2) The fabricated device with valves opened. (a-3) The fabricated device with valves closed. (b-1) A schematic view of hydrogel blocks incorporated as a membrane actuator. (b-2) Valve closed (b-3) Valve opened. The graphics were cited from an article with permission.[46]

Although these phase transition valves have a simple device structure, the relatively slow response time of the open/close operation (~seconds) limits the application to analyses that do not require quick response.

Mechanical passive valves

Mechanical passive valves are valves having moving parts to seal/open channels, but not requiring actuators. The valves open when pressurized by fluid pressure, but only against one direction, which is similar to a diode. Most passive valves are incorporated in inlets and outlets of micropumps using membrane valves. Therefore, the behavior of the check valves are important for a suitable performance of pumping.

Cantilever-type valves has a simple structure and fabricated by various materials such as PDMS,[52] metal,[53] PET,[54] *etc.* For example, Ma *et al.* fabricated a cantilever-type valve from PDMS and combined it with a membrane valve (Fig. 1-10(a)). A simple vibration

of the membrane at the frequency of 70–180 Hz generated a maximum pumping rate of 72 mL/min. Although cantilever-type valves are easy to design and operate, the simplicity lowers the endurance of the valve.

In contrast, membrane-type passive valves have several edges fixed to the substrate and achieved higher endurance (Fig. 1-10(b)). Therefore, the size of the membrane can be enlarged, resulting in a large pumping rate (*e.g.* 395 mL/min[55]).

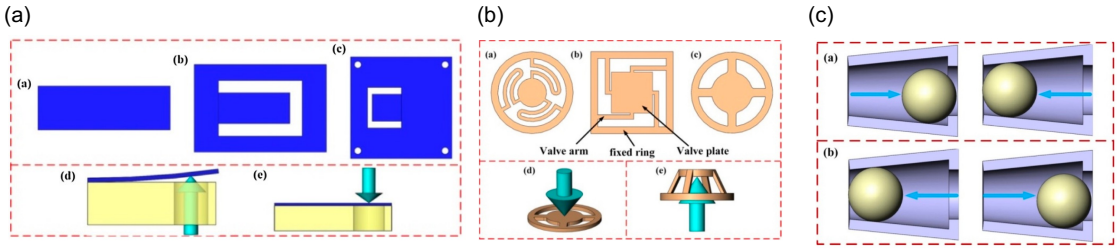

Figure 1-10: Schematic images and working principles of (a) a cantilever valve (b) a membrane-type check valve (c) a ball valve. The graphics were cited from a review with permission.[56]

Other types of passive valves are ball valves,[57,58] wheel valves,[59,60] umbrella valves,[61] *etc.* These type of valves also achieve a well pumping rate or pressure capacity, but the complexity of the fabrication and the valve volume limits their use to simple fluid controls.

Non-mechanical passive valves

The idealistic way to control the flow is to achieve flow control without using additional components such as valves. That is because the fabrication process will be simple and no actuators for the valve is required. There are a few reports on such "valveless" flow control method.[62,63] In this method, the flow is controlled by designing the fluid resistance from the channel structure. Although the main flow can be controlled in this way, there is always a reverse flow, and the flow cannot be fully stopped unless the channel is

partitioned. Another approach is to utilize the surface properties that derive from the large surface-to-volume ratio in microspace. By changing the channel size, capillary force, or Laplace pressure on the gas/liquid interface can be controlled. This means the fluid can be transported to the aimed space at an arbitrary moment. However, it only works when there is a gas/liquid interface and its performance would be degraded as the hydrophobicity of hydrophilicity of the channel changes after repeated time of use.

This type of Laplace valve can be applied to glass-made devices. Mawatari *et al.* fabricated nano-sized pillars with a radius of 70 nm and a height of 50 nm with a pitch of 160 nm inside a nanochannel (1700 nm wide and 200 nm deep).[64] The nano-sized pillars and the nanochannels were hydrophobically modified. By controlling the structure and wettability of the surface in such a way, water introduced into the channels will stop before the nano-sized pillar area (Fig. 1-11). When a pressure over 200 kPa was applied, the gas/liquid interface passed through the pillar area. Thus, a stop-and-go valve was demonstrated. Nevertheless, this type of valves could no longer be used after the hydrophobic modification is once wet. Therefore, it is difficult to be integrated into nanofluidic analytical devices.

Among the various types of valves in micro-/nanofluidics, channel open/close valve has the fastest response time, smallest dead volume and most of all, a simple working principle, which allows integration and application to versatile analyses. With this type of valve developed in a glass-made micro/nano integrated fluidic device, the designing concept of micro-/nanochannels and the flow controlling system will greatly change. If the channels could be partitioned using valves, many reagents could be used at once without causing problems of contamination or loss of reagents. Since open/close valves can not

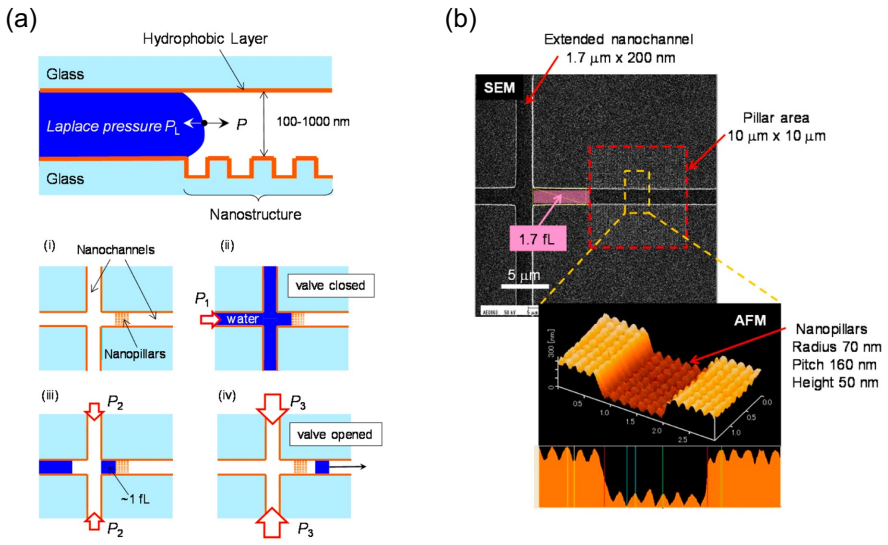

Figure 1-11: (a) The working principle of the Laplace valve with hydrophobic nanochannels and nanopillars (b) SEM and AFM image of fabricated nanochannels and nanopillars

only stop the flow but also control the flow rate, the current flow driving system consisting of several pressure controllers for each reagent will be unnecessary. This will further realize easy and precise fluid control and all users other than technicians could operate the analysis. Based on this concept, I conceived a channel open/close valve for glass micro/nano integrated fluidic device.

1.2 Objective

The aim of this study is to create a channel open/close valve for micro-/nanofluidic devices made of glass. Using glass deformation at nanoscale, where glass deforms elastically, nanochannels are opened and closed controlling the femtoliter volume fluid. The developed valve will be implemented to a micro-/nanofluidic device and applied to femto-liter analysis. The objectives of each chapter are as follows.

In chapter 2, a valve using glass deformation is designed, fabricated, and its perfor-

mance is evaluated. First, the conceptual design of the valve using glass deformation is proposed. Based on the conceptual design, a valve that meets analytical and mechanical requirements is designed in detail. Next, a top-down nano-fabrication process is proposed for the valve and the valve is fabricated. Finally, the fluidic and mechanic performance of the valve is evaluated.

In chapter 3, fluid operations using the valve is verified. Fluid operations in analytical chemistry can be divided into single-phase system and multi-phase system. For a single-phase system (*e.g.* liquid/liquid system), a valve chamber with a curved structure is proposed and fabricated in order to prevent leakage through the valve chamber caused by molecular diffusion. For a multi-phase system (*e.g.* gas/liquid system), a valve chamber with hydrophobic modification is proposed.

In chapter 4, a fluid controlling system integrated with a flow driving apparatus, a detector, and a flow controlling part, which is an array of multiple valve actuators is designed and established.

In chapter 5, using the developed valve and the fluid controlling system, a device integrated with multiple valves is designed and fabricated, and femto-liter analysis is demonstrated using the device.

Chapter 2

Development of a nanochannel open/close valve utilizing glass deformation

2.1 Introduction

2.1.1 Background

In this chapter, a channel open/close valve using glass deformation is designed and developed. In order to realize such a valve, the least requirement is that the glass does not break when deformed. That is, the stress on the glass must be less than the breaking stress of glass. The breaking stress of the glass used in this research was 1.16 GPa, which was experimentally evaluated. The details of the experiments are shown in the Appendix section. To meet this requirement, the relationship between the deformation value, glass thickness, and channel width was roughly estimated based on mechanics of material. Since the channels in the actual devices are in a closed system bonded with glass substrates, the edge of the deformation part is fixed, so a model of deflecting a plane with clamped edges under a concentrated load was applied for the estimation.

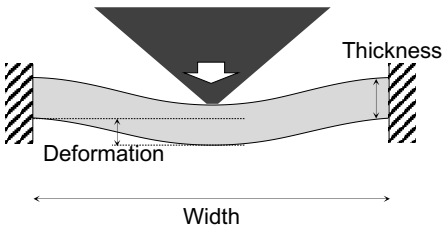

Figure 2-1: Deformation of a beam with clamped edges

Under this condition, the maximum value of deflection and stress on the glass is expressed as

$$w_{\max} = \frac{Fl^3}{16ht^3E} \tag{2.1}$$

$$\sigma_{\max} = \frac{3Fl}{4ht^2} \tag{2.2}$$

where F is the load applied to the glass, l is the width of the plane (corresponding to the

channel width), t is the thickness of the glass, E is the Young's modulus, and h is the length through the back side of the page.

First, the stress created on glass when deforming glass to seal microchannels was estimated. In order to seal a microchannel with the width and depth of 10^2 μm (a general size of microchannels), the stress on the glass is estimated to be 10^2 GPa ($\gg$ 1.16 GPa). Since this is much greater than the breaking stress, it is estimated impossible to realize an open/close valve for microchannels in a practical size using glass deformation.

Here, I conceived the idea of opening/closing nano-sized channels utilizing nano-scale deformation of glass. The depth of nanochannels is 10^2 nm, which is the same order of the range of elastic deformation of glass. Therefore, open/close of nanochannels could be realized in this way.

Based on this idea, the width and depth of the nanochannel and the thickness of the glass deformation part was roughly calculated. As a result, in order to obtain a deflection value of 10^2 nm while the stress generated on the glass is below 1 GPa, the channel width is required to be 10^2 μm and the thickness of glass should be 10^1 μm . Based on this rough estimation of glass deformation, designing a valve that can stop the flow and can endure repeated use is required.

2.1.2 Objective

To address this requirement, a design of the valve based on fluidics and mechanics was proposed. The objective of this chapter is to design and fabricate a nanochannel open/close valve and evaluate its performance. In section 3.2.2, the design of the valve is described. In section 2.3, the fabrication process of the valve is briefly explained, and in section 2.4,

the operation of the valve is confirmed, and the performance of the valve is evaluated.

2.2 Design of a nanochannel open/close valve

Conceptual structure of the valve

Based on the basic design of the valve described in section 2.1, the conceptual structure of the valve was designed. First, a nanochannel with a width of 900 nm and a depth of 900 nm was designed. In order to close this channels and stop the flow, a channel with the structure designed in section 2.1 is required. Therefore, the 900 nm-deep nanochannel was partially replaced by a valve chamber as shown in Fig.2-2. The valve chamber was designed as a circle, because otherwise the stress generated at the corners would be the critical area of glass breaking. For example, using a square-shaped valve chamber, whose length of one side is equal to the diameter of a circle-shaped chamber, the maximum stress on the glass is calculated to be five times greater than the circle-shaped chamber.[65]

The depth of the valve was designed to be 100 nm so it could be applied to analyses using proteins, whose sizes are generally ~10 nm. Under this condition, the diameter of the valve was designed to be 75 μm so that the volume of the valve chamber is at the same order of that of nanochannels (10^2 fL).

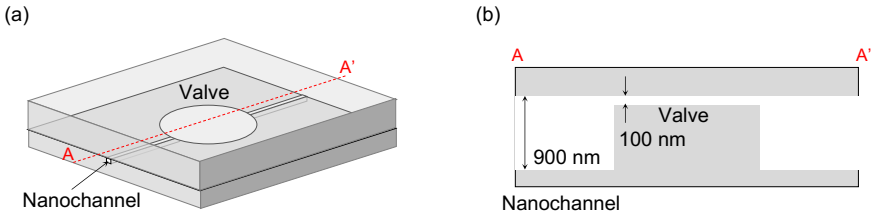

Figure 2-2: Basic structure of a channel open/close valve utilizing glass deformation

Requirements for the valve

The required valve performance is dependent on fluid operations in nanofludic analyses such as single molecule ELISA[36] or nanofluidic chromatography.[34] In such analyses, the ratio of the flow rate when the valve is open and closed should be under 1 % for accurate flow switching. That is, the flow rate decreases to less than 1/100 when the valve is closed. Next, not only precise fluid control but also rapid switching is required especially in nanofluidic chromatography. In this case, the switching time is at the order of 10^{-1} s. Finally, for repeated experiments, the valve is required to have a high endurance. For example, if one valve controls a flow of a certain reagent and the reagent is used 10 times in one cycle of analysis, the valve should endure 1,000 times of open/close operations in order to repeat the analysis 100 times.

The requirements for the valves are summarized below.

Table 2-1: Requirements for the nanofluidic valve

Flow rate	Response time	Endurance
$< 1\%$ (Closed/Open)	$< 10^{-1}$ s	$> 1,000$ open/close cylces

Design of nanochannel open/close valve

As shown in Fig. 2-2, the channels deform as load is applied to the valve by an actuator. This can be considered as a deflection model of a circular plate with clamped edges, and the deflection curve can be described as follows.[65] The deflection for the outer portion and the inner portion of a plate with a built-in edge can be expressed respectively as

$$w_{\text{outer}} = \frac{F}{8\pi D_{\text{f}}} \left\{ \frac{(a^2 - r^2)(a^2 + b^2)}{2a^2} + (b^2 + r^2) \log \frac{r}{a} \right\} \tag{2.3}$$

$$w_{\text{inner}} = \frac{F}{8\pi D_{\text{f}}}\left\{\frac{(a^2+r^2)(a^2-b^2)}{2a^2} + (b^2+r^2)\log\frac{b}{a}\right\} \tag{2.4}$$

where $a,\ b$ is the radius of the valve chamber and the tip of the actuator respectively, r is the distance from the center of the valve chamber, and D_{f} is the flexural rigidity. D_{f} is defined as in equation (2.5) using the Young's modulus E, the thickness of the material t, and the Poisson ratio ν of the material defined as below

$$D_{\text{f}} = \frac{Et^3}{12(1-\nu^2)} \tag{2.5}$$

Therefore, the maximum deflection can be obtained by substituting $r = 0$ in equation (2.4) which is

$$w_{\max} = \frac{F}{8\pi D_{\text{f}}}\left\{\frac{a^2-b^2}{2} + b^2\log\frac{b}{a}\right\} \tag{2.6}$$

On the other hand, the maximum stress generated on the deflected glass surface differs according to the ratio of the radius of the actuator and the circular plane.

When $b/a < 0.32$,

$$\sigma_{\max} = \frac{3F}{4\pi t^2}(1+\nu)\left(\frac{b^2}{a^2} + 2\ln\frac{a}{b} - 1\right) \tag{2.7}$$

When $b/a > 0.32$,

$$\sigma_{\max} = \frac{3F}{2\pi t^2}\left(\frac{b^2}{a^2} - 1\right) \tag{2.8}$$

Considering the deflection curve of the glass expressed by equations (2.3) and (2.4), the dead volume of the rectangular shaped valve chamber will be large. The open space remaining when the valve is closed would also cause leakage and therefore controlling the flow would be difficult (Fig. 2-3(b)). Since the flow in small spaces such as in microchannels and in nanochannels is a laminar flow (as explained in chapter 1), the flow rate in the valve chamber can be roughly estimated as

$$Q = \frac{{D_{eq}}^4}{128\mu L}\Delta P \tag{2.9}$$

where Q is the flow rate, μ is the viscosity, D_{eq} is the equivalent diameter of the channel, L is the channel length, and ΔP is the pressure drop through the channel. Using the sectional area $A = \frac{{D_{eq}}^2}{4}$, equation (2.9) can be rewritten as

$$Q = \frac{A^2}{8\pi\mu L}\Delta P \tag{2.10}$$

Equation (2.10) indicates that the flow rate is proportional to the square of the sectional area. Therefore, the ratio of the sectional area when the valve is closed and open should be 0.1 in order to achieve a flow rate ratio under 1 % .

In order to achieve a sufficiently small sectional area, a four-stepped valve chamber that resembles the deflection curve of the glass was proposed. Each step is 25 nm high and the diameters are 26 μm , 38 μm , 50 μm , 75 μm .

Next, a design to achieve a response time of 10^{-1} s was proposed. The deformation speed can be estimated as the speed of sound of the material, which is in this case 5,770 m/s under 20 °C for glass. Since the deflection is only 10^2 nm, the time consumed for deflection can be neglected and the response time of the valve would be dependent on the response time of the actuator. Therefore, we adopted a piezoelectric actuator, whose response time is shorter than 0.1 second.

Finally, the thickness of the deforming glass was designed so that the glass does not break during open/close operation. In architecture or strength of mechanics, a parameter called safety factor n, which is defined as

$$n = \frac{\text{Stress generated on the material}}{\text{Breaking stress of the material}} \tag{2.11}$$

is considered when designing. It is known that when $n = 2$, the breaking probability

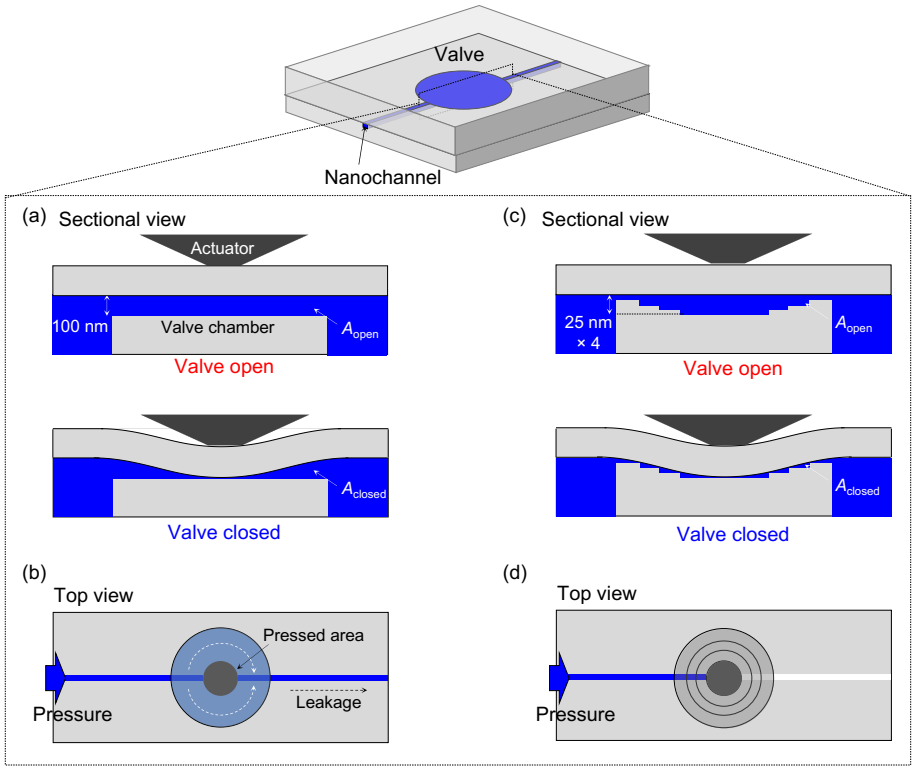

Figure 2-3: (a) A rectangular (one-stepped) chamber (b) Conceptual image of liquid flowing through the opening space of the valve chamber (c) A four-stepped chamber resembling the curve of glass deflection (d) Conceptual image of liquid stopped at the stepped-structure

of the material is under 1/1000.[66] Therefore, the glass thickness was designed so that the stress on the glass when deformed was less than half of the breaking stress of glass (< 580 MPa).

The load applied to the valve was set to 1 N. Under this condition, the relation between the deflection value of glass w, the stress generated on the deformed glass σ, and the thickness of the glass t was calculated using equations (2.3)〜(2.8).

As shown in Fig. 2-4, glass deflects more than 100 nm when the thickness of glass is thinner than 32 μm . On the other hand, the glass must be thicker than 29 μm in order to reduce the stress on glass less than half of the breaking strength. Thus, the thickness of glass was designed as 30 μm .

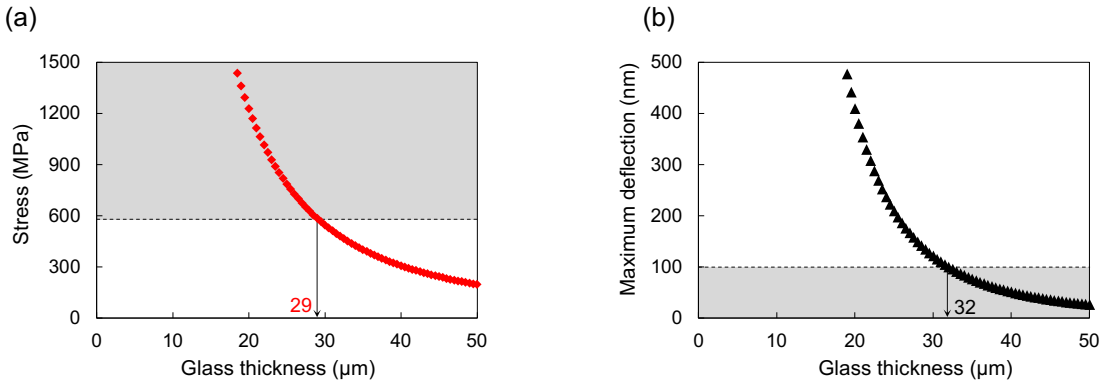

Figure 2-4: (a) Relation between glass thickness and stress generated on glass (b) Relation between glass thickness and deformation value of glass

Integration of valve with micro/nano fluidic device

In order to use the valve for micro-/nanofluidic analysis, it must be integrated in the device. However, such devices consist of several microchannels and nanochannels and therefore glass substrate with a thickness of several hundred μm is necessary. To make the valve (thickness: 30 μm) and the device (thickness: ~10^2 μm) compatible, a structure that has a deformation part fabricated on a small part of the substrate was proposed (Fig. 2-5). With this structure, the rigidity of the substrate is maintained while the valve area has the sufficient thickness to safely close the channel.

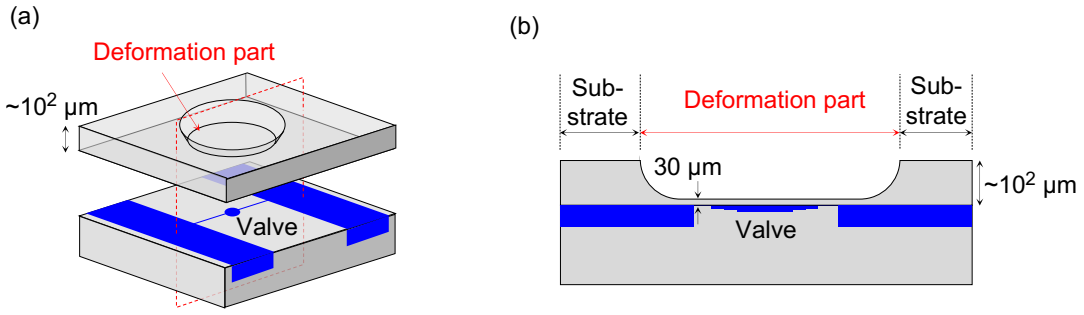

Figure 2-5: Structure for integrating valves into micro-/nanofluidic devices made from glass substrates.

2.3 Device fabrication

Based on the design, the device was fabricated. The details of the fabrication process is explained in the Appendix section. Here, the process will be briefly explained. Fused silica substrates (VIO-SILSX, Shin-Etsu Quartz Co., Ltd., Tokyo, Japan) were used for the device. On the upper substrate, deformation parts for the valve were fabricated. A 0.3 mm-thick substrate was sputtered with chromium and a circle pattern with a diameter of 1 mm was patterned by photolithography. The substrate was then immersed in 30% HF solution for 0.27 mm-deep etching. In this way, a 30 μm -thick deformation part was fabricated. Microchannels, nanochannels, and valve chambers were fabricated on the lower substrate with a thickness of 0.7 mm. First, the nanochannels were fabricated by conventional electron beam (EB) lithography and reactive ion etching (RIE).[25] Next, the valve chambers with a four-stepped structure were fabricated. In order to achieve such a structure, a multistep nano-fabrication process was proposed. One step (25 nm deep) of the valve was fabricated by EB lithography process followed by RIE. This process was repeated four times while changing the diameter of the valve pattern. Then, microchannels were fabricated by conventional photolithography and RIE. The two substrates were washed with piranha solution ($H_2SO_4 : H_2O_2 = 3 : 1$) for 8 minutes and sonicated in ultra-pure water for 10 minutes. Next, the surface of the substrates was activated by irradiating oxygen an fluorine plasma, and bonded at 110 °C under a pressure of 5000 N for 3 hours.[67] The fabricated device is shown below in Fig.2-6.

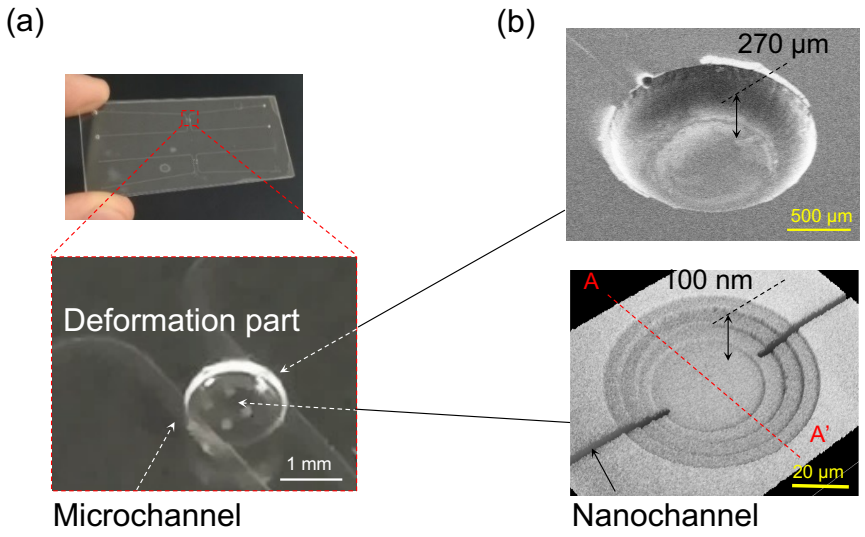

Figure 2-6: (a) Image of fabricated device and the deformation part (b) SEM image of the deformation part on the upper substrate and a 3D depth profile of the valve chamber fabricated on the lower substrate.

2.4 Evaluation of valve performance

2.4.1 Experiment

Valve actuating system

A system for evaluating the valve performance was developed as illustrated in Fig.2-7. The valve control system consists of a stainless pin attached to a piezoelectric driven actuator and a force sensor (Nano-Control Co., Ltd., Tokyo, Japan). The combined actuator and the force sensor was integrated in a XYZ control stage to align the pin. The device was placed on a stainless jig and the whole actuating system was combined to the jig in order to prevent external vibration or alignment errors. The channels and the valves were observed using an inverted fluorescence microscope (IX71, Olympus Corp., Tokyo, Japan), a 20x objective lens with a numerical aperture of 0.4 (LCPlanFL, Olympus Corp., Tokyo, Japan), and an electron multiplying charge-coupled device (EMCCD)

camera (C9100-13, Hamamatsu Photonics K. K., Hamamatsu, Japan). A small hole (diameter: 5 mm) was opened only at the valve area so that the deformation of the whole device can be prevented. Using this system, the operation of valve open/close was first confirmed. Next, flow stop/go by opening/closing the valve was verified. Finally, the flow rate when the valve was closed and the endurance of the valve was evaluated.

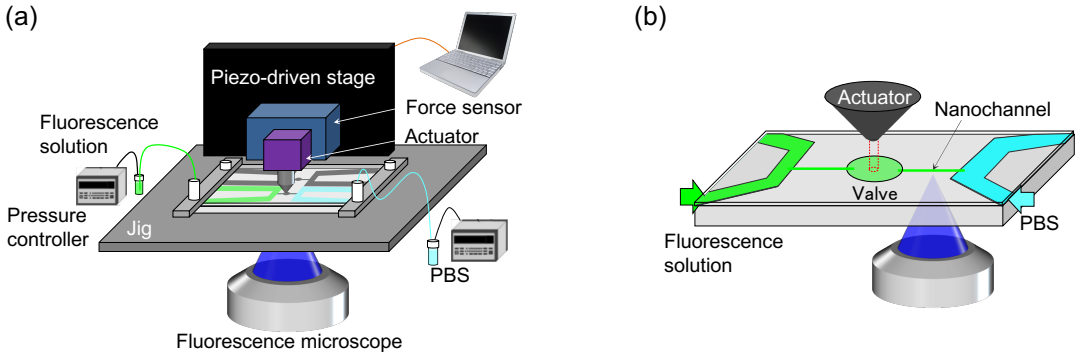

Figure 2-7: (a) Setup of experiment. The valve is opened/closed with a piezoelectric actuator. (b) A magnified image of the device. Fluorescence solution is flowed in the microchannels, nanochannels, and in the valve. The open/closed state of the valve or the flow in the nanochannel is measured with a fluorescence microscope.

Confirmation of valve open/close operation

100 μM Alexa Fluor^{TM}488 NHS Ester (Succinimidyl Ester) (Thermo Fisher Scientific, MA, USA) solution (hereinafter called "Alexa solution") was prepared by dissolving Alexa Fluor^{TM}488 in phosphate saline buffer (PBS). was used for the fluorescence measurements. This was introduced in the microchannels, nanochannels, and in the valve chamber. The valve was pressed with a load of 0.9 N. Under this load, the glass is calculated to deform 116 nm, which is sufficient to close the valve. The open/close state was observed by measuring the fluorescence intensity of the valve chamber.

Confirmation of stop/go using the valve and evaluation of flow rate

First, the microchannels, nanochannels and the valve chamber were filled with PBS from one side. Next, the valve was closed and Alexa solution was flowed in from the other side of the valve. Finally, the load applied to the valve was removed and the flow in the nanochannel was observed.

Evaluation of endurance

The microchannels, nanochannels, and the valve chamber was filled with Alexa solution and the open/close operation of the valve was repeated. During this process, the open/close state was observed with a fluorescence microscope in order to confirm whether the valve is working without breaking.

2.4.2 Results and Discussion

Confirmation of valve open/close operation

The fluorescence images of the valve at the open state and the closed state and the fluorescence intensity at the valve chamber are shown in Fig. 2-8.

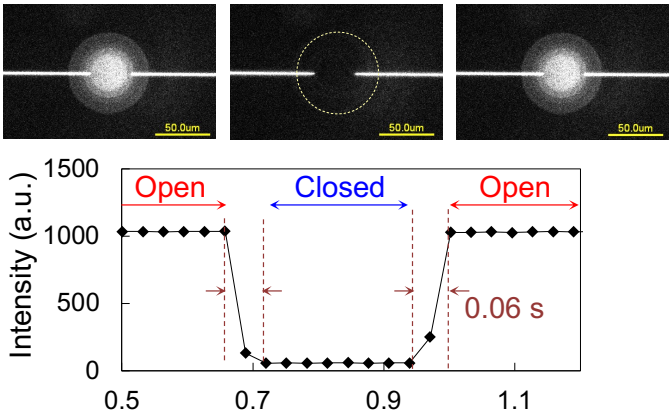

Figure 2-8: Fluorescence intensity at the valve chamber

Since the fluorescence intensity is proportional to the depth of the channel, the fluorescence intensity of the valve chamber represents the opening space of the valve. From the results shown in Fig. 2-8, the fluorescence intensity at the valve chamber decreased by 97% when the load was applied to the valve.

From this result, the deformation of glass and opening/closing of the valve was verified. In addition, from the time required for opening and closing the valve, the response time of the valve was 0.06 s, which reflects the high response time of the actuator and satisfies the requirement ($< 10^{-1}$ s).

Furthermore, in order to investigate the tolerable alignment error of the pressing position, the open/close operation of the valve when the pressing pin was out of alignment from the center of the valve was verified. The valve chamber was filled with fluorescence solution and the open/close operation of the valve was tested while the position of the actuator was varied from 0 μm to 80 μm from the center of the valve chamber. The results are shown below.

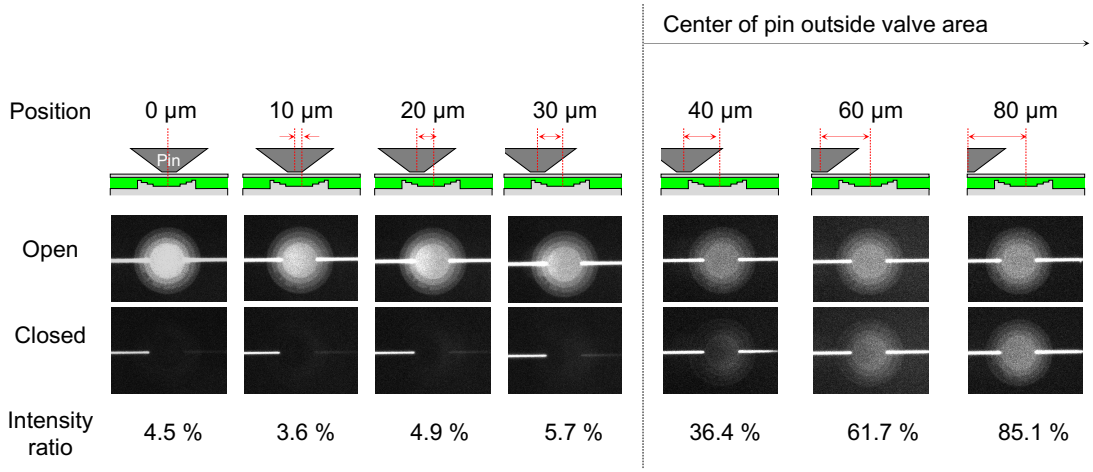

Figure 2-9: Fluorescence image of the valve chamber at the open and closed state and the ratio of the fluorescence intensity of the valve chamber (valve closed / valve open).

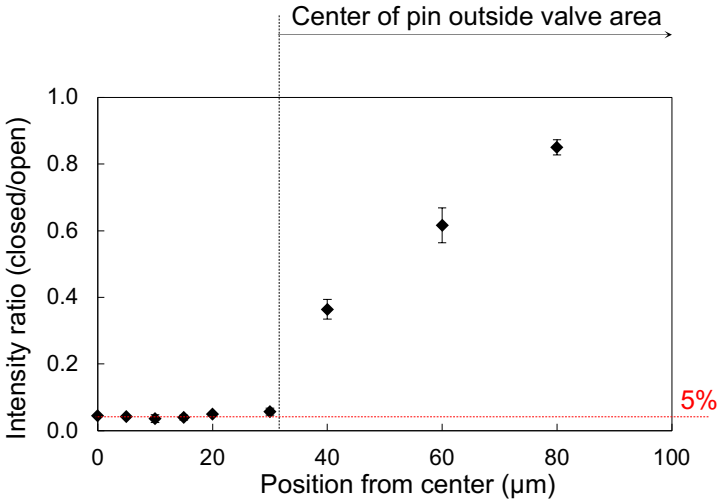

Figure 2-10: Relationship between the distance of the actuator from the center of the valve and the closing efficiency of the valve.

As shown in Fig. 2-10, the fluorescence intensity ratio does not greatly change while the center of the pin is in the area of the valve chamber (alignment error $<$ valve radius 37.5 μm). However, once the center of the pin is outside of the valve area (alignment error $>$ valve radius 37.5 μm) the intensity ratio greatly rose, which indicated insufficient closure of the valve. From this result, the valve could work normally while the alignment error is within 20 μm . Therefore, the tolerable alignment error was determined as $<$ 20 μm .

Verification of flow stop/go using valve

Alexa solution was flowed in with 100 kPa and the flow was observed as the valve opened. The fluorescence intensity in the downstream nanochannel and the fluorescence images of the valve are shown in Fig. 2-11.

When the valve was opened, fluorescence solution instantly flowed through the valve. The fluorescence intensity at the downstream nanochannel when the valve was closed was

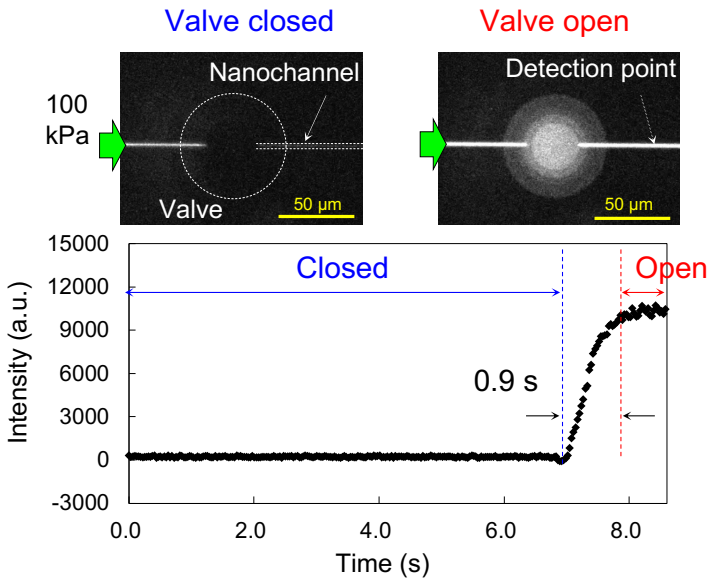

Figure 2-11: The fluorescence intensity in the downstream nanochannel and the fluorescence images of the valve

0.1% compared to that when the valve was opened. Considering the limit of detection in this system (defined as the range of 2σ), fluorescence ratio under 0.5% could not be detected. Therefore, we concluded that the flow was stopped when the valve was closed. The time to replace the nanochannel with fluorescence was 0.9 s, which is applicable to general nanofluidic analysis such as ELISA. This response time for switching flows could be controlled by designing the fluid resistance generated by the valve size, but it can be changed more easily by simply varying the driving pressure.

Evaluation of flow rate

To quantify the flow rate, the following experiment was carried out. The fluorescence in the nanochannel could not be detected when the valve was fully closed so the flow rate could not be directly evaluated. Therefore, the relation between the applied load and the flow rate was evaluated and used to estimate the flow rate when the valve was fully

closed. After closing the valve and introducing Alexa solution , the load was partially removed leaving a certain load (0.11 N, 0.22 N, 0.33 N) to the valve (Fig. 2-12(a)). The fluorescence intensity was measured at two points (distance Δx of the two points: $\Delta x = 100$ μm) at the downstream nanochannel (Fig. 2-12(b)). Using the time difference Δt of the arrival time of fluorescence, the flow velocity u was calculated $\left(u = \dfrac{\Delta x}{\Delta t} \right)$ and the flow rate obtained by multiplying the sectional area of the nanochannel. The relation between the extent to which the valve is closed and the flow rate is shown in Fig. 2-12(c). The extent to which the valve is closed was estimated as

$$\zeta = 1 - \frac{J_x}{J_0} \tag{2.12}$$

where ζ is the ratio of the extent to which the valve is closed, and $J_x,\ J_0$ is the fluorescence intensity of the valve chamber under a certain load and without any load ($i.e.$ fully opened) respectively.

As shown in Fig. 2-12, the flow rate decreased as the applied load increased. When the applied load was over 0.33 N, the signal of fluorescence in the nanochannel was covered by the noise and difficult to determine the arrival time of fluorescence. The obtained relation was using a quadratic function. From the closing ratio ζ when the valve chamber was fully closed, the estimated flow rate was 0.1 %. Furthermore, from the obtained flow rate shown in Fig. 2-12 (63–1300 fL/s), the valve could be used to control flow rate within the range of fL/s.

Evaluation of endurance

The open/close operation of the valve was repeated (open time: 0.25 s, closed time: 0.25 s) and the endurance of the valve was evaluated.

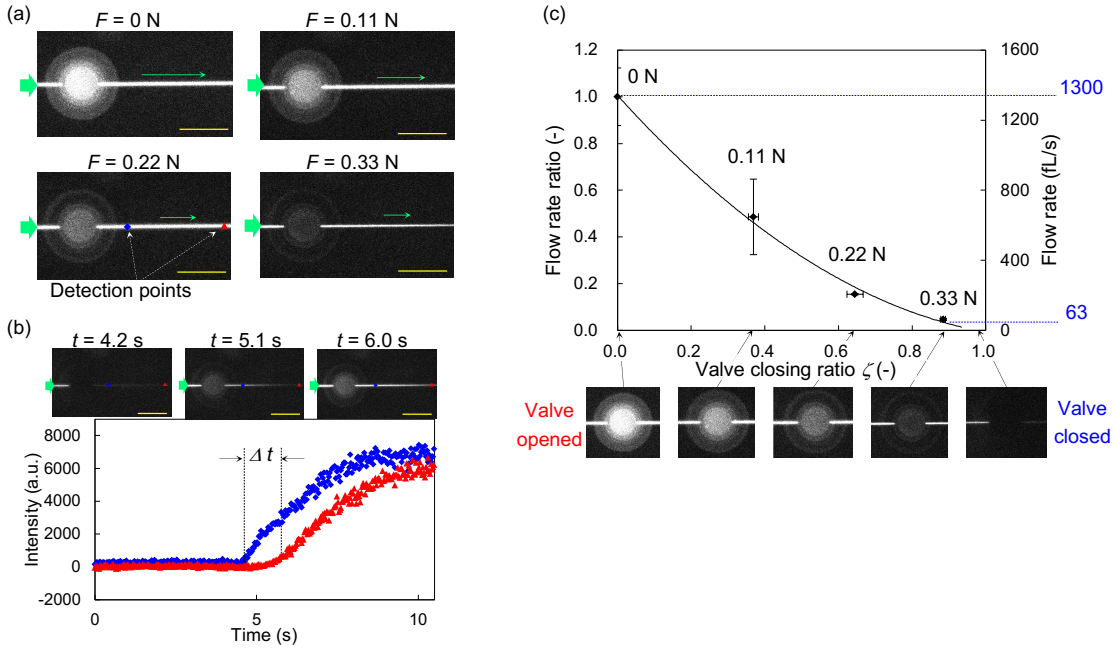

Figure 2-12: (a) Fluorescence images under loads of $F = 0, 0.11, 0.22, 0.33$N (b) An example of flow rate measurement. The flow velocity was calculated from the difference of the arrival time of the fluorescence at two points. (c) Relation between the valve closing ratio ζ and the flow rate

As a result, the operation of the valve could be repeated more than 100,000 times, which was two orders of magnitude greater than the original goal (1,000 times). While the number of operation increased, the fluorescence intensity at the valve chamber also increased, until the intensity finally reached 1.3 times higher than the original state. This implies that the deflection of the valve was greater than designed and that the valve chamber deformed to the shape of the curve of the glass deflection while it was repeatedly struck and became deeper. Although the deformation may be larger than designed, an endurance of more than 100,000 times of open/close operation was confirmed.

Numerical simulation of flow in the valve chamber

We carried out a numerical simulation to characterize the valve using finite element method. The mass balance and the momentum balance of the fluid are expressed by

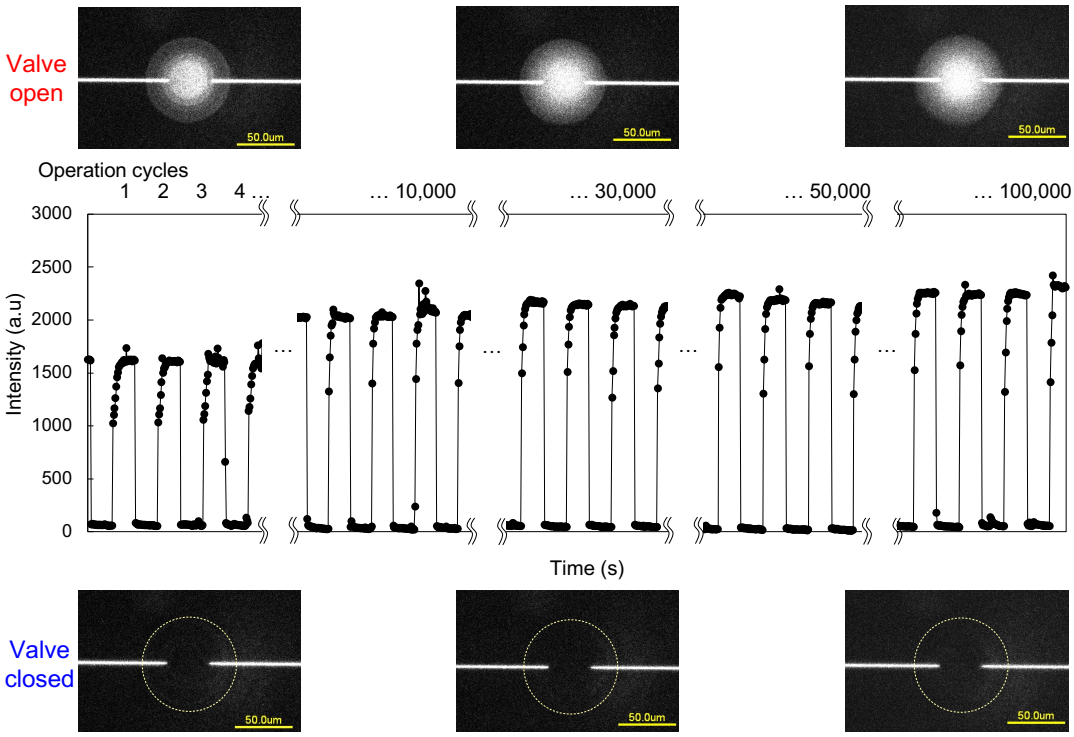

Figure 2-13: Fluorescence intensity at the valve chamber and fluorescence images during repeated open/close operation.

the equation of continuity and the Navier-Stokes equation respectively and the boundary condition was set so that the flow velocity is zero at the channel surface. The calculation was operated with COMSOL (Keisoku Engineering System Co., Ltd.). The results of the simulations are shown in Fig. 2-14 and in Fig. 2-15.

The horizontal axis represents the ratio of the extent to which the valve is closed (ζ in equation (2.12)) The vertical axis represents the flow rate ratio. Theoretically, a small volume remains open even though the deformation of the glass reaches the chamber depth, so the theoretical maximum value of the sectional area is 0.9. As a result of the simulation, the flow rate decreases as the sectional area of the valve chamber decreases, which means that the fluid resistance is increasing. However, the flow rate obtained from the experiment was lower. Considering from the results that the valve chamber could be distorted to the shape of deformation after several thousand operations, the actual de-

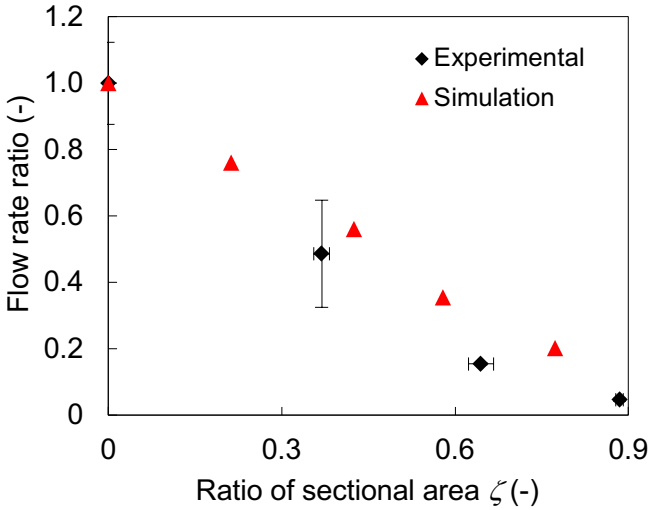

Figure 2-14: Comparison of the experimental and simulation results of flow rate control

formation value could be approximately 1.5 times more than designed as mentioned in section 3.2.2. Therefore, the fluid resistance could be higher than expected, which results in lower flow rate. Another possible factor is increase of the viscosity of liquid (which is water in this experiment) confined in nanospace. When the valve is deformed, the valve chamber that the fluid flows through can be assumed as a plate-shaped channel with the depth of ~10^1 nm and an aspect ratio of more than 1000 (width/depth). In such a space, our group revealed that water gets 1.2 times more viscous.[30] Therefore, the increase of the viscosity of water could also be a possible cause for the lower flow rate. Despite the fact that the actual flow rate was lower than expected, this will be an advantage for the valve to control low flow rates. From this result, it would be possible to estimate the range of flow rate control and the approximate load applied to the valve in order to obtain a certain flow rate.

(a)

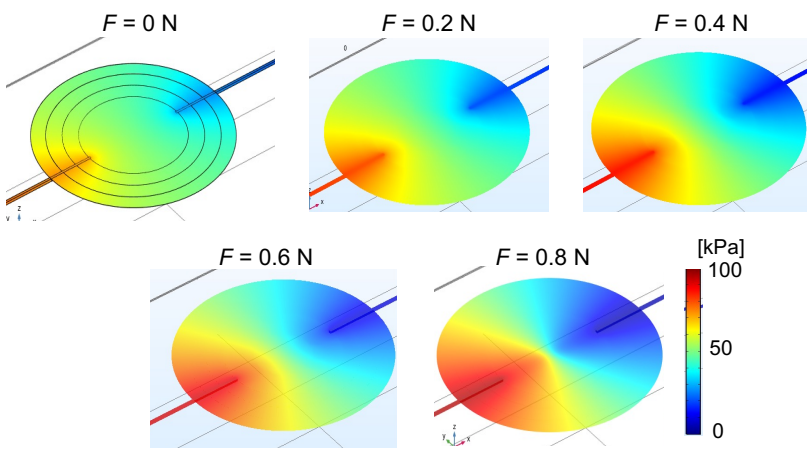

(b)

Force	0 N	0.2 N	0.4 N	0.6 N	0.8 N
Pressure drop	41.1 kPa	60.7 kPa	70.9 kPa	81.5 kPa	89.7 kPa
Flow rate	4523 fL/s	3434 fL/s	2535 fL/s	1607 fL/s	912 fL/s

Figure 2-15: Detailed simulation results of flow rate control

2.4.3 Comparison with other reported valves

The performance of the valve developed in this chapter is compared with other types of valves (Fig. 2-16).

Among the various valves developed nowadays, channel deformation valves, so-called "Quake valves," are most widely used for integrated analytical systems. Compared to the channel deformation valves, the nanochannel open/close valve achieved a similar performance in terms of pressure capacity and the response time. Because these performances surpass those of other types of valves, it could be said that this valve also has a sufficient performance for integration into analytical devices. What is more, most valves nowadays are made from polymers such as PDMS, which limits their application to only aqueous analyses. By contrast, this nanochannel open/close valve is made from glass. Hence, there is almost no limitations in using organic/inorganic solvents and it could pave the

	Active valves			This study	Passive valves	
	Channel deformation	Membrane	Phase transition	Channel deformation	Check	Burst
Pressure capacity	10^2 kPa	10^1 kPa	10^2 kPa	500 kPa	10^1 kPa	10^2 kPa
Response time	10^{-2} s	10^{-2}-10^0 s	10^0-10^1 s	0.06 s	—	—
Fabrication for valve	Control channel	Membrane Control channel	Incorporation of polymer	Deformation part Valve chamber	Cantilevers	Surface modification
Device material	Polymer	Polymer Metal	Polymer	Glass	Polymer Metal	Polymer
Reports on integration	Many	Many	Few	Not yet	Combined with others	Combined with others
Versatility	△	△	△	◎	○	△

Figure 2-16: Comparison of the nanochannel open/close valve developed in this chapter with other micro-/nanofluidic valves.

way for realizing integrated nanofluidic analyses.

2.5 Conclusion

In chapter 2, the basic design of a nanochannel open/close valve utilizing glass deformation was proposed and the valve was developed.

In section 2.1, the requirements to realize a valve utilizing glass deformation was discussed and based on the idea of a nanochannel open/close valve, the conceptual design of the valve was proposed.

In section 2.2, the valve was designed in detail. Considering the requirements for the valve to be used in nanofluidic analyses, a four-stepped structure was proposed for the valve and the thickness of the glass deformation part was designed based on mechanics of materials. Furthermore, in order to implement the valve into nanofluidic devices, the idea to fabricate a deformation part on the substrate was proposed.

In section 2.3 and 2.4, the open/close operation and the performance of the valve was

evaluated. The flow rate when closing the valve was 0.1 % , the response time was 0.06 s, the endurance of open/close operation was over 100,000 times. In addition, we verified its use as a flow rate controlling valve.

Chapter 3

Fluid operation using nanochannel open/close valve

3.1 Introduction

3.1.1 Background

In the previous chapter, stopping and releasing the flow, which is the most basic fluid operation using valves were verified. In this chapter, the valve will be applied to fluid operations required in analyses using micro/nano integrated devices.

Fluid operations can be roughly divided into single-phase operations and multi-phase operations. An example of a single-phase operation is switching flow of reagents with different concentrations. It can be assumed from the results of chapter 2 that forming flows of different reagents will be easily achieved by opening the valve. However, it is also necessary to partition multiple reagents so that they do not get mixed and contaminated. In terms of multi-phase operations, a general example of a system is a gas/liquid two-phase system. For chemical reactions or volume regulation of liquid solutions, air would also be introduced in the analytical devices. Therefore, switching the reagents in the nanochannels from liquid to gas and vice versa is an important and required fluid operation.

By using a nano-sized valve for these operations, certain problems can be assumed that derives from its small space (~10^1 nm). The diffusion velocity of molecules is proportional to the square root of its diffusion coefficient D, so generally, the diffusion velocity of molecules is 10^1 μm/s. Therefore, diffusion through the valve that is only 100 nm deep occurs within the order of ms. Because the valve developed in chapter 2 has a stepped structure, a small space remains open even when the valve is closed. Although the flow can be stopped even with this remaining open space, molecules could diffuse through this space, which results in solute leakage. A subtle solute leakage would not be a major

problem in analyses in microspace, but in analyses in nanospace, where the sample could be countable molecules, it would cause a critical problem. On the other hand, the small space in the valve chamber enhances the surface effect even greater than in nanochannels. Because the interaction with the surface will be dominant, the wetting property of the surface would be critical in the case of flow operations in gas/liquid two-phase system.

3.1.2 Objective

The objective of this chapter is to realize fluid operations in a single-phase system and a gas/liquid two-phase system using the valve developed in chapter 2.

In section 3.2, a curved valve chamber is proposed for single-phase operation to prevent leakage caused by diffusion. In order to obtain such a curved structure, a fabrication method using plastic deformation of glass is also proposed. The fabrication process is verified and the leakage caused by diffusion is evaluated using the curved valve chamber. In section 3.3, a hydrophobic valve chamber is proposed to control the surface properties for a gas/liquid two-phase system. A method to control the gas/liquid interface by generating pressure using the open/close operation of the valve is also proposed and verified.

3.2 Single-phase fluid operations

3.2.1 Subjects of fluid operation

Operation using stepped-structured valve chamber

As designed and evaluated in chapter 2, the valve has a four-stepped valve chamber which resembles the deflection curve of the glass. However, there is still a small space remained open at the edge of the steps. This space is estimated to have a height of only 25 nm and have no negative effects on stopping the flow, but considering molecule diffusion, this space would be large enough for molecules to transfer through the valve (Fig. 3-1(a)).

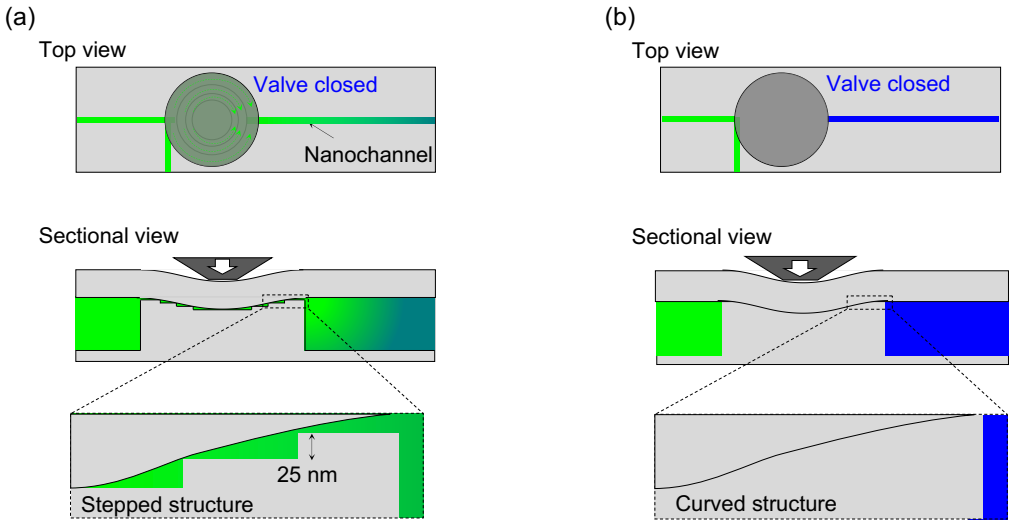

Figure 3-1: Molecular diffusion in a stepped valve chamber and a curved valve chamber

To this subject, using a curved valve chamber would be ideal (Fig. 3-1(b)). If the valve chamber perfectly fits the glass deflection curve, not only the leakage caused by diffusion would be reduced, but the flow leakage when the valve is closed would also improve.

Fabrication of a curved structured valve chamber

The curved structure required here is a curve of the glass deflection, which is theoretically described with the equations (2.3) and (2.4). This is an almost flat structure with a

high aspect ratio of 750 (width 75 μm / depth 100 nm) and the maximum slope degree of $0.15°$. A general method for fabricating a curved surface on a glass substrate is wet etching.[68] It has been reported that the isotropic etching procedure can be controlled by temperature and the composition of the etchant or the mask.[69–71] However, the structures produced by this method have too low aspect ratios or slope angles for the required structure and therefore wet etching cannot be used to fabricate the nanofluidic valve. Laser ablation[72] and nanoimprinting lithography[73] are also examples of methods to fabricate curved surfaces. However, the surface roughness caused by laser ablation and the difficulty of creating valve-shaped molds make these methods difficult to apply. Therefore, fabrication of such a structure is challenging.

Here, I conceived the idea of using plastic deformation of glass. Glass is generally known to be a rigid and brittle material. That is, as the stress generated inside the glass increases, it breaks right after its limitation of elastic deformation range without deforming plastically. However, under a specific circumstance, plastic deformation of glass is reported. An example using this is the hardness measurement of glass using a Vickers indenter. A Vickers indenter is an indenter with a square-based pyramid made of diamond on the tip. By pressing the sharp tip of the indenter on a glass surface, the surface deforms up to ~μm without breaking.

Therefore, the valve chamber could be deformed to the shape of the glass deflection curve by using the deflected glass itself as a indenter. To achieve this, a fabrication process using plastic deformation of glass was proposed. As shown in Fig. 3-2, after fabricating a four-stepped valve chamber, the valve is repeatedly opened and closed. Each open/close cycle applies pressure to the surface of the valve chamber. Since each step is only 25 nm high, a nanoscale plastic deformation at the edges of the steps would result in smoothening

the surface of the valve chamber.

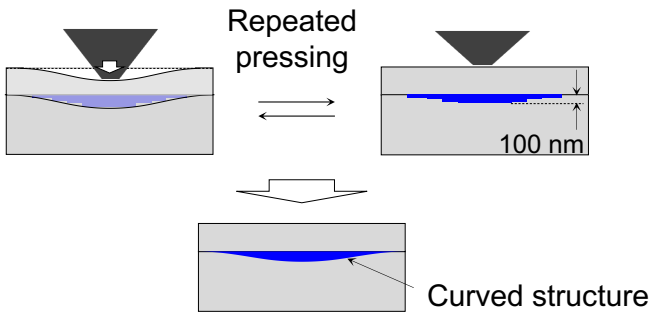

Figure 3-2: Concept of the fabrication process for a curved valve chamber

3.2.2 Experiment

Fabrication of device

The nanofluidic device was fabricated in the similar way as described in section 2.3. A 30 μm -thick deformation part was fabricated on a 250 μm -thick substrate by etching the glass 220 μm deep with HF solution using a Cr/Au/Cr mask. On another substrate, nanochannels (width: 1000 nm, depth: 900 nm) and a four-stepped valve chamber were fabricated. In order to evaluate leakage through the valve, an L-shaped nanochannel was fabricated at the upstream of the valve chamber so that fresh reagent could be introduced just before the valve chamber even when the valve is closed. Microchannels (width: 400 μm , depth: 7 μm) were then fabricated on the same substrate. The substrates for the device to evaluate the fabrication method were loosely bonded after being washed only with piranha solution followed by sonication in ultra-pure water. This loose bonding condition is for the detaching process of the substrates and evaluation of the valve shape afterward. For the substrates for the device to evaluate leakage, the substrates were bonded after additionally irradiating oxygen and fluorine plasma after washing with piranha solution and sonication in ultra-pure water. Finally, the substrates were bonded at 110 °C under a

pressure of 5000 N for 3 hours. Then, the valve was repeatedly pressed with 1.1 N using the same system used in section 2.4 with a period of 250 ms. This pressing process was carried out in room temperature (25 °C). The shape of the valve was evaluated for the initial valve chamber and after repeated pressing of 5,000, 10,000, and 20,000 times.

Another approach to fabricate a curved chamber is to increase the number of the steps and create a structure that resembles the deflection curve of the glass more closely. In addition to the valve chamber with four steps, valve chambers with eight steps (diameters of each step were 18, 26, 32, 38, 44, 50, 58, 75 μm and each step were 13 nm deep) and 12 steps (diameters of each step were 15, 21, 26, 30, 34, 38, 42, 46, 50, 55, 61, 75 μm and each step were 8 nm deep) were fabricated for comparison of the availability of the fabrication method and the performances using the fabricated valve chambers.

Evaluation of leakage

100 μM Alexa Fluor^{TM}488 dissolved in PBS (hereinafter called "Alexa solution") was used to evaluate the leakage. First, the microchannels, nanochannels, and the valve chamber were filled with PBS (Fig. 3-3(a)). The valve was then closed by a load of 1 N and Alexa solution was introduced with a low driving pressure (20 kPa) into the upstream L-shaped nanochannel as illustrated in Fig. 3-3(b). As soon as the upstream nanochannel was filled, the pressured was turned off (Fig. 3-3(c)). The solute diffusion through the small remaining open space of the valve was observed by fluorescence measurement, using the same system described in chapter 2.

To evaluate the dynamics of the diffusion, the diffusion flux through the valve was estimated. According to Fick's law, the diffusion flux J under this condition can be calculated as

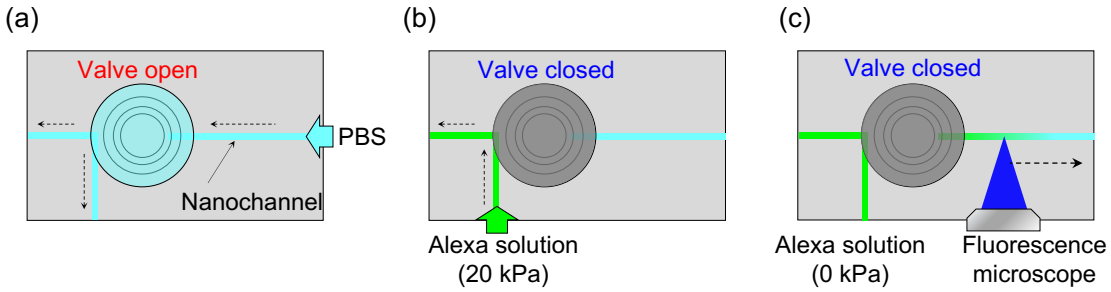

Figure 3-3: The procedure of the experiment to evaluate solute leakage caused by molecular diffusion through the valve

$$J = -D\frac{\partial C}{\partial x} \tag{3.1}$$

where C is the concentration of the solution, x is the position, and D is the diffusion coefficient of the solute. The fluorescence intensity at 11 points (a total distance of 300 μm) in the downstream nanochannel was measured (Fig. 3-3(c)).

Demonstration of switching reagents

Utilizing the similar device, reagents, and setup, switching and partitioning operations in a nanochannel were demonstrated. The process is illustrated in Fig. 3-4. An external pressure of 100 kPa was applied to Alexa solution in the straight nanochannel, and that of 40 kPa was applied to PBS solution in the L-shaped nanochannel. By opening the valve for 30 s, the fluorescence solution was provided into the L-shaped nanochannel for switching. The time of closing the valve was varied from 1 to 30 minutes in order to investigate effects of solute leakage through the closed valve.

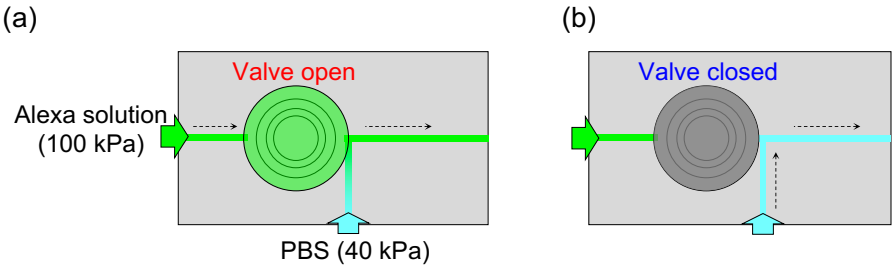

Figure 3-4: Schematic image of switching two reagents (a) When the valve is opened, the flow of Alexa solution is formed in the downstream nanochannel. (b) When the valve is closed the flow switches to that of PBS.

3.2.3 Results and discussion

Fabrication of a curved valve chamber

The microchannels, nanochannels, and valve chamber were successfully fabricated. After pressing the valve repeatedly, the substrates were detached by inserting a razor blade between the substrates for surface shape measurement. The shape and the depth profile of the valve chamber was obtained using an optical profiler (WYKO NT9100A, Bruker Co.) and a stylus profiler (Dektak XT-S, Bruker Co.). The results of the measurements of the chamber shapes and depth profiles before/after pressing are shown in Fig. 3-5. After pressing 5,000 times, the stepped structure can still be recognized but the edges of the steps were apparently smoothened. After pressing 10,000 times the steps in the valve chamber were gradually demolished, and after 20,000 times the steps were almost completely demolished, and a curved surface was obtained. Although the steps of the initial valve chamber were demolished, the shape of nanochannel was maintained. In addition, as the pressing number increased, the valve chamber gradually became deeper. The depth of the valve chamber after pressing 20,000 times was 130 nm, which implies that the valve chamber was mechanically deformed by repeated pressing. From these

results, we successfully verified the proposed fabrication method by applying impulsive forces and demonstrated the fabrication of nanoscale curved structure with an aspect ratio of 750 (width: 75 μm , depth: 100 nm), which has been difficult for conventional fabrication methods.

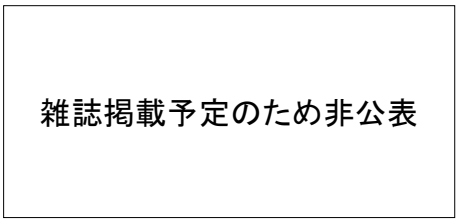

Figure 3-5: 3D depth profiles and 2D sectional depth profiles of the valve chambers of the initial four-stepped structure and after being pressed 5,000, 10,000, 20,000 times

As for the eight-stepped valve chamber and 12-stepped valve chamber, a shape closer to a curved structure was obtained as well (Fig. 3-6). However, as the number of steps increase, the alignment precision for each step during the fabrication gets stricter. For example, the tolerable alignment error of each step in the 12-stepped valve is less than 2 μm , which is difficult to achieve by manual operation. For this reason, it can be assumed that an ideal curved structure cannot be achieved by increasing the number of steps.

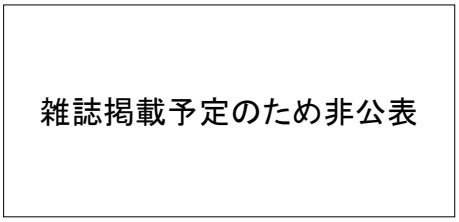

Figure 3-6: 3D depth profiles and 2D sectional depth profiles. (a) Eight-stepped valve chamber (b) 12-stepped valve chamber.

Evaluation of diffusion flux

The fluorescence images are shown in Fig. 3-7. No apparent fluorescence was observed in the downstream nanochannel at the moment Alexa solution was introduced in the upstream nanochannel, but significant fluorescence was observed after 30 minutes especially with the four-stepped valve chamber (Fig. 3-7(a)). However, the brightness of the downstream nanochannel decreased as the pressing number of the valve chambers increased. This implies that the valve chamber resembled the deflection curve of the glass more closely as the pressing number increased and thus the open space remaining when the valve was closed decreased.

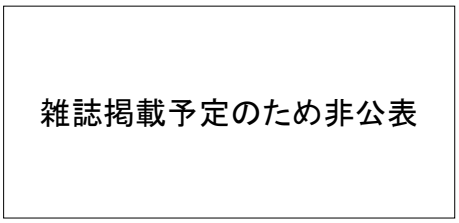

Figure 3-7: Fluorescence images of valves. The top and bottom rows show the images right after fluorescence solution was introduced in the L-shaped nanochannel and 30 minutes after. (a) Four-stepped valve and after pressed (b) 5,000 times (c) 10,000 times (d) 20,000 times.

Since no fluorescence was observed at the end of the nanochannel, where it is connected to the microchannel filled with PBS, the fluorescence concentration can be consid-

ered as zero. Therefore, a one-dimensional diffusion model was applied to characterize the diffusion in the nanochannel. Using equation (3.1) and that fluorescence intensity is proportional to the concentration of the fluorescent solution, the diffusion flux can be estimated from the linear slope of the fluorescence intensity in the downstream nanochannel after reaching its stationary state. For all conditions, the absolute value of the slope of the fluorescence intensity in the nanochannel increased and had no significant change after 30 minutes. The diffusion flux was estimated at this stationary state. Figure 3-8 shows the results of each conditions. The summarized results of the absolute value of the slope after 30 minutes are shown in Fig. 3-9. The diffusion flux decreased by 81 % when the pressing number was 5,000 times. As the pressing number was increased, the diffusion flux further decreased, and finally reached a decrease of 94 % after 20,000 times of pressing. Considering that the edges of the valve chamber started to smoothen after being pressed 5,000 times and further smoothened as the pressing number increased, the edges of the stepped valve chamber could be the dominant factor of causing solute diffusion.

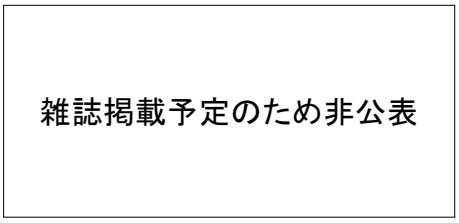

Figure 3-8: Fluorescence intensity in the downstream nanochannel for each valves

Under a one-dimensional diffusion model, the diffusion flux J can be calculated as

$$J = \frac{DC_1}{L} \tag{3.2}$$

where C_1 is the initial concentration of fluorescence solution where the downstream nanochannel and the valve is connected, and L is the length of the nanochannel (L =300 μm). Since the diffusion coefficient D in the nanochannel and the length of nanochannel

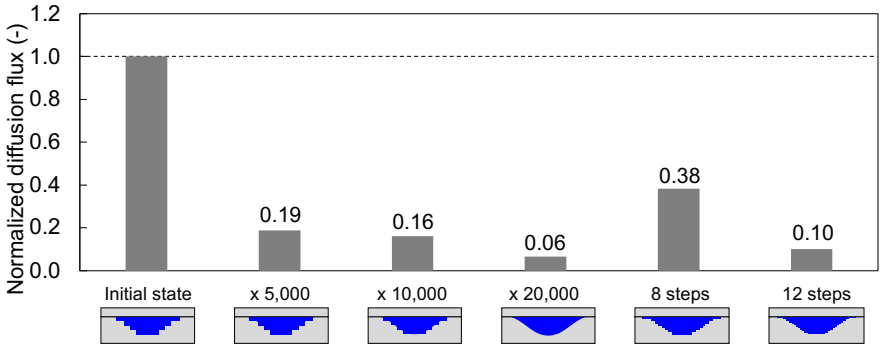

Figure 3-9: The summarized results of diffusion flux

L is constant, the diffusion flux is proportional to C_1. Considering that the depth of the nanochannel (900 nm) is small enough compared to the length of the nanochannel (300 μm), the time for diffusion in the depth direction can be negligible. In addition, C_1 is determined by the diffusion of the fluorescence molecules from the nanochannel at the upstream of the valve so C_1 has a proportional relation with the remaining open space of the valve chamber and a positive correlation with the diffusion coefficient D' in the valve chamber. Thus, diffusion flux in the downstream nanochannel can be assumed to be dependent on both the opening space of the valve chamber and the value D'. When considering a static diffusion system in the valve chamber, D' can be estimated by applying Stokes-Einstein equation (3.3),

$$D' = \frac{k_{\mathrm{B}}T}{6\pi\eta r} \tag{3.3}$$

where k_{B} is the Boltzmann constant, T is the temperature, η is the viscosity of the solution, and r is the radius of the molecule. As this equation indicates, D' is inversely proportional to the viscosity of the solution. The remaining open space in the valve is considered to be a 1D plate nanochannel with a width of ~μm and a height of ~10 nm. In such a confined space, it has been revealed by our group that the viscosity of water rises.[30] Considering this effect of the space size on the viscosity, reducing the open space in the valve could also

reduce the diffusion coefficient of the solute molecules in the valve chamber. Although these two effects cannot be discussed separately from the obtained results, the result that the diffusion flux was reduced by 94 % when pressing the valve 20,000 times implies that a curved valve chamber that resembles the deflection curve of the glass was successfully achieved and the open space remaining had decreased. On the other hand, when using the eight-stepped valve chamber and the 12-stepped valve chamber, the diffusion flux was reduced by 62 % and 90 % respectively (Fig. 3-9). Therefore, increasing the steps of the valve chamber also contributes to decreasing the diffusion flux, but considering the fabrication precision mentioned before, there is a limit for this method. Moreover, the results shown in Fig. 3-9 imply that a valve chamber with less edges is more effective for reducing leakage. Therefore, fabrication by pressing the valve repeatedly is a simpler and a more promising method to realize a curved structure resembling the glass deflection.

Evaluation of leakage

The average fluorescence intensities in the upstream (I_0) and downstream (I_1) nanochannels were measured, and the total amount of leakage was estimated from the ratio of the average fluorescence intensity (I_0/I_1). Figure 3-10(a) shows the results of the leakage of the valves after pressing 0, 5,000, 10,000, and 20,000 times. The leakage reaches a plateau after about 7 minutes and the value decreased as the pressing number increased. We evaluated the leakage as far as the signal-to-noise (S/N) ratio was over two, which corresponds to leakage of 0.5 %.

The amount of leakage after 30 minutes for the initial four-stepped valve chamber and the pressed chambers are compared in Fig. 3-10(b). When the valve was pressed 5,000 times, the leakage greatly decreased by 88 % compared to the initial valve chamber,

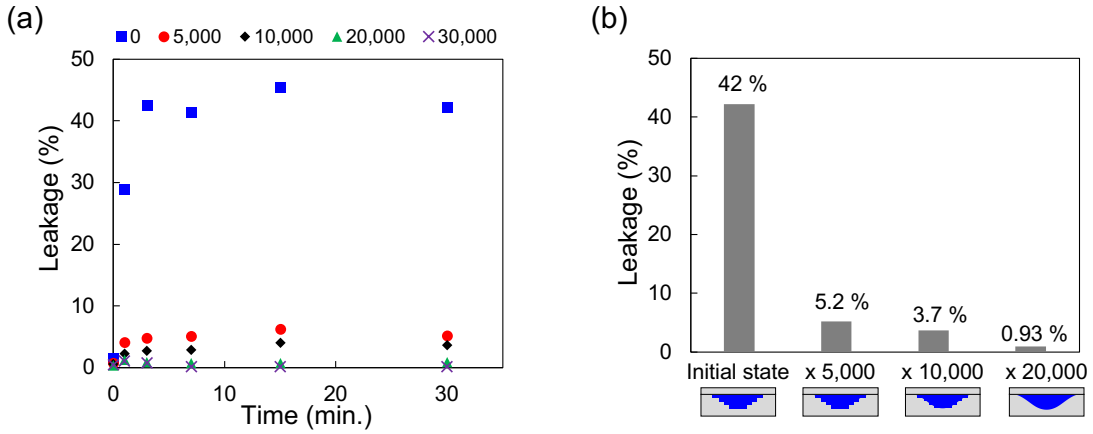

Figure 3-10: (a) The amount of leakage caused from the four-stepped valve and valves pressed 5,000, 10,000, 20,000, and 30,000 times (b) Comparison of the amount of leakage caused by diffusion for valve chambers with different pressing numbers

which is a similar tendency to the results of the diffusion flux. When the pressing number was 20,000, the estimated leakage was 0.93 %, which is more than 40 times smaller than the four-stepped valve (42 %). Therefore, sampling or partitioning a certain volume within this degree of error is possible using this valve. Because the sampling tolerance in general analyses (*e.g.* using micropipettes) is around 1 %, and even larger for small sample volumes, this error can be considered sufficiently small. Judging from the results of pressing the valve, the remaining open space would decrease as the pressing number increases, and therefore the leakage could be further decreased by increasing the pressing number. To verify this, the leakage of a valve chamber that was pressed 30,000 times was also evaluated. The calculated leakage was 0.21 %, which was less than the limit of quantification. Therefore, the idea of further reduction of leakage by increasing the pressing number was verified and the estimated leakage was less than 0.5 %. These results support that a curved valve chamber was fabricated by repeated pressing of a stepped-structured valve chamber and that leakage could be greatly reduced using this method.

Although the four-stepped valve possesses a satisfactory performance to stop the flow as evaluated in chapter 2, the experiment in this section indicates that molecules can still flow through the valve chamber by diffusion (*e.g.* 42 % of leakage in a four-stepped valve). Therefore, in order to control mass transfer by opening and closing the valve, controlling only the macroscopic flow of the fluid is insufficient and additional control of microscopic molecular diffusion is also necessary especially for nanofluidic analysis, where the sample could contain only countable molecules. The results in this section revealed this critical problem, and in addition, presented a promising solution to prevent leakage caused by molecular diffusion. Furthermore, by controlling and quantifying the remained open space in the closed valve chamber, the valve could be used to investigate molecular behaviors in a small space that is nearly the same size as the molecules. As a result, new information on diffusion coefficients of molecules or molecular interactions in such an extra-confined space could be obtained.

Switching of reagents

Finally, switching and partitioning of reagents in pressure-driven flows was demonstrated using the valve with the curved surface by the pressing number of 30,000. The results are shown in Fig. 3-11. Alexa solution and PBS were introduced from the upstream straight nanochannel and the downstream L-shaped nanochannel respectively. When the valve was opened, the fluorescence solution was instantly flowed in to the downstream nanochannel at a velocity of 2.65 mm/s, with a response time of 0.4 s. When the valve was opened for 30 s, 72 pL of the fluorescence solution was provided to the downstream nanochannel. The valve was kept closed for 1, 3, 7, 15, and 30 minutes in order to verify flow switching during a long time interval. After each intervals, the valve was

opened again for 30 s. Since the solute leakage at the valve closed state was sufficiently suppressed by the curved valve chamber, even when the time interval of the switching became longer, almost no leakage was observed, and the initial state before opening the valve could be maintained. Therefore, using the valve with the curved structure, switching and partitioning of pL reagents in nanochannels can be achieved without contamination of reagents by unexpected mixing.

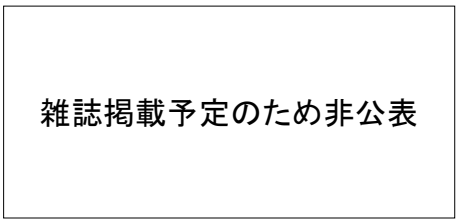

Figure 3-11: Fluorescence intensity at the downstream nanochannel during flow switching. The images on the top and bottom are fluorescence images of the valve when opened and closed respectively.

3.3 Multiple-phase fluid operations

3.3.1 Subject

In order to replace liquid in the nanochannels to air using valves, the gas/liquid interface must be transported through the valve. In order to achieve this, the Laplace pressure at the gas/liquid interface must be overcome using the driving pressure of air. The Laplace pressure is calculated from the Young–Laplace equation and for rectangular channels such as the micro-/nanochannels in this study, it can be expressed as follows.[74,75]

$$P_{\mathrm{L}} = -\gamma \left(\frac{\cos\theta_{\mathrm{t}} + \cos\theta_{\mathrm{b}}}{h} + \frac{\cos\theta_{\mathrm{l}} + \cos\theta_{\mathrm{r}}}{w} \right) \tag{3.4}$$

where P_{L} is the Laplace pressure, γ is the interfacial tension of the liquid, h, w are the channel height and width respectively, and θ_{t}, θ_{b}, θ_{l}, θ_{r} are the top, bottom, left, and right

contact angles of liquid against the four channel walls. When the materials and the surface conditions are same for all four walls ($\theta_{\mathrm{t}} = \theta_{\mathrm{b}} = \theta_{\mathrm{l}} = \theta_{\mathrm{r}} = \theta$), equation (3.4) can be simplified to

$$P_{\mathrm{L}} = -2\gamma \cos\theta \left(\frac{1}{h} + \frac{1}{w} \right) \tag{3.5}$$

Although the valve chamber is not a rectangular shape exactly, the Laplace pressure can roughly be estimated using the equation (3.5). The valve chamber is 75 μm in width and the depth is 100 nm at maximum and 25 nm at minimum. Thus, the Laplace pressure is estimated to be 1.5 MPa. On the other hand, the maximum pressure generated from the compressor (TFP04C-10C, ANEST IWATA Corp., Kanagawa, Japan) is 0.8 MPa. Hence, once the valve chamber is filled with water, it cannot be replace with air using the driving pressure from the compressor.

To address this subject, hydrophobic modification of the valve chamber was proposed to control the Laplace pressure inside the valve. By hydrophobically modifying the surface of the valve chamber, introduction of water can be prevented. The valve chamber could be replaced from water to air in this way, but still, the gas/liquid interface remains at the exit junction of the valve chamber and the nanochannel. The Laplace pressure here is also estimated to be 1.5 MPa and would prohibit introduction of air. In order to conquer this subject, I additionally proposed a method to generate pressure on-chip using the closing operation of the valve. Judging from the experiment in section 2.4, the volume of the valve chamber is estimated to be compressed to 10 % when closed. Plus, the time taken for the glass to deform was estimated from the theoretical response time of the piezoelectric actuator, which is 2.4 μs. Considering the speed of air compression inside the valve chamber and the speed of air escaping from the upstream nanochannel,

the maximum pressure obtained was calculated to be 4.3 MPa. Therefore, this process could be applied to overcome the Laplace pressure at the gas/liquid interface in the valve chamber and achieve gas/liquid switching in the downstream nanochannel.

3.3.2 Experiment

Fabrication of device

The design of the valve chamber and the nanochannels are same as the design in section 3.2.2. Octadecyldemethyl-N, N-diethylaminosilane (ODS-DEA) (Gelest Inc., PA, USA) was used for hydrophobic modification of the valve chamber and the nanochannels. The nanochannels and the valve chamber was washed and replaced with ethanol, acetone, toluene in this order, and ODS/toluene (20% v/v) was introduced for two hours. The valve chamber and the nanochannels were washed with toluene for 30 minutes and ODS/toluene was introduced for another two hours. After washing with toluene again for 30 minutes, the valve chamber and the nanochannels were replaced with acetone, ethanol in this order and finally dried to air. The chip was heated to 70 °C on a hot plate during introduction of ODS/toluene and washing with toluene. Next, the valve was closed and water was introduced into the L-shaped nanochannel. The water was then replaced to $1\mathrm{M}$ NaOH and the nanochannels were treated with NaOH for 15 minutes. Because the valve chamber is hydrophobically modified, the water and NaOH will only be introduced in the L-shaped nanochannel. Thus, hydrophobic modification of the valve chamber was completed.

Gas/liquid switching in nanochannel

The proposed process for switching water in the nanochannel to air is shown in Fig.

3-12. The valve is opened at first and air is flowed into the valve chamber (Fig. 3-12(a)). Because the upstream nanochannel and the valve chamber is hydrophobically modified, the Laplace pressure works in the same direction of the air flow and the valve chamber is filled with air. Next, by maintaining the driving pressure of air, the valve is closed. Using the pressure generated at the moment the valve is closed, the gas/liquid interface pinned at the junction of the nanochannel and the valve chamber is pushed out into the downstream nanochannel (Fig. 3-12(b)). Although the downstream nanochannel is hydrophilic and therefore the Laplace pressure works against the air flow, the Laplace pressure in nanochannels is sufficiently small (~10^1 kPa) that it can be controlled with air pressure. For that reason, the downstream nanochannel can be fully replaced with air by finally opening the valve and introducing air (Fig. 3-12(c)).

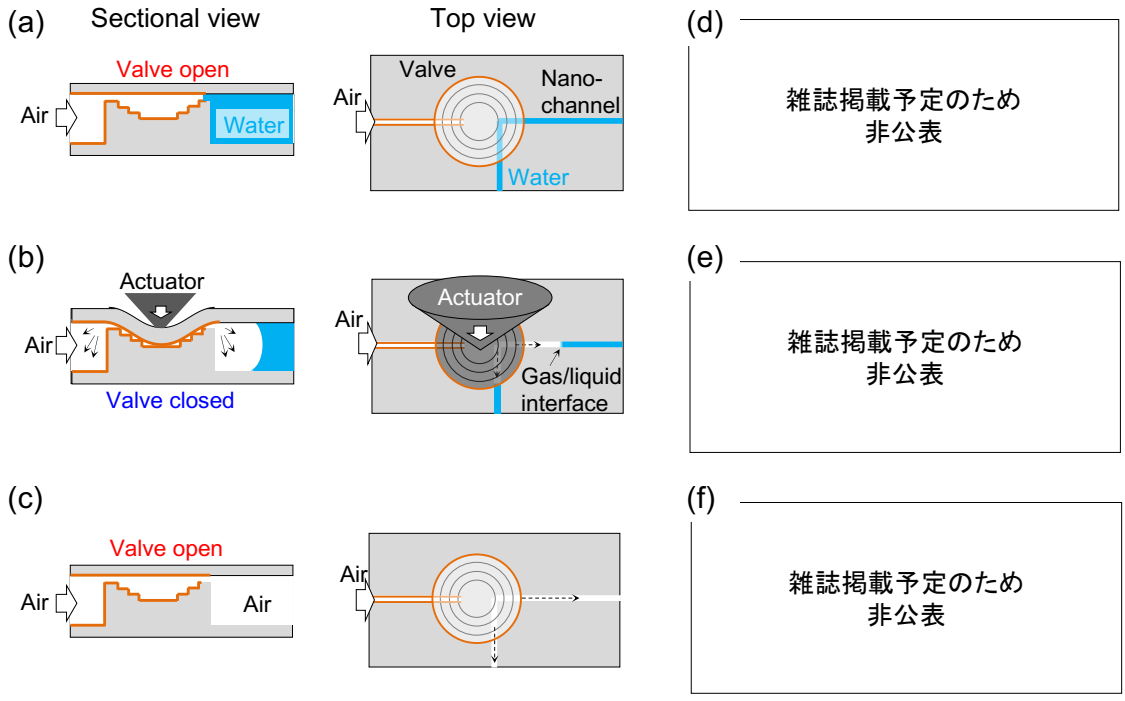

Figure 3-12: (a)–(c) Proposed process of gas/liquid replacing in nanochannel (d)–(f) Microscopic images of the valve chamber and the nanochannels during the replacing process

3.3.3 Results and discussion

Hydrophobic modification of valve chamber

The valve chamber and the nanochannels were observed in a coaxial lighting system using white light emitted from a mercury lamp used in the previous section. Because the transmitted light cannot be observed due to the valve actuating system covering the top of the device, the fluid inside the channels were observed by light scattering. The channels filled with air look bright and white and channels with liquid look dark and rather gray. First, partial modification of the valve chamber and the nanochannels were verified. Water was introduced into the L-shaped nanochannel using capillary force while the valve was kept opened. As shown in Fig. 3-13, water was only introduced in the L-shaped nanochannel and did not enter the valve chamber. From this result, partial hydrophobic modification of the valve chamber was confirmed.

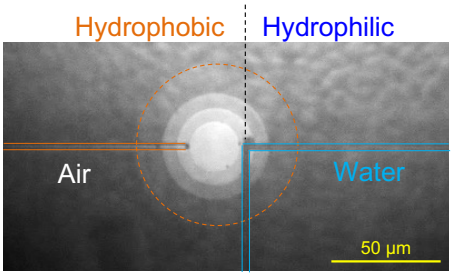

Figure 3-13: Microscopic image of valve chamber after partial hydrophobic modification

Gas/liquid switching in nanochannel

The results of gas/liquid switching is shown in Fig. 3-12 (d)–(f). Water was first introduced in the L-shaped nanochannel with 50 kPa, and then the pressure was cut off. Air was then introduced from the left at the pressure of 500 kPa and filled the valve chamber (Fig. 3-12(d)). At this moment, the gas/liquid interface in the valve chamber could not be pushed out to the downstream nanochannel. This indicates that gas/liquid switching cannot be achieved only with hydrophobic modification. Next, when the valve was closed, the gas/liquid interface instantly moved into the downstream nanochannel (Fig. 3-12(e)). Finally, when the valve was opened and air was continuously introduced with 500 kPa, the nanochannel was replaced with air (Fig. 3-12(f)).

In this way, gas/liquid switching was verified using the open/close valve. Hence, fluid operations that require gas/liquid two-phase system such as reaction/condensation using a gas reagent or isolating liquid samples for volume regulation can be achieved using the open/close valve and the verified switching process.

3.4 Conclusion

In this chapter, fluid operations for analyses using the valve developed in chapter 2 were verified.

In section 3.2, a curved valve chamber was proposed in order to prevent leakage caused by molecular diffusion through the valve chamber and to achieve fluid switching in a single-phase system. To achieve a curved structure that fits the deflection curve of the glass, a fabrication method using plastic deformation of glass was proposed. As a result of repeating the open/close operation for more than 20,000 times against a four-

stepped valve chamber, the steps consequently demolished and a curved valve chamber resembling the shape of the deflection of the glass was obtained. Using this curved valve chamber, the amount of leakage caused by diffusion was evaluated to be under 0.5 %.

In section 3.3, switching water inside the nanochannel into air was performed as a typical example of a fluid operation in a gas/liquid two-phase system. A hydrophobic valve chamber and a valve operation to generate pressure inside the chip was proposed. Using the driving pressure alone, air could not go through the valve chamber. However, additional use of the pressure generated from the valve closing operation could push out the gas/liquid interface into the nanochannel. Thus gas/liquid switching was achieved using the valve.

From the verified fluid operations in this chapter, the valve can be implemented into analytical devices not only to stop and flow reagents but also be used for partitioning reagents, regulating volume of the sample, and even to reactions or sophisticated fluid control using multi-phase flows.

Chapter 4

Fluid control system integrated with nanochannel open/close valves

4.1 Introduction

4.1.1 Background

In chapter 2 and chapter 3, the basic fluid operations using the nano-sized valve was verified. In this chapter, a fluid control system for micro/nano integrated devices with multiple valves integrated is established. Such system requires a reagent injection part, a flow control part, and a detection part. Reagents are set in a vial and introduced in the device through a connected capillary. Therefore, a jig, or a chip holder, is necessary to connect the capillary. For the flow control part, integrated multiple valves will play the role of flow control. Here, several actuators, must be implemented into the system for controlling the valves. In addition, a detector must also be integrated in the same system to carry out nanofluidic analysis. On the other hand, by pressing several parts of the device when operating multiple valves, the device could deflect and affect the open/close state of the valves.

4.1.2 Objective

Considering these requirements and probable subjects, a system that consists of pressure controllers, actuators, and a detector is designed.

In section 4.2, the system was designed based on the boundary conditions set from the limitation of miniaturization of the actuators and the size of the detector. The deformation of the device when multiple valves are actuated was calculated based on strength of materials, and a design to reduce the deformation was proposed.

In section 4.3, open/close operation of the multiple valves using the system was verified.

4.2 Design and establishment of fluid control system

4.2.1 Design

Integration of chip holder, actuators, and detector

The design of the fluidic control system for devices integrated with valves is shown in Fig. 4-1. A chip holder for introducing reagents was firstly designed. The holder clamps the edges of the device and capillaries for introducing reagents can be connected to Teflon screws tightened to the holder.

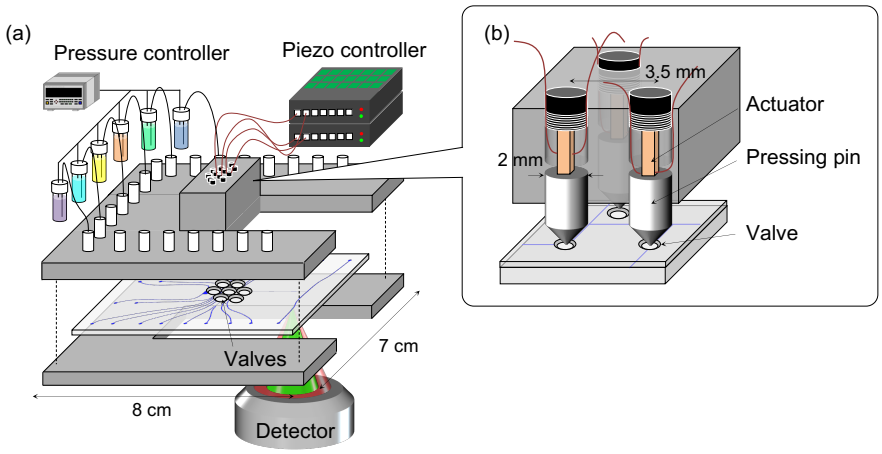

Figure 4-1: Design of fluid control system integrated with actuators and a detector.

For the valve operation, the actuator used in chapters 2 and 3 cannot be applied to this system because the actuator consists of a pressing pin, a force sensor, and micrometers to control the position of the actuator, which makes the total system too large (~10 cm). In order to integrate multiple actuators on a hand-sized device, the force sensor and the micrometers were removed, and a piezoelectric element was fabricated as small as possible. A small piezoelectric actuator with a bottom area of 1.1 mm $\times$ 0.8 mm and a height of 10 mm was purchased from TOKIN Corp., Japan. This actuator is used within the voltage range 0 to 150 V and the maximum displacement is 9.1 μm . The actuator was then attached to a stainless pressing pin with a diameter of 2 mm by inserting the actuator

into a hole fabricated on the pressing pin. Each pressing pin was arrayed through a hole (hereinafter called "actuator holes") fabricated directly on the chip holder. In order to densely array the actuators, the holes fabricated on the chip holder must be dense as well. However, due to the machining limits to maintain the shape of each holes, the thickness of the stainless remaining between each holes must be larger than 1.5 mm. For this reason, the actuator holes were placed in a distance of 3.5 mm from each other (Fig. 4-1(b)). A pressing pin attached to a piezoelectric actuator is set to each hole and the actuator is sealed with a screw from the top. When voltage is applied to the piezoelectric element, the actuator is displaced in the vertical direction, which makes the pin press the valve deformation part (Fig. 4-2). On the other hand, the chip holder combined with actuators must be compatible with the detection system. In general, an optical detection systems consist of an objective lenses observing the detection area. Therefore, the size and the position of the actuator holes was determined considering the occupied space by the objective lens (~cm). As a result, up to 12 actuators could be integrated with the system.

Alignment of actuators and valve chambers

In order to operate the valves with the actuators based on the design explained above, alignment of the actuators and the valve chamber is essential. There are three technical subjects to complete the alignment: (1) Determining the coordinates of the valve chambers, (2) Adjusting the XYθ position of the actuators, and (3) Adjusting the Z position of the actuators.

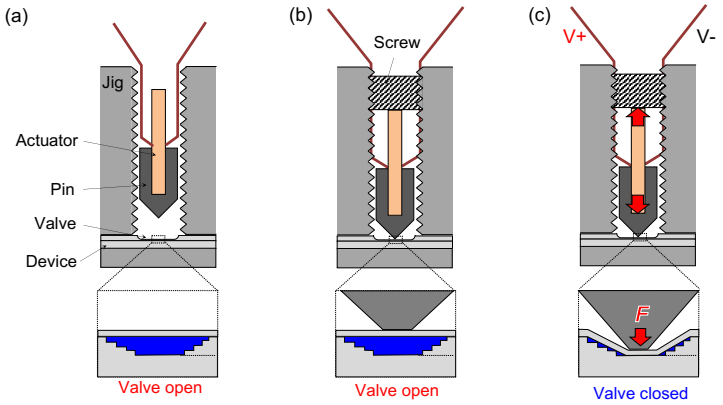

Figure 4-2: Valve open/close scheme using a miniaturized actuator. (a) A stainless pressing pin was attached to the actuator was attached to the actuator. (b) The actuator was fixed with a screw from the top and tightened until it makes contact with the valve. (c) Voltage is applied to the actuator and the valve is closed.

(1) Determining the coordinates of the valve chambers

Although the valve chambers and the actuator holes are designed at the same position, a position error is inevitable in the actual fabricated system due to the precision of fabrication. The actuator holes, fabricated by machining, are positioned with a precision around 10^2 μm . On the other hand, the valve chambers, fabricated by top-down nano-fabrication, are positioned with a precision around ~μm. Therefore, by obtaining the coordinates of the fabricated actuator holes beforehand and then determining the coordinates of the valve chambers, the relative coordinates of the valve chambers and the actuator holes are arranged while the alignment error can be theoretically kept within ~ μm . The experiment setup and results to obtain the coordinates of the actuator holes are described in the Appendix section A.4.

(2) Adjusting the XYθ position of the actuators

After arranging the coordinates of the valve chambers and the actuator holes, the device implemented with valves is set to the lower jig and the actuators are set through

the actuator holes on the upper jig. The lower and upper jigs are then combined to fix the device and the actuator. Here, the mechanical tolerance and human error when combining the jigs will result in a positioning error. To address this subject, a system to align the actuators and the valves is required. Because the relative position of the actuators and the valves are determined after (1), controlling the XY position and the angle of the top jig that holds all the actuators is sufficient. An alignment system to achieve such a process was established as shown in Fig. 4-3. The device is first set to the lower jig using screws on the sides and then the jig is fixed onto the stage of the system. Next, the top jig with actuators is clamped by an arm that can control its XY position and its angle in the XY plane. The valves and the actuators are observed from below by a microscope. Using this system, the actuators and the valves can be aligned within the presicion of ~1 μm , and the tolerable alignment error (< 20 μm) obtained in section 2.4.2 can be achieved. When the alignment is completed, the top and bottom jig is combined, and the position of the actuators are fixed.

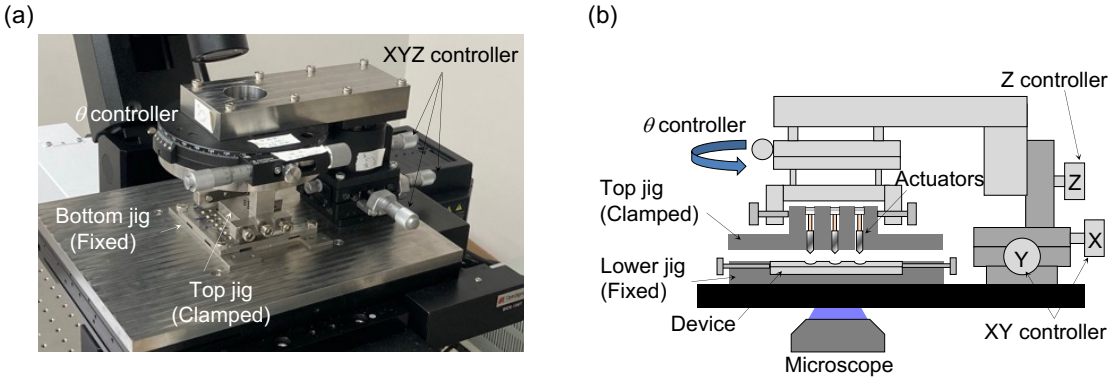

Figure 4-3: (a) The system established for alignment of actuators and valves. (b) Schematic side view of the alignment system.

(3) Adjusting the Z position of the actuators

Finally, the Z position of the actuators must be adjusted to make sure the displacement of the piezo-driven actuators is conveyed to open/close the valves. The open/close operation process is as follows. The actuators are set in the actuator holes and by tightening a screw from above, the Z position of the actuators are lowered until it makes contact with the valves. After contact, 100 V is applied to the actuator to close the valve and the voltage is turned off to open the valve. During this process, the backlash of the screw would be a factor to cause an error in the Z position. A backlash is a small space (~10^1 μm) intendedly made between the male thread and the female thread. Backlash is essential for threads to be tightened smoothly by reducing the friction. However, in the case of fixing the actuators to apply deformation to the valve, it may take up the displacement of the actuator and few displacement is applied to the valve. In order to investigate the effect of backlash, an actuating procedure that could eliminate the effect of backlash was proposed. First, voltage is applied to the actuators and the screws were tightened until the valve is fully closed. At this point, the actuator is pressurized backwards from the closed valve, so the backlash is already absorbed in the displacement of the actuator (Fig. 4-4(a)). Next, the voltage is turned off and the valve opens. The results using this process and the initial process is shown in Fig. 4-4(b). This result implies that the backlash of the screw causes an error in the Z position, and that the proposed process is a reasonable way to overcome this subject. In this way, the Z position of the actuators were adjusted. There are other possible factors that could cause an error in the Z position such as the tilt of pressing pin, the tilt of actuators, and the actuator pushing the screw back. The effect caused by these factors were also investigated, which is described in the appendix section A.5.

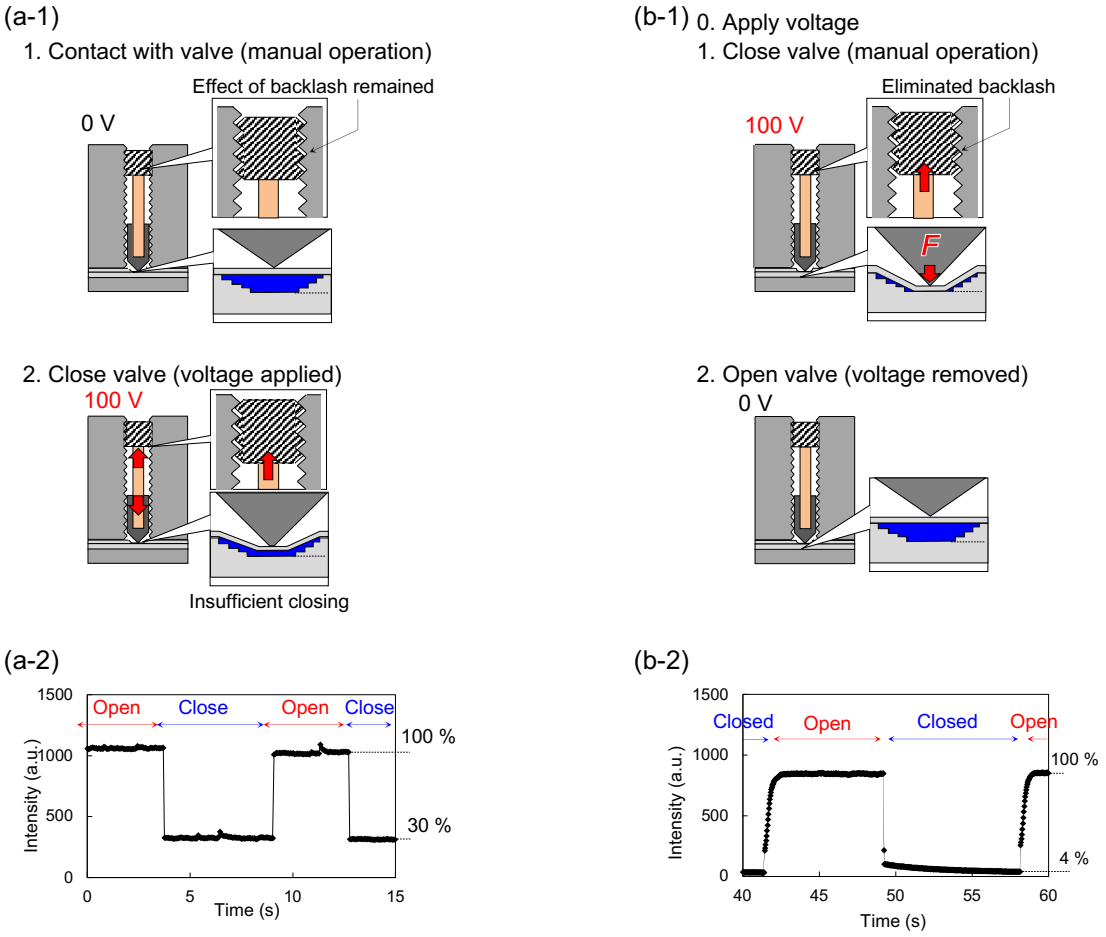

Figure 4-4: (a-1) The initial process for valve open/close operation (a-2) Fluorescence intensity of the valve chamber during the initial open/close process (b-1) The newly proposed process for valve open/close operation (b-2) Fluorescence intensity of the valve chamber during the new open/close process

Calculation of device displacement

When a detector is integrated as described in the previous section, an area of 34 mm×51 mm becomes an opening space with no support of the jig (Fig. 4-1). This is a normal situation in the chip holders used in general micro-/nanofluidic devices without valves, but when a load is applied to the device for valve operation, the deformation of the total device could be a problem. For example, deformation produced by a single valve actuation can affect the open/close state of other valves or change the focal point of the detector and affect the detection efficiency. The distribution of the deformation was

calculated by finite element method (Fig. 4-5).

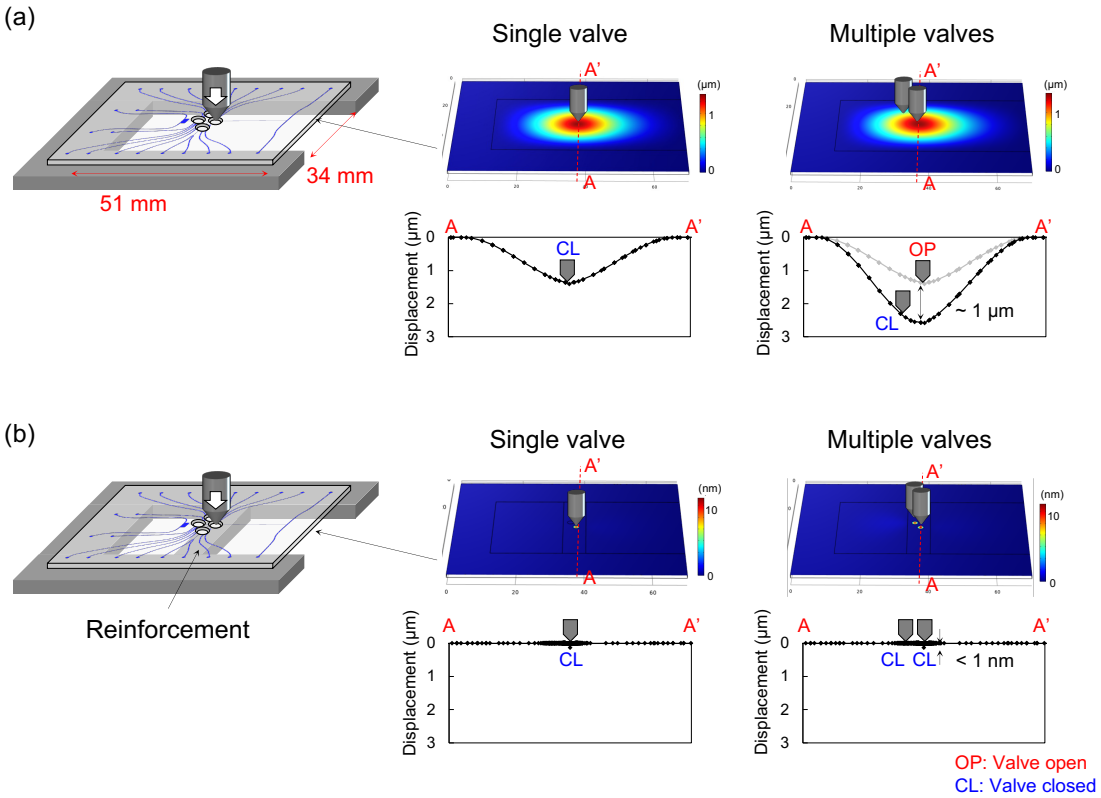

Figure 4-5: Calculation of device displacement when one and two valves are pressed. (a) Jig without reinforcement (b) Jig with reinforcement

During this calculation, the displacement of the areas that are supported by the chip holder was set to zero. When a single valve was closed, the maximum displacement of the device was calculated to be 1.2 μm . When another valve was pressed, the device was deformed even more. The displacement itself is not a problem when only one valve is actuated, but when multiple valves are actuated, the displacement will affect the opening/closing of other valves. At the position of the first valve, the device was additionally deformed by 1 μm , which is greater than the valve depth (Fig. 4-5(a)). This means that the closed valve will open when another valve is pressed.

To address this subject, a reinforcement set below the valve area was proposed. The

reinforcement area was designed so that is prevents deformation of the total device when a valve is actuated and that its size and position does not interfere with the detection system. The effect of the reinforcement was estimated as well. The additional displacement of the device when the second valve was actuated was less than 1 nm. This could be considered sufficiently small to control open/close states of multiple valves independently.

4.2.2 Establishment of system

Established system

The established system is shown in Fig. 4-6. Pneumatic pumps for fluid introduction are connected to the vials containing the reagents. A reinforcement part is incorporated in the chip holder where the valves are positioned. The fluid operation is carried out by controlling the open/close state of the valves, and the operation is confirmed with observation by a microscope. For detection, the jig is moved to the stage of the DIC-TLM.

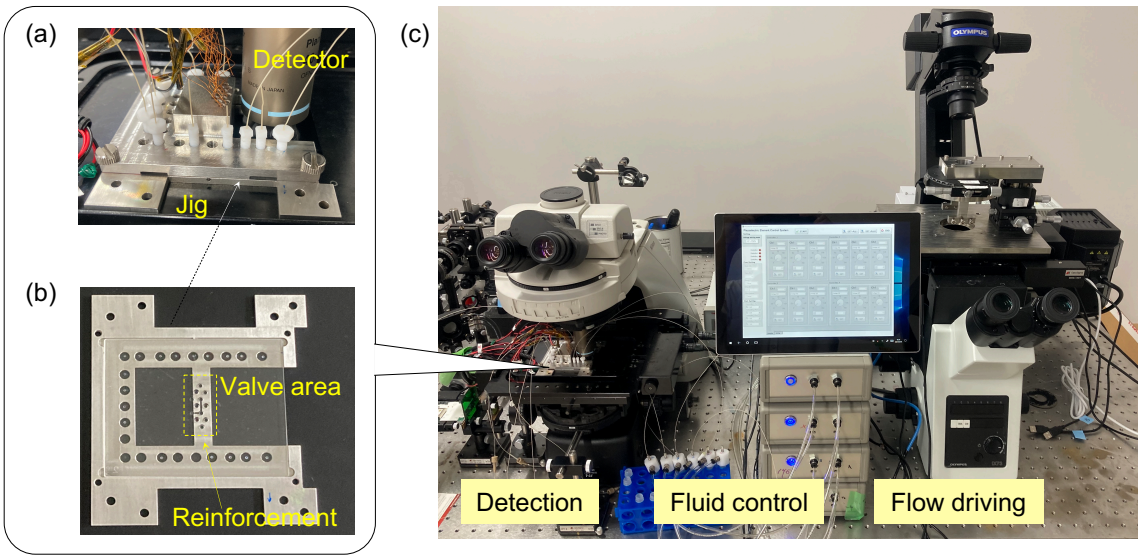

Figure 4-6: (a) Fabricated jig integrated with a detector. (b) Lower jig with a reinforcement part around the valve area. (c) Total image of the established system.

4.3 Verification of fluid control system

4.3.1 Verification of open/close operation of multiple valves

Operation of two valves

With the established fluid control system, open/close operation of two valves was verified. The results are shown in Fig. 4-7. Valve B was closed at first, and then valve A was repeatedly opened and closed. During this operation, valve B remained closed. Therefore, it was verified that open/close operation of one valve does not affect other valves.

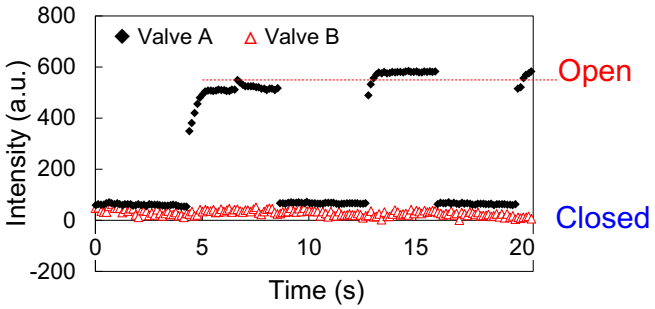

Figure 4-7: Fluorescence intensity of two valve chambers. During the open/close operation of valve A, the closed state of valve B was maintained.

Injection operation using valves for chromatography

As a simple demonstration of a fluid operation using multiple valves, the injection process of a sample in nanofluidic chromatography was verified. The injection process in general chromatography consist of two steps: Loading the sample and transporting the sample to the separation channel. This switching process could be achieved using valves as follows (Fig. 4-8). Valve A, which controls the flow of the eluent, is at first closed. When valve B, which controls the flow of the sample, is opened for a certain time τ, the sample is loaded into the nanochannel. Finally, by opening valve A at the moment valve

B is closed, the loaded sample would be injected into the separation channel. For the experiment, PBS and 100 μM Alexa Fluor^{TM}488 solution were used as model reagents for the eluent and the sample respectively and τ was set to $\tau = 1$ s.

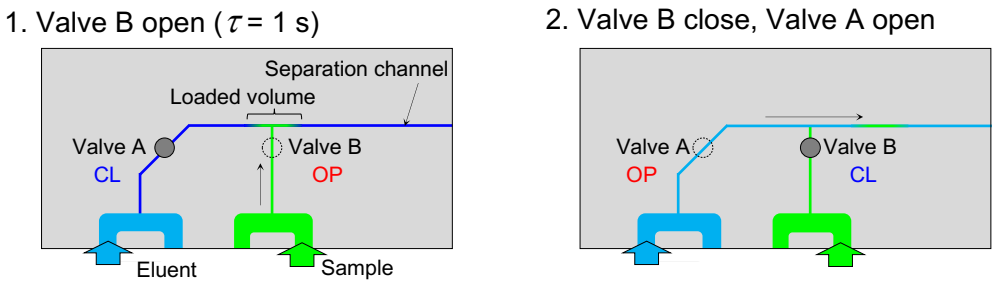

Figure 4-8: Valve operation for sample injection into separation channel

The results are shown in Fig. 4-9. The device was successfully fabricated (Fig. 4-9(a)). The nanochannels were 5 μm wide and 2 μm deep. Using this device, fluorescence solution and PBS was flowed into the device from a single pressure source. That is, the flows were controlled only by valves A and B. When valve A was closed and valve B was opened for loading fluorescence solution, the loaded fluorescence band spread to the downstream of the separation nanochannel. This indicates that valve A, which is placed at the upstream of the nanochannel, has stopped the flow of PBS. When valve B was closed and valve A was opened, the flow was switched to the eluent flow within less than 0.25 s and the loaded fluorescence was transported downstream (Fig. 4-9(b)). In order to investigate the reproducibility of this injection system, the total process (loading fluorescence for $\tau = 1$ s and switching to the flow of PBS for 5 s) was repeated 10 times. The fluorescence intensity was measured at 600 μm downstream of the loading point. Figure 4-9(c) represents the results. The relative standard deviation (RSD) of the 10 peak areas was 1.6 %. In general chromatography, the minimal requirement of the RSD of the peak area for quantification is considered to be less than 5 %.[76] Furthermore, the RSD

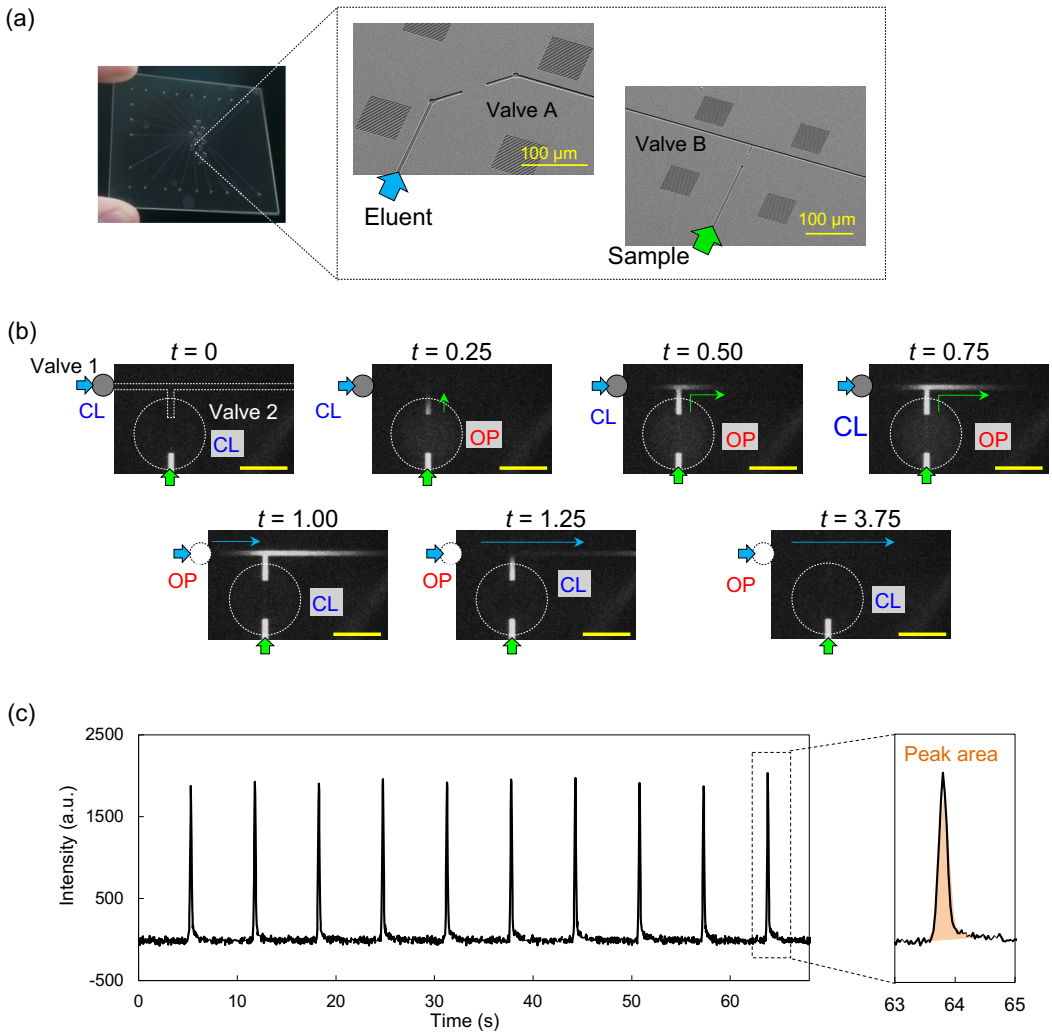

Figure 4-9: (a) Image of the fabricated device and SEM image of the fabricated nanochannels and valves (b) Fluorescence image of valve B during the injection process (c) Fluorescence intensity measured at 600 μm downstream from the loading point.

of the peak area achieved in injection systems developed in microfluidics are mostly 3 % or more.[77–81] Therefore, the injection performance achieved here was relatively higher than other reports. This could be explained by the quick and promising flow control by the open/close valves. Thus, the injection process for nanofluidic chromatography was verified as a precise and robust fluid operation using multiple valves.

4.4 Conclusion

In this chapter, a fluid control system for a nanofluidic device integrated with valves was established. The structure of the system was designed based on the limitation of the size of the actuators and the detector. In order to incorporate actuators at the highest density, a chip holder that is combined with an actuator holder was designed, and to integrate a detector, an opening space for the objective lens was created. Furthermore, the effect of deformation of the total device caused by the opening space and the operation of the valves was considered. By creating a reinforcement in a minimum area around the valves, the deformation was sufficiently reduced. Thus, the fluid control system was established and the basic function of the system to independently operate multiple valves was verified. In addition, a sample injection process assuming nanofluidic chromatography was verified as an example of fluid control in nanofluidic analyses. As a result, a quick response and a robust fluid control with a high reproducibility was achieved.

Chapter 5

Application to femto-liter analyses

5.1 Introduction

5.1.1 Background

In this chapter, the valve developed in chapter 2 and chapter 3, and the fluid control system established in chapter 4 is applied to femto-liter analysis.

In the current analytical devices handling fL sample volume such as single molecule ELISA,[36] nanofluidic chromatography,[34] single cell protein analysis[82], various reagents are used and several fluid operations are required. Since the fluid in nanofluidic devices are controlled by external pressure, even the simplest fluid operations such as introducing/switching reagents and regulating volume of reagents require precise but instable control at all channels. Accordingly, the complex process could only be achieved by highly skilled technicians. Here, using the valve developed in the previous chapters would change the fluid operation to an easier and more stable operation.

5.1.2 Objective

Herein, valves were implemented on a device for single-cell protein analysis and fluid operations to perform immunoassay in fL space was verified. First, the device is designed based on our integration concept of MUO/NUOs. Next, the device is fabricated and the fluid operations were verified. Finally, IL-6 in standard solution is detected by ELISA and the performance of the device integrated with valves is discussed.

5.2 Design of the device

5.2.1 MUO/NUOs in single-cell analysis

The device was designed based on the methodology of MUO/NUOs. The left column in Fig. 5-1 shows the chemical processes in single-cell protein analysis. The process is divided into a total of 11 unit operations, and each of these were converted into MUOs and NUOs as shown in the middle column in Fig. 5-1. In order to connect each MUO/NUOs by controlling the fluid, a total of seven valves were designed on the device. The design of the device is illustrated in the right column in Fig. 5-1. A total of four kinds of surface is prepared in the channels. In order to isolate a single cell during stimulation, the cell chamber is kept hydrophilic while the microchannel connected to the cell chamber is hydrophobically modified. The surface of the nanochannel where ELISA is performed (hereinafter called "ELISA channel"), has a region where antibodies to capture the analyte is immobilized and other regions in the ELISA channel are modified with polyethyleneglycol (PEG) to prevent non-specific adsorption of proteins.

5.2.2 Design of fluidic channels

Size of microchannels, nanochannels, cell chamber, and pipette

The microchannels are 400 μm wide and 20 μm deep, and the nanochannels are 3 μm wide and 1.2 μm deep. The size of the cell chamber (75 μm in diameter, 20 μm deep, 88 pL volume) and the pipette (25 pL volume) between valves 2 and 3 was determined based on the performance achieved in the previous work.[82]

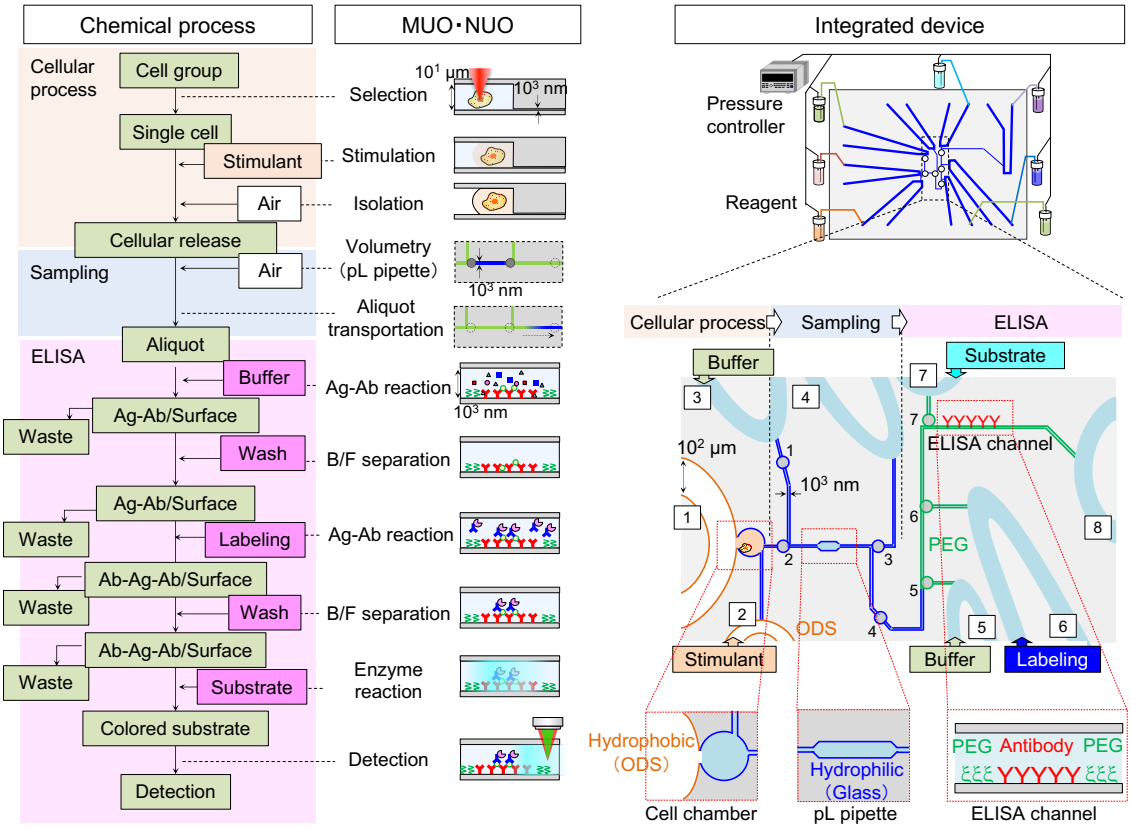

Figure 5-1: Concept of integrating chemical processes of single-cell analysis into a micro/nano integrated device.

Fluid operations for ELISA using valves

The fluid operations during the ELISA process is carried out as follows.

(1) Sample introduction

The sample is introduced from microchannel 1. During this process, valves 1 and 4 are closed and the sample flows through valves 2 and 3 and to the drain. Valves 5, 6, 7 are also closed in order not to release reagents into the ELISA channel (Fig. 5-2(1)).

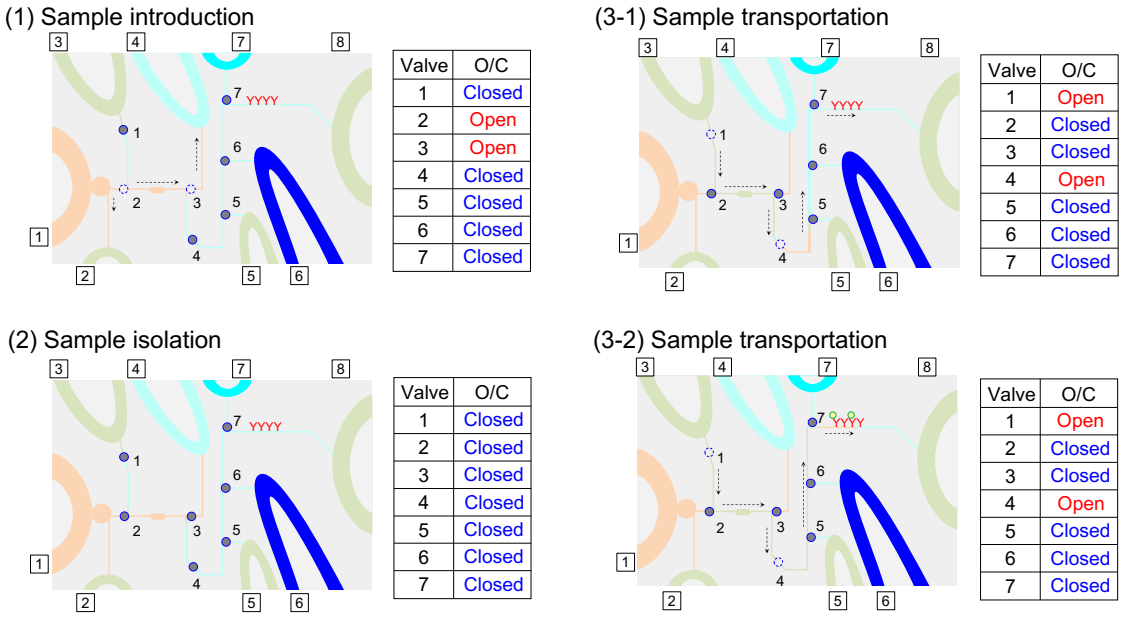

Valve	O/C
1	Closed
2	Open
3	Open
4	Closed
5	Closed
6	Closed
7	Closed

Valve	O/C
1	Open
2	Closed
3	Closed
4	Open
5	Closed
6	Closed
7	Closed

Valve	O/C
1	Closed
2	Closed
3	Closed
4	Closed
5	Closed
6	Closed
7	Closed

Valve	O/C
1	Open
2	Closed
3	Closed
4	Open
5	Closed
6	Closed
7	Closed

Figure 5-2: The fluid operations designed in the ELISA process. (1) Sample introducing (2) Sample isolation (3) Sample transportation

(2) Sample isolation

After the pipette is filled, valves 2 and 3 are closed. At this moment, the sample volume injected is determined as the sample isolated between valves 1, 2, 3, and 4 (Fig. 5-2(2)).

(3) Sample transportation

Next, valves 1 and 4 are opened and the isolated sample is transported to the ELISA channel using the flow of washing buffer from microchannel 3 (Fig. 5-2(3-1)(3-2)).

(4)–(7) B/F separation, labeling, enzyme reaction, and detection

The ELISA channel is then washed with washing buffer (B/F separation) by opening valve 5 for 5 minutes. The washing buffer consists of 2 wt% BSA, 0.05 % Tween 20, and 10 mM PBS. After B/F separation, valve 5 is closed and valve 6 is opened to introduce 10 nM HRP-labeled antibody solution into the ELISA channel for three

minutes. Valve 6 is closed and the ELISA channel is washed again with washing buffer from microchannel 8 for five minutes. Then, valve 7 is opened to introduce tetramethylbenzidine (TMB). After introducing TMB solution for two minutes, the flow is stopped for 90 seconds for enzyme reaction by closing valve 7. Finally, valve 7 is opened and the flow in the ELISA channels is regenerated. The colored substrate is detected at the downstream using DIC-TLM.

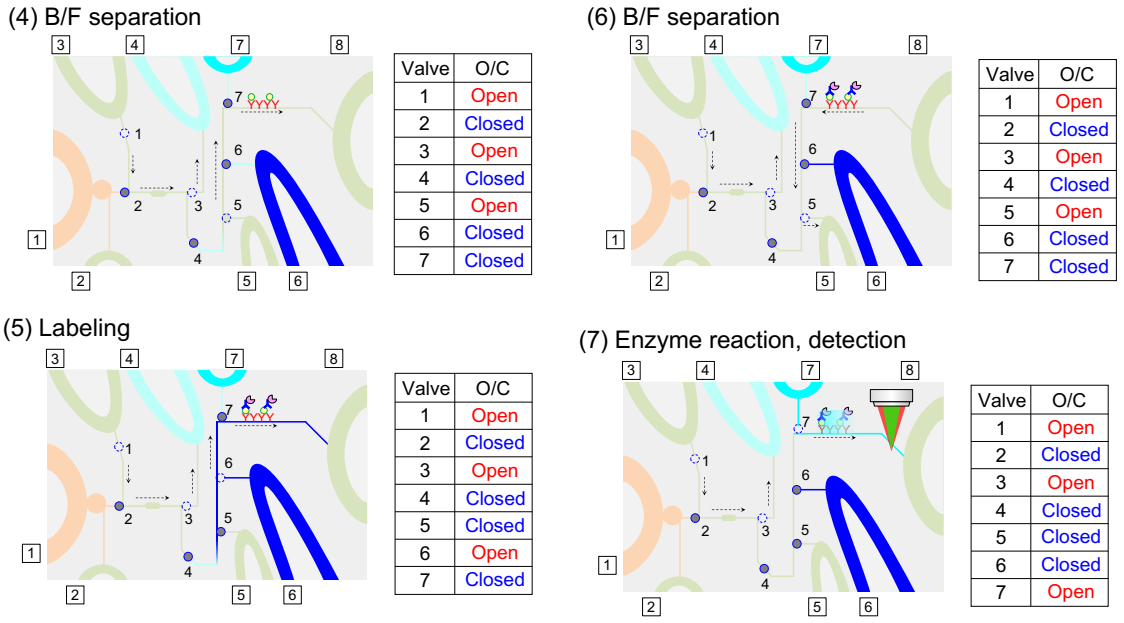

Valve	O/C
1	Open
2	Closed
3	Open
4	Closed
5	Open
6	Closed
7	Closed

Valve	O/C
1	Open
2	Closed
3	Open
4	Closed
5	Open
6	Closed
7	Closed

Valve	O/C
1	Open
2	Closed
3	Open
4	Closed
5	Closed
6	Open
7	Closed

Valve	O/C
1	Open
2	Closed
3	Open
4	Closed
5	Closed
6	Closed
7	Open

Figure 5-3: The fluid operations designed in the ELISA process. (4) B/F separation (5) Labeling the captured antigen (6) B/F separation (7) Enzyme reaction between HRP and TMB followed by detection with DIC-TLM

5.3 Experiment

5.3.1 Device fabrication

Fabrication of nanochannels, valves, and microchannels

The device was fabricated in the same way as in chapters 2 and 3 using EB lithography, photolithography and dry etching. After fabricating the nanochannels, valves, and

the microchannels, the ELISA channel was modified with aminopropyltetraethylsilane (APTES) for immobilizing capture antibodies afterwards. The details of this process is explained in the appendix section. The substrates were bonded under a condition of 5000 N, 110 °C for three hours.

Among the seven valves designed on the device, valves 5, 6, and 7 are closed for a long term preventing leakage from each reagent introduced at microchannels 5, 6, and 7 respectively. As revealed in chapter 3, the property of the valve to prevent solute leakage caused by molecular diffusion can be improved by repeated pressing of the valve. Since leakage of HRP antibody and TMB into the ELISA channels will cause a critical effect on the analysis, valves 6 and 7 were repeatedly pressed 20,000 times in order to curve the valve chamber and reduce leakage.

Modification of fluidic channels

After the substrates were bonded, the surface of the channels were modified in the following procedure. The chemical materials and protocol used here are similar to our previous report with minor modification.[82]

(1) PEG modification in ELISA channel

PEG was modified by flowing PEG silanization reagent in the nanochannel (Fig. 5-4). First, all the microchannels and nanochannels were filled with ethanol. A powder of trimethoxysilane-PEG (MW=5,000, NANOCS, NY, USA) was dissolved in water/ethanol (5/95) at the concentration of 0.1 wt%. After the channels were filled with ethanol, valve 4 was closed to partition the ELISA region and the sampling region. Next, PEG solution was introduced into the ELISA nanochannel from

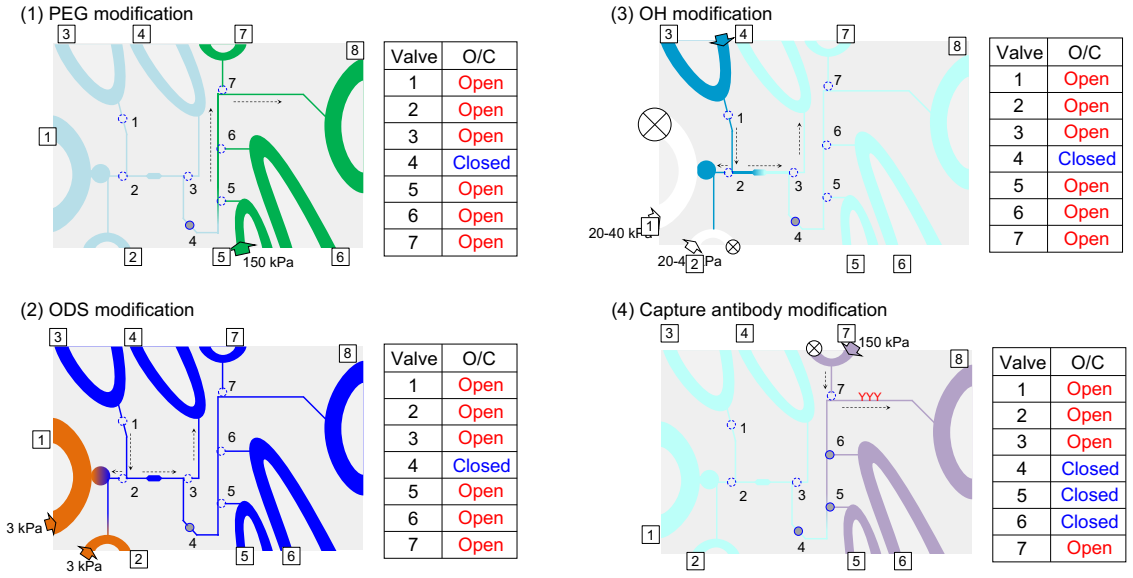

Valve	O/C
1	Open
2	Open
3	Open
4	Closed
5	Open
6	Open
7	Open

Valve	O/C
1	Open
2	Open
3	Open
4	Closed
5	Open
6	Open
7	Open

Valve	O/C
1	Open
2	Open
3	Open
4	Closed
5	Open
6	Open
7	Open

Valve	O/C
1	Open
2	Open
3	Open
4	Closed
5	Closed
6	Closed
7	Open

Figure 5-4: (1) Modification of PEG in ELISA channel (2) ODS modification of microchannels 1 and 2 (3) Silanization of cell chamber (4) Immobilization of capture antibody in ELISA channel

microchannel 8 at 150 kPa for 45 minutes. During this procedure, a mild flow of ethanol was formed in the other microchannels. The pressure at microchannel 8 was switched off and PEG solution was then introduced from microchannel 5 at 150 kPa for modification of another 45 minutes. After modification, the microchannels and the nanochannels were washed with ethanol for 15 min at 30–150 kPa.

(2) ODS modification in microchannels

The surface of microchannels 1 and 2 were modified with hydrophobic molecules (octadecylsilane) as described in a previous report.[82] The microchannels and nanochannels were first replaced from ethanol to acetone, toluene in this order. ODS-DEA was diluted in toluene at 20 % (v/v) and flowed into microchannels 1 and 2 at 20 kPa. After the microchannels were replaced with ODS, the pressure was lowered to 3 kPa. A back pressure of 40 kPa was applied from microchannel 3 generating a flow in the direction from valve 2 to the cell chamber to prevent ODS molecules

entering the pipette region. The modification was carried out at 70 °C for 2 hours. Then, microchannels 1 and 2 were washed with toluene, acetone, ethanol, water in this order and dried with air.

(3) OH modification in cell chamber

After all microchannels and nanochannels were replaced to water, valve 4 was closed and 1 M sodium hydroxide (NaOH solution) was introduced from microchannel 3 so that NaOH solution does not reach the APTES modified region. Water in microchannels 1 and 2 were replaced with air. Once the NaOH solution filled the cell chamber, the interface of NaOH solution and air was controlled by adjusting the pressure of air at microchannels 1 and 2. NaOH solution was pumped in and out so that fresh NaOH solution was provided. The modification time was 15 minutes. After the modification, valve 4 was opened and all the channels were washed with water.

(4) Immobilization of capture antibody in ELISA channel

Next, capture antibody was immobilized on the surface of the ELISA channel as shown in Fig. 5-4(4). Valve 4 was closed and all the solutions were introduced into the nanochannel from microchannel 8 and 9. 2.5 % glutaraldehyde in borate buffer pH 7.2 was introduced into nanochannel from microchannel 8 at 150 kPa for 1 hour. After washing the nanochannel with water for 10 minutes, 25 μg/mL anti-IL-6 antibody (MAB206-500, clone 6708, R& D systems, Inc., MN, USA) in PBS was introduced from microchannel 7 at 150 kPa for 1 hour with the outlet of microchannel closed. After washing the nanochannels with PBS for 10 minutes, 0.5 M ethanolamine was introduced at 100 kPa for 10 minutes. This is for endcapping

of the unreacted reaction sites of glutaraldehyde. Then, 2 wt% BSA (Bovine Serum Albumin) in PBS was introduced at 150 kPa for 30 min for blocking of the surface of nanochannels and the valves. All the modification steps here were conducted in room temperature.

5.4 Results

5.4.1 Fabricated device

The fabricated device is shown in Fig. 5-5. On a 70 mm × 60 mm fused silica substrate, microchannels, nanochannels and seven valves were successfully fabricated as designed.

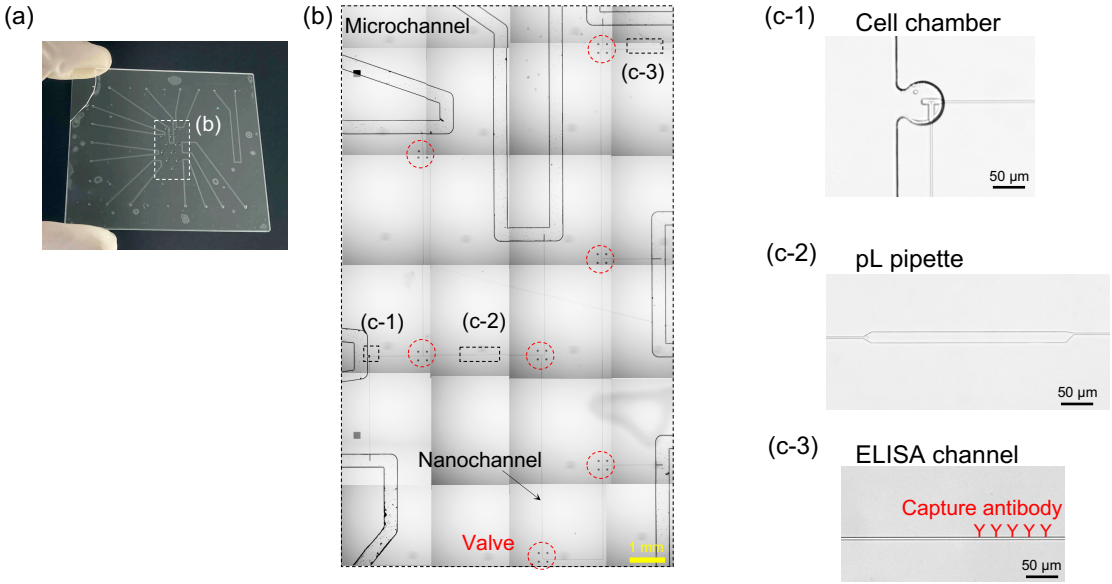

Figure 5-5: Image of the fabricated device. (a) Total device (size: 60 mm× 70 mm) (b) Microscopic image of the microchannels and the nanochannels (c) Microscopic image of the cell chamber, the pico-liter pipette ,and the ELISA channel.

5.4.2 Performance of ELISA

Confirmation of fluid operations

Seven actuators were set to the actuator holes on the jig, corresponding to the position of the fabricated valves 1–7. Each actuators were aligned to the valve chambers using the alignment system developed in chapter 4. Here, the fluid operations beginning from the injection of the sample to the detection of the colored substrates are described.

(1) Sample loading

Valves 4, 5, 6, and 7 were closed at the initial state, and wash buffer was flowed in at 120 kPa from microchannel 3. The sample was introduced from microchannel 1 at 20 kPa. For the experiment of blank sample, Alexa Fluor^{TM}488 was mixed in the sample in order to confirm the fluid control (Concentration; 50 μM). After the microchannel was replaced with the sample, the exit was closed and the pressure was raised to 40 kPa. At the same time, a back pressure of 50 kPa was applied from microchannel 2. At this moment, the flow from microchannel 3 is dominant and the sample could not enter the pipette. When valve 1 was closed and the flow from microchannel 3 was stopped, the sample was introduced into the pipette and flowing out to the drain (Fig. 5-6(1)). The time for filling the pipette was two minutes.

(2) Sample volumetry and transport

The introduced sample was isolated by additionally closing valves 2 and 3 (Fig. 5-6(2)). At the same time, valves 1 and 4 were opened and a flow to the ELISA channel was generated. Here, it was observed that the sample was partitioned at valve 2 and the aliquot inside the pipette was flowed to the downstream (Fig. 5-6(3-1)(3-2)). The transported aliquot was confirmed by fluorescence observation at two

points in the downstream; before valve 5 and at the antibody immobilized region. As shown in Fig. 5-7(3-3) and (3-4), the sample was successfully transported to the ELISA channel.

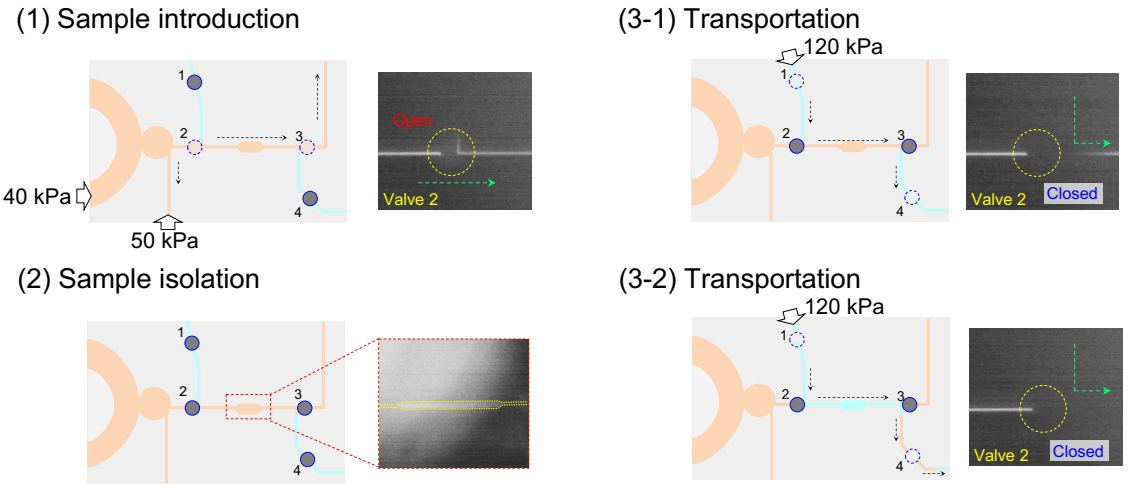

Figure 5-6: Fluid operations and fluorescence images during the actual operation. (1) Sample introduction (2) Sample isolation (3-1)(3-2) Sample transportation

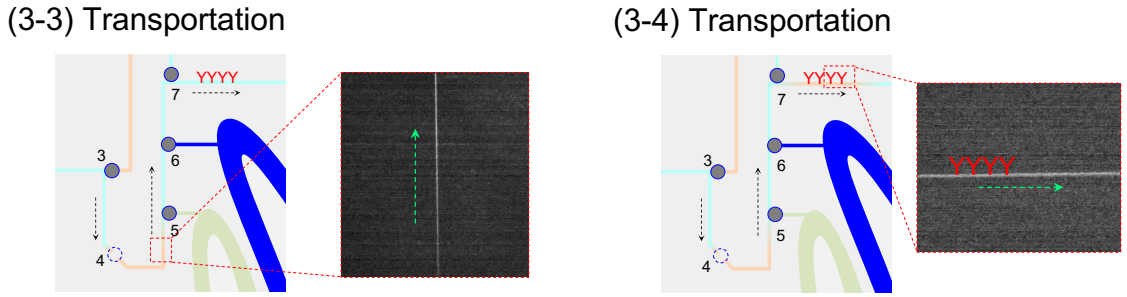

Figure 5-7: Fluid operations and fluorescence images during transportation of the aliquot. (3-3) Transportation image before valve 5 (3-4) Transportation image at ELISA channel

(4)–(7) B/F separation, labeling, enzyme reaction, and detection

After confirmation of the aliquot transportation, the device was set to the stage of the detector (DIC-TLM) so the fluid operations could not be observed.

Valve 4 was closed and the ELISA channel was washed with washing buffer by opening valve 5 for 5 minutes. The washing buffer was flowed at 200 kPa. Then

valve 5 was closed and valve 6 was opened to introduce HRP-labeled antibody solution at 200 kPa into the ELISA channel for three minutes. Valve 6 was then closed and the ELISA channel was washed again with washing buffer from microchannel 8 at 200 kPa for five minutes in the direction to microchannel 5. After washing, valve 7 is opened to introduce TMB solution. TMB was introduced at 200 kPa for two minutes, and valve 7 was closed to stop the flow for 90 seconds. Finally, valve 7 is opened again to regenerate the flow in the ELISA channels and the colored substrates were detected by DIC-TLM. The total operation was performed for a blank sample (0 M) and a standard solution of 100 pM IL-6. The detected signal is shown in Fig. 5-8.

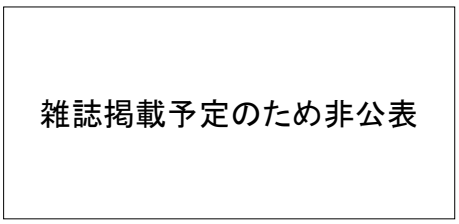

Figure 5-8: Obtained ELISA signals from 100 pM IL-6 standard solution and the blank solution.

5.5 Discussion

The flow velocity in the ELISA channels was measured to determine the arrival time of the signal from the antibody immobilized region (velocity; 315 μm/s). Considering the distance between the detection point and the antibody immobilized region (16.9 –19.9 mm), the arrival time is estimated to be in the range of 53.6–63.1 s in Fig. 5-8, which is indicated as a purple area. Therefore, among the two peaks detected in Fig. 5-8, the latter peak is assumed to be the peak derived from the analytes specifically captured by

the antibodies. On the other hand, the former peak is assumed to be a peak derived from non-specific adsorption in the ELISA channel. The peak areas of specific signal peaks were calculated with a peak fitting software (Igor, WaveMetrics, Inc., OR, USA), and the sum of the peak areas was defined as "ELISA signal." From the concentration of the standard solution (100 pM) and the volume transported to the ELISA channel (25 pL), the obtained ELISA signal derives from 1500 molecules, or 2.5 zmol. Consequently, femto-liter analysis utilizing a valve-implemented micro/nano fluidic device was successfully operated for the first time.

Compared to the conventional analytical system, which requires high skill and experience in order to control several pressure values at once and to adjust and maintain the pressure balance at all channels, the system developed in this study requires only a simple open/close operation of two valves for each fluid operations. Since fluid control based on open/close valves is digital, that is, the flow is either "stopped" or "released," it is also possible to control the system automatically in the future. As a result, this will realize an analytical system that can be operated not only by highly-skilled technicians but by all users. Moreover, the valve system is essential for micro-/nanofluidics in order to realize sophisticated analyses. Single-cell proteomics is an example of such analyses, which consists of various components such as a picoliter reactor for protein digestion,[83] nanofludic chromatography column for separation,[34] a droplet shooter for connection to a mass spectrometer,[84] *etc.* Although each unit operations were verified in the previous work, it was impossible to carry out the fluid operations by conventional pressure control when the unit operations were integrated. Thus, the development of the valve and the established system is a fundamental and essential technology to realize such sophisticated analyses.

5.6 Conclusion

In this chapter, a device for single cell protein analysis integrated with valves was fabricated and the fluid operations to perform ELISA was verified. First, the required fluid operations and position of the nanochannels and the valves were designed based on our methodology of MUO/NUOs. Next, the device was fabricated and modification of the channels to obtain four kinds of channel surfaces; hydrophobic (ODS), hydrophilic (OH), PEG, and capture antibody was carried out. Then, fluid operations to perform ELISA was conducted using the valves. Fluid operations of sample introduction, sample volumetry, transportation of the aliquot, and switching flows of reagents were successfully achieved by simple opening/closing of the valves. As a result, 1500 molecules (2.5 zmol) from the standard solution was detected. From these results, a nanofluidic analytical system using a valve-implemented micro/nano fluidic device was successfully operated for the first time.

Chapter 6

Conclusion

6.1 Conclusion

In this thesis, a nanochannel open/close valve for femto-liter analyses was developed. Our group has established the concept of MUO/NUOs, and integrated various chemical processes into a micro-/nano integrated fluidic device. Such a device can not only realize rapid and highly efficient chemical reactions but handle samples of ultra-small volume (aL–fL), and recently, quantification of cytokine molecules secreted from a single B cell was realized. Although micro-/nano integrated fluidic devices had the potential to achieve such novel analyses, the fluid control was extremely difficult. For this reason, there were problems such as low reproducibility and difficulty of further integration of chemical processes. To address these problems, development and implementation of a valve applicable to nanofluidics was conceived.

In chapter 2, the basic design of a nanochannel open/close valve utilizing glass deformation was proposed based on the strength of materials and fluid engineering. In order to achieve sufficient fluid resistance when the valve is closed, a four-stepped structure was proposed to reduce the dead volume. In addition, incorporating a deformation part on the glass substrate used for the device was proposed for integration of the valve into a nanofluidic device. The performance of the valve was then evaluated. The flow rate when closing the valve was 0.1 % , the response time was 0.06 s, the endurance of open/close operation was over 100,000 times. These performances satisfied the requirements for application to nanofluidic analyses.

In chapter 3, fluid operations for analyses using the valve were verified. Two types of fluid operation was verified, that is, fluid operations in a single-phase system and in a multi-phase system. For fluid operations in a single-phase system, a curved valve cham-

ber was proposed in order to prevent leakage caused by molecular diffusion through the valve chamber. A fabrication method using plastic deformation of glass was proposed. By repeating the open/close operation and pressing the valve chamber for more than 20,000 times using a four-stepped valve chamber, the steps consequently demolished and a curved valve chamber was obtained. The amount of leakage caused by diffusion from this curved chamber was evaluated to be under 0.5 %. For fluid operations in a multi-phase system, typically a gas/liquid two-phase system, a hydrophobic valve chamber and a valve operation to generate pressure on-chip was proposed to switch water in the nanochannels to air. The hydrophobic modification of the valve chamber kept the water out of the valve chamber and by using the pressure generated from the quick valve closing operation, gas/liquid switching in the nanochannel was verified.

In chapter 4, a fluid control system for a nanofluidic device integrated with valves was established. A chip holder combined with an actuator holder was designed to incorporate actuators at the highest density. An opening space for the objective lens of the detector was also created in the chip holder. In addition, in order to reduce the effect of deformation of the total device caused by operation of the valves and realize independent operation of multiple valves, a reinforcement was set around the valves. Furthermore, a sample injection process assuming nanofluidic chromatography was verified. As a result, a quick response and a robust fluid control with a high reproducibility was achieved.

In chapter 5, the operation of ELISA in a single-cell analysis device implemented with valves was confirmed. Seven valves were implemented into the device to operate the flow. Sample volumetry of 25 pL was achieved and the aliquot was successfully transported to the ELISA channel. As a result of antigen-antibody reaction and enzyme reaction, a signal from a standard solution of IL-6 was obtained. 1500 molecules (2.5 zmol) of the

standard solution was detected, and a valve-implemented micro/nano fluidic device was successfully developed and operated for the first time.

With micro/nano integrated fluidic devices implemented with valves, the designing concept of micro-/nanochannels and the flow controlling system would greatly change. The fluid control using valves would be an easy and precise process so that all users could operate sophisticated analyses that can only be controlled by technicians today. Furthermore, chemical processes could be integrated easier and various functions could be added to the device. In this way, the nanochannel open/close valve would greatly contribute in advancing the field of nanofluidics.

6.2 Future prospects

The nanochannel open/close valve utilizing glass deformation developed in this research is a fundamental technology for sophisticated integration of chemical processes on glass-based micro-/nanofluidic devices. As is the case with the development of microfluidics, which owes a great part to the emergence of the PDMS valve ("Quake valve"), highly integrated analytical devices could be realized by implementing the nanochannel open/close valves. For example, it is indispensable for the realization of single-cell protein analysis, which is currently attracting attention in the fields of medicine and biology.

Cell analyses have mostly been performed using a large number of cells (~10^6 cells) due to the restriction of the sample volume or the analytical systems. The field of cell biology have been advanced in this way. Recently, however, it has come to be widely known that the behavior of individual cells are different even if they are genitically identical.[37–39] In order to investigate the unique character of individual cells, an analytical tool for a sin-

gle cell is necessary. Otherwise, analyses using a large number of cell would mask these properties of each cells. However, the number of proteins expressed in one cell is as much as ~10^4 kinds, plus, the absolute number is very small (zmol ~amol). Although analysis targeting specific proteins has been realizing these days,[85–87] comprehensive analysis of proteins from a single cell is not yet achieved.

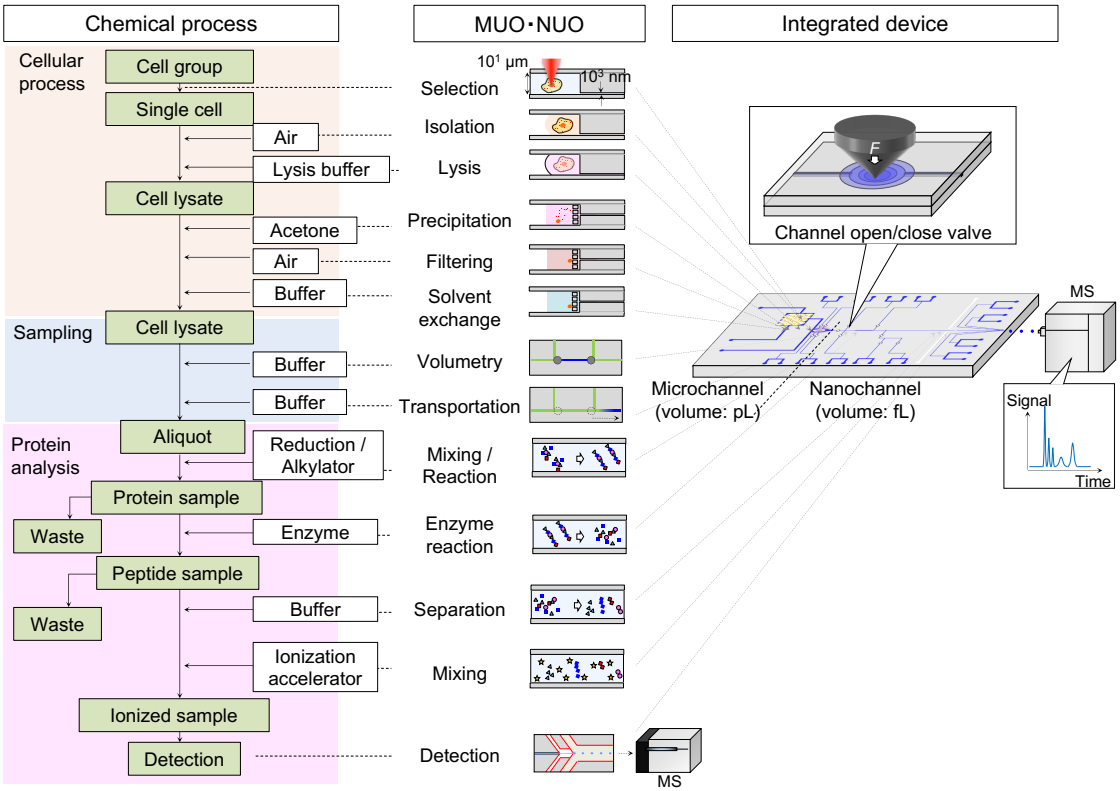

Figure 6-1: System design of single cell proteomics

Our group has been tackling this subject using micro-/nanofluidic devices based on our concept for integrating chemical processes.[14–16] The processing flow of protein analysis from a single cell is illustrated in Fig. 6-1. First, cell suspension is introduced in a microchannel and a single cell is selected and captured by an optical tweezer. After adding the lysis buffer, the cell is isolated by a gas/liquid interface.[82] The protein in the lysate is then perticipated, filtered, and purified.[88] The sample is introduced in the nanochannels

and the sample volume is regulated (fL–pL). The aliquot is mixed with reducing agent followed by protein digestion in a pL enzyme reactor.[83] The obtained peptides are separated by nanofluidic chromatography,[34] ionized after adding an ionization accelerator, and finally introduced in a mass spectrometer with a fL droplet shooter.[84] Although all the unit operations described above are already established, the current fluid control using pressure balance was too complex to connect the operations and complete the analysis. Therefore, the nanochannel open/close valve and the fluid control system developed in this study is essential. Integration of the valves would make it possible to connect unit operations by sophisticated fluid control, and pave the way to realize comprehensive analysis of proteins from a single cell.

Appendix要約

A.1 Evaluation of glass breaking stress

In chapter 2, the thickness of the glass defomation part for the valve was designed based on the breaking strength of glass. Here, the strength test of fused silica is explained.

A model similar to a three-point bending test, which is a general strength test for materials, was constructed. The set up is shown in Fig. A-1. The sample used for the test was 0.17 mm-thick substrate of fused silica. This was set on supporting beams placed with a gap of 5 mm. The actuating system for operating a single valve was used for pressing. The pressing pin was placed at the middle of the two supporting edges and the zero-point height was determined using the force sensor and the moment of contact was detected. Starting from this height, the sample was pressed downwards using the z axis micrometer of the actuator until the sample was broken.

The deflection of sample before breaking was approximated by a circular arc and the curvature was estimated from the following equation.

$$\rho = \frac{8w}{4w^2 + d^2} \tag{A.1}$$

where ρ is the curvature of the glass, w is the maximum deflection, and d is the gap between the supporting edges ($d = 5\mathrm{mm}$). Therefore, the stress on the glass surface can be estimated using the obtained value of w, Young's modulus $E = 73$ GPa, and the thickness of the material ($t = 170$ μm). As a result, the deflection of the glass when breaking was 619 ± 33 μm ($N = 4$). Thus, the breaking stress of glass was estimated to be 1.16 GPa.

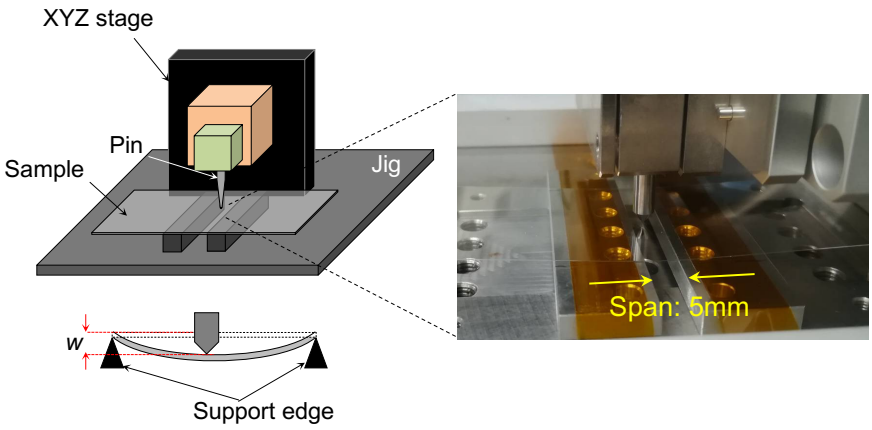

Figure A-1: Experimental setup of strength evaluation.

A.2 Fabrication process

Here, the details of the fabrication process of the device implemented with valves is described. The device consists of an upper substrate with a deformation part and a lower substrates with microchannels, nanochannels, and valve chambers.

A.2.1 Upper substrate

Fabrication of glass deformation part for valve

(1) Cr/Au/Cr sputtering

A fused silica substrate with a thickness of 0.25 mm (Shinetsu VIOSIL) was first washed with piranha solution for 8 minutes. Then, a three layered film consisting of Cr (50 nm), Au (300 nm), Cr (150 nm) was sputtered on the surface using a sputtering equipment (CFS-4EP-LL i-Miller; Shibaura Mechatronics Corp., Yokohama, Japan).

(2) Photolithography

The patterns for the deforamtion part (1 mm in diameter) was designed on the

Cr/Au/Cr layer by photolithography.

(3) Wet etching

The substrate was immersed in hydrofluoric acid and the substrate was etched for a depth of 220 μm . Because wet etching proceeds isotropically, the maximum diameter of the final deformation part spreads to approximately (Designed diameter)+2× (Etching depth), which is about 1.5 mm. However, the diamter of the area with a 30 μm thickness would be 1 mm as designed.

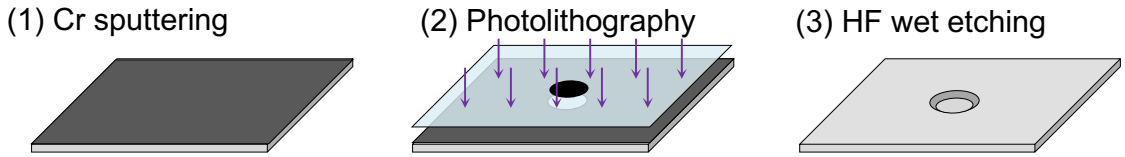

Figure A-2: The fabrication process of the upper substrate.

A.2.2 Lower substrate

Fabrication of nanochannels

(1) Cr sputtering

Chromium was sputtered on the surface using a sputtering equipment. The thickness of the chromium was 100 nm.

(2) Electron beam (EB) resist coating

ZEP-520A (Zeon Corp., Tokyo, Japan) was used as the EB resist material and spin-coated onto the substrate at 5000 rpm. The obtained thickness of the resist is about 300 nm. After coating, the substrate was baked on a hot plate with 180 °C for two minutes.

(3) EB lithography

EB lithography was performed by ELS-7800 (Elionix, Tokyo, Japan). For the devices used in chapters 2 and 3, the exposure time was 0.4 μs/dot and the dot size was $5\mathrm{nm} \times 5\mathrm{nm}$ per dot. For the devices used in chapters 4 and 5, the exposure time was 1.4 μs/dot and the dot size was $30\mathrm{nm} \times 30\mathrm{nm}$ per dot. This was because the nanochannels designed on the devices used in chapters 4 and 5 were wider and the total area was greater.

(4) Development

After EB lithography, the resist was developed by immersing the substrate in $o-$xylene for 5 minutes. Then, the substrate was rinsed to stop the developing by gently shaking in isopropanol for about 10 seconds. After washing the substrate with ultra pure water, the substrate was immersed in Cr etchant (HICRETCH S–1, FUJIFILM Wako. Pure Chemical Corp., Osaka, Japan) for 1–2 minutes. The EB resist was then removed by sonication in a mixture of *o*-xylene and acetone, and finally washed with piranha solution.

(5) Reactive ion etching (RIE)

The nanochannels were fabricated by a RIE process using an NLD-570 system (ULVAC Co., Ltd., Kanagawa, Japan). A mixture gas of $\mathrm{SF_6}$ and $\mathrm{CHF_3}$ was used for etching $\mathrm{SiO_2}$.

(6) Removing Cr

Finally, the Cr film was removed by immersing the substrate in Cr etchant.

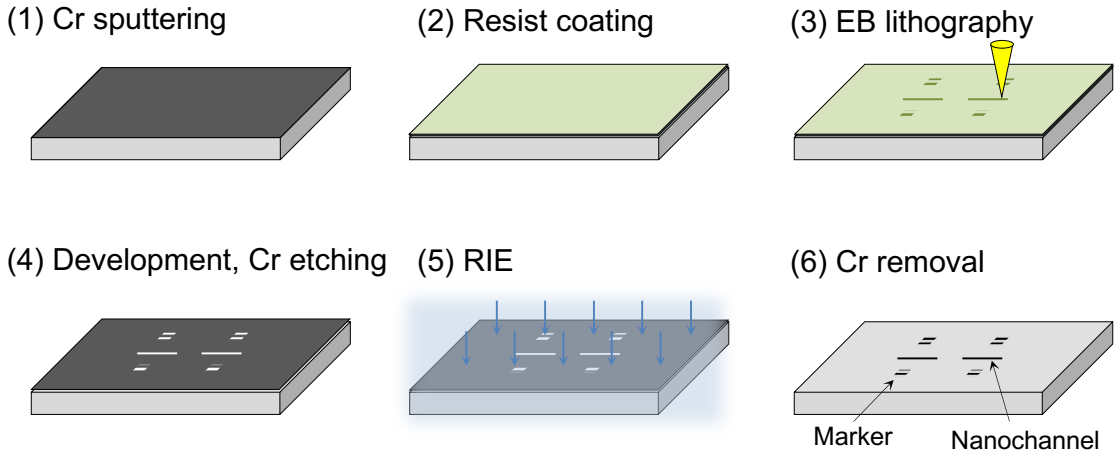

Figure A-3: The fabrication process of the nanochannels on the lower substrate.

Fabrication of valve chamber

The four-stepped valve chamber was fabricated one steps each by repeating the following process (1)–(3). The steps were fabricated from the step with the smallest diamter in order. In this way, the nonuniformity of the resist coating will less effect the fabrication of the steps afterwards.

(1) EB resist

Similar to the EB lithography process above, ZEP-520A (Zeon Corp., Tokyo, Japan) was spin-coated onto the substrate at 5000 rpm and the substrate was baked on a hot plate with 180 °C for two minutes. After cooling the substrate down to room temperature, conductive polymer (Espacer 300, Showa Denko, Tokyo, Japan) was spin-coated at 1000 rpm for one minute.

(2) EB lithography

The substrate is set to the EB lithography machine (ELS-7800). The fabricating position of the valve is determined by the alignment markers fabricated at the same time of fabricating nanochannels. When the machine recognizes the position of the

markers, it automatically corrects the position and the angle of the substrate in order to expose electron beam to the right position. After EB exposure, the conductive polymer on the surface is washed with water. The developing process is the same as mentioned above only that piranha solution is unnecessary before RIE.

(3) RIE

Then, the substrate is set to NLD and the surface is etched for 25 seconds resulting in a shallow valve step of 25 nm height. After etching, the EB resist was removed by sonication in a mixture of $o-$xylene and acetone. When the resist is hard to be removed piranha solution can also be used.

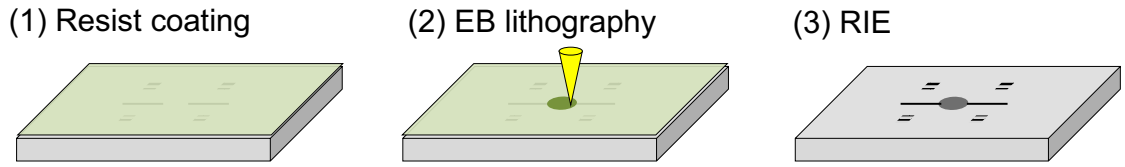

Figure A-4: The fabrication process of the valve chamber on the lower substrate.

Fabrication of microchannels

(1) KMPR

The substrate was first washed with piranha solution followed by sonication in ultra pure water. Then, the surface of the substrate was modified with 1,1,1,3,3,3–hexamethyldisilazane (HMDS; FUJIFILM Wako. Pure Chemical Corp., Osaka, Japan). As a photoresist, KMPR®1035 (Microchem Corp., MA, USA) was spin-coated at 2000 rpm at room temperature, and baked on a hot plate (110 °C) for 30 minutes.

(2) Photolithography

KMPR®1035 is a negative resist, that is, the area where light is exposed will be cured. Considering this character, a photomask was prepared using a Direct Write Lithography system (DWL66+, Heigelberg, Germany). A mask aligner (MA6, SÜSS MicroTec SE, Germany) was used to align the photomask and the substrate, and ultraviolet light was exposed. After exposure, the substrate was removed from the machine and baked on a hot plate at 80 °C for three minutes.

(3) Developement

The substrate was immersed in SU–8 developer and sonicated. After five minutes of sonication, the solution was replaced and sonicated for another two minutes. Then, the substrate was rinsed in isopropanol for about 10 seconds and dried with air blow.

(4) RIE

The substrate was set to NLD and the microchannels were etched for 3000 seconds (for the device used in chapter 5). Using a mixture of Ar, C_3F_8 and CHF_3 as the etching gas, the rate of SiO_2 can be enhance to 5–7 nm/s.[89] Therefore, as a result of the process, microchannels with a depth of 20 μm can be fabricated.

(5) Removing resist

KMPR®1035 was removed by immersing the substrate in piranha solution. In addition, the surface was cleaned by irradiating O_2 plasma for 20 minutes in using NLD.

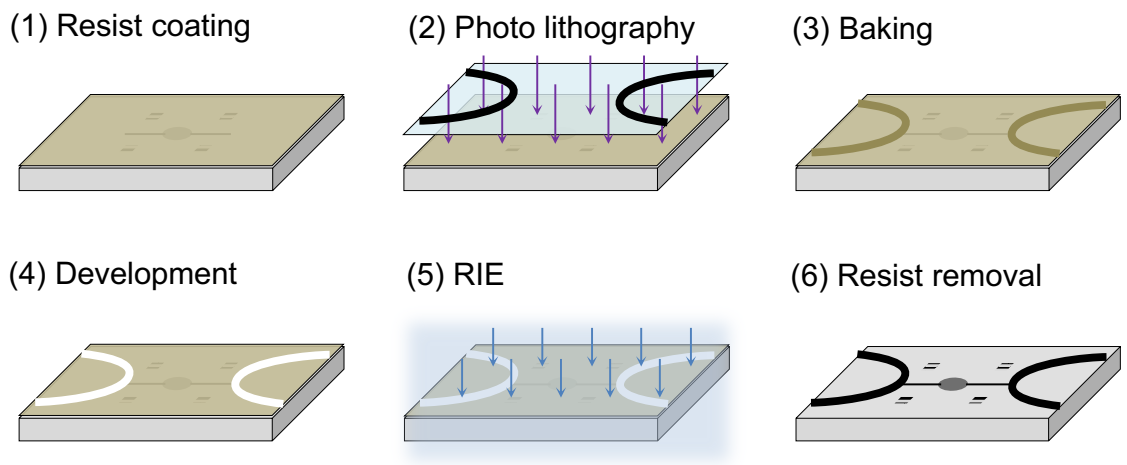

Figure A-5: The fabrication process of the microchannels on the lower substrate.

A.2.3 Bonding

Modification of the ELISA channels with APTES

The lower substrate was modified with APTES (Tokyo Chemical Industry, Tokyo, Japan) in a gas phase. Beforehand of modification, the substrate was washed with piranha solution for 8 minutes followed by sonication in ultra-pure water for 10 minutes, and finally the surface was activated with O_2 gas plasma for 250 W, 40 seconds. The substrate was placed in a separable flask with a vial containing 200 µL of APTES solution, which was then sealed. All the procedures above were conducted in a cleanroom.

The flask was evacuated using a vacuum pump for 3 minutes and then Ar was introduced into the flask. This Ar replacing process was repeated twice. The flask was evacuated for another 5 minutes and then heated in an oil bath at 120 °C . After 2 hours of reaction, the substrate was removed from the flask and sonicated in toluene for 10 minutes. The substrate was then rinsed with ethanol and ultra-pure water in this order and was dried with flowing air.

Bonding two substrates

The lower substrate (APTES-modified substrate) was placed in a vacuum ultraviolet (VUV) irradiating machine (E500-172-120-A2, Excimer Inc., Japan) and a chromium mask (the entire mask was 15 cm $\times$ 15 cm and the masked area was 135 μm $\times$ 3 mm placed at the center of the mask) was aligned to the capture antibody immobilizing area. The substrate was irradiated with VUV light at an intensity of 5 $\mathrm{mW/cm^2}$ for 15 minutes. After irradiation, the APTES-patterned substrate was sonicated in ultra-pure water and dried with flowing air.

The upper substrate was washed with piranha solution for 8 minutes followed by sonication in ultra-pure water for 10 minutes, and finally the surface was activated with $\mathrm{O_2}$ gas plasma (60 Pa, 250 W) for 40 seconds. The substrate was removed from the plasma chamber and washed with ultra-pure water. After drying the substrate with flowing air, the two substrates were brought into contact in a way that the holes fabricated on the upper substrate is aligned to the ends of the microchannels fabricated on the lower substrate (Fig. A-6). With this alignment process, the deformation parts should be automatically aligned right above each valves. In order to increase the bonding energy of the substrates, the device was pressurized at 5,000 N for 3 hours under 110 °C using a bonding machine (Bondtech Co., Ltd., Japan).

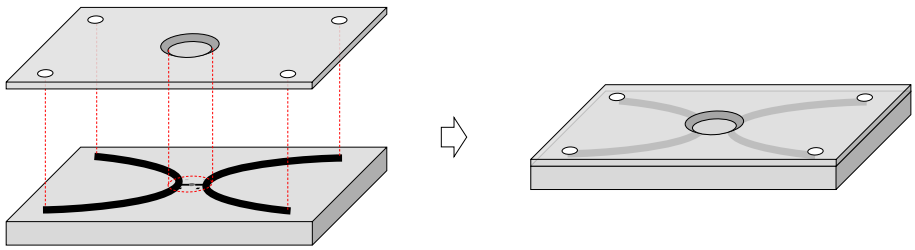

Figure A-6: Alignment of the upper substrate and the lower substrate

A.3 Deformation of the upper substrate after repeated pressing

Plastic deformation of the four-stepped valve chamber fabricated on the lower substrate was described in chapter 3. The deformation of the upper substrate caused by repeated pressing was also investigated and is described here. Figure A-7 shows the results.

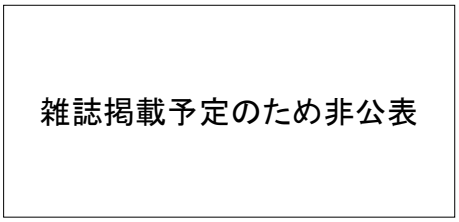

Figure A-7: A 3D depth profile of the upper/lower substrate and a sectional depth profile along the plane A–A' (a) Before pressing (b) After pressing 30,000 times

Before pressing the valve, which is the state just after the fabrication of the channels and the valve was completed, the surface of the upper substrate was smooth with a roughness less than 1 nm, and the four steps of the valve chamber could clearly be observed. After pressing the valve chamber for 30,000 times, the steps in the valve chamber had deformed. On the other hand, the surface of the upper substrate has also deformed in a way as if it were embossed with the valve chamber and the nanochannels. Because the deformed values were similar for both the upper substrate and the lower substrate (~8 nm), it is implied that the deformation is caused by the repeated pressing. Furthermore, judging from the results in section 3.2.3 that solute diffusion through the valve could be greatly reduced using the pressed valve, it is probable that the roughness on each substrate meshes with each other reducing the opening space in the valve chamber when the valve is closed.

A.4 Determining the coordinates of the valve chamber

Here, the experiment for determining the coordinates of the valve chamber is explained.

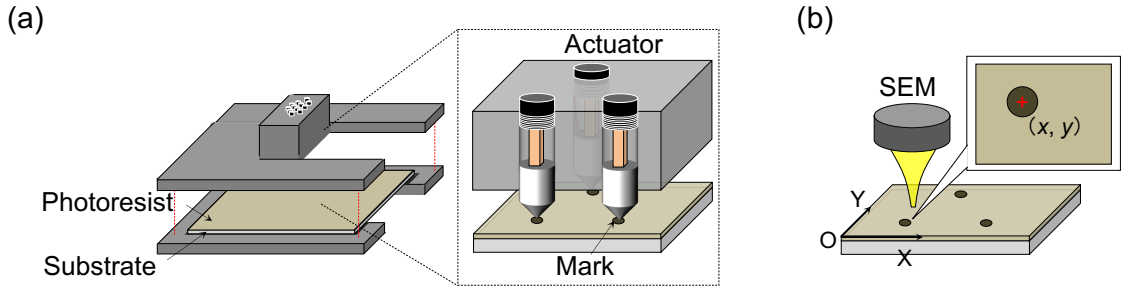

Figure A-8: Experiment for obtaining coordinates of actuator holes. (a) The actuators were set through the actuator holes and the position of each holes were marked on the photoresist. (b) The surface of the substrate is observed by SEM and the coordinates were obtained.

First, a photoresist (THB-111N; JSR Corp., Tokyo, Japan) was spin-coated on a glass substrate and fixed on a jig. Then, 12 actuators were set through the actuator holes and the pressed area was marked on the photoresist. The substrate was then coated with a conductive polymer (Espacer 300, Showa Denko, Tokyo, Japan) and the surface was observed by a scanning electron microscope (SEM) (ELS-7800). The center point of the mark on the photoresist was searched and the coordinates at the point were obtained (Fig. A-8). Hole No.4 was set as the base of alignment and the other coordinates were converted so that the square residuals sum is the smallest is the minimum. The results are shown in Table A-2.

Table A-2: The obtained coordinates of the actuator holes and the error from the designed position.

Hole No.	Coordinates (mm)	Error from design (μm)
1	(34.0086, 32.9933)	9.3
2	(34.0165, 26.9828)	17
3	(35.7265, 36.0018)	38
4 (base)	(35.7650, 30.0000)	–
5	(35.7837, 23.9896)	21
6	(37.4676, 39.0089)	48
7	(37.4950, 33.0034)	20
8	(37.5107, 27.0032)	5.3
9	(37.5474, 20.9969)	32
10	(39.2102, 35.9894)	56
11	(39.2625, 30.0054)	6.0
12	(39.2994, 24.0089)	35

A.5 Possible factors for Z positioning error

When the valve open/close is operated in the initial way described in chapter 4, which is a process to apply voltage to the actuator after making contact with the valve, the valve would not fully close as shown in Fig. A-9.

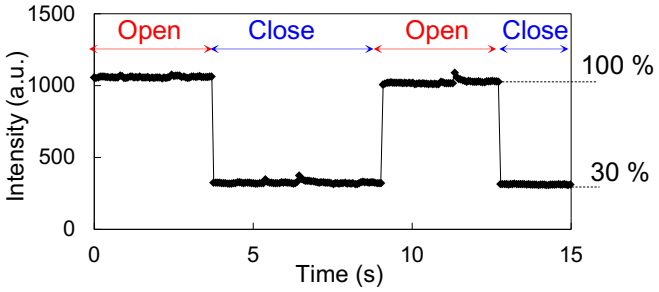

Figure A-9: Fluorescence intensity at the valve chamber during the open/close operation using the system.

Here, the possible factors causing a Z position error other than the backlash of the screw is investigated. The other possible factors are (a) Tilt of pressing pin, (b) Tilt of actuator, and (c) Pushing screw back (Fig. A-10).

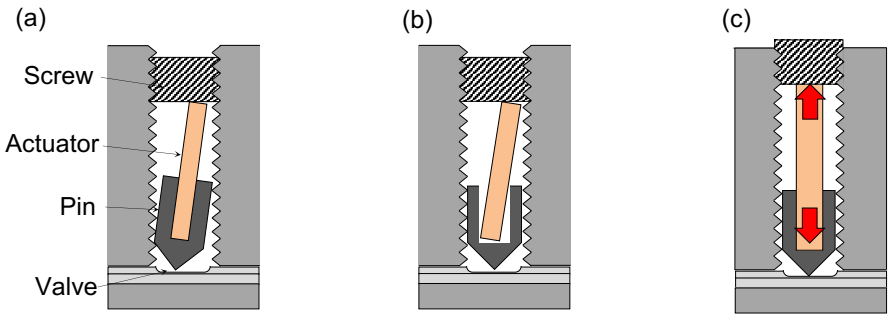

Figure A-10: Possible cause for insufficient deformation. (a) Tilt of pressing pin (b) Tilt of actuator (c) Pushing screw back

(a) Tilt of pressing pin

The diameter of the pressing pin was originally design as 2 mm so the diameters of the "actuator holes" were 2 mm as well. However, due to the mechanical tolerance, the actual

inner diameters of the threaded screw holes were 2.04 mm. With this 40 μm –gap, the pin could tilt inside the holes and the pressing area would not be the center of the valve. In order to investigate the effect of the tilt, a pressing pin with a diameter of 2.04 mm was fabricated. Still, the insufficient closing of the valve had not improved (Fig. A-11). Therefore, the tilt of pressing pin was not the dominant factor.

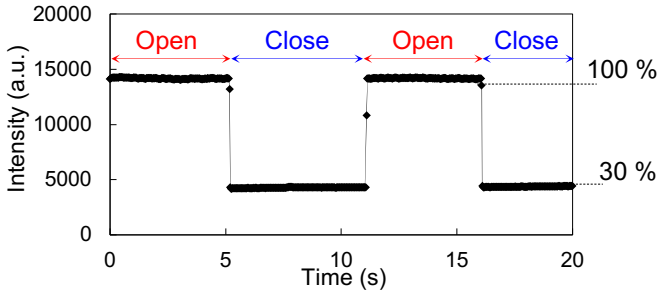

Figure A-11: Fluorescence intensity at valve chamber while open/close operation using a pressing pin with a diameter of 2.04 mm.

(b) Tilt of actuator

The holes fabricated on the pressing pins are slightly larger than the size of the actuators, which could cause a tilt of the actuators. However, the calculated value of the tilting angle is 0.02 rad. This indeed decreases the amount of displacement of the actuator, but still the deformation value is 7.8 μm , which is enough for valve closing. Judging from this estimation, the tilt of the actuators was concluded not to be the dominant factor for insufficient closing.

(c) Pressing back screw

When a voltage is applied to the actuators, they not only press the valve deformation parts but also push the screw used to fix the actuator. If the actuator pushes the screw back, the displacement of the actuator is absorbed in the upward direction and result in insufficient displacement.

Here, the axial force, or the tightening force of screw can be expressed as follows.

$$F = \frac{T}{kd} \tag{A.2}$$

where T is the tightening torque, k is the torque coefficient, and d is the diameter of the screw. The diameter of the screw is 2.5 mm, k is a constant value generally within 0.15–0.20, and T is determined by the ISO standard according to the diameter of the screw; in the case of $d = 2.5$, the value of T is 0.36. Based on this equation, the axial force is estimated to be 720–960 N. Therefore, it is impossible to push back with the actuator.

From the results above and the results described in section 4.2.1, the backlash of the screw was concluded to be the dominant factor of insufficient closing. For the actuation of the valves in the actual fluid control, the process verified above was adopted.

List of Abbreviations

AFM	atomic force microscope	24
APTES	aminopropyltriethoxysilane	93
BSA	bovine serum albumin	96
CFCP	Continuos Flow Chemical Processing	10
DIC-TLM	differential interference contrast-thermal lens microscopy	13
ELISA	enzyme linked-immunosorbent assay	14
HMDS	1,1,1,3,3,3-hexamethyldisilazane	115
HRP	horseradish peroxidase	91
LIF	Laser Induced Fluorescence	8
MUO	Micro Unit Operation	9
NUO	Nano Unit Operation	12
ODS-DEA	octadecyldemethyl-N, N-diethylaminosilane	68
PBS	phosphate buffered saline	38
PC	polycarbonate	10
PDMS	polydimethylsiloxane	11
PEG	polyethyleneglycol	89
PET	polyethyleneterephthalate	11
PMMA	polymethylmetacrylate	10
PNIPAM	poly(N-isopropylacrylamide)	20
SEM	scanning electron microscope	24
TLM	thermal lens microscopy	8
TMB	3,3',5,5'-tetra-methylbenzidine	92

List of Related Publications

Publications

(1) Hiroki Sano, Yutaka Kazoe, Kyojiro Morikawa, and Takehiko Kitamori, "Fabrication of a nanoscale curved structure for a nanofluidic valve utilizing glass deformation," *Journal of Micromechanics and Microengineering*, submitted

(2) Hiroki Sano, Yutaka Kazoe, Kyojiro Morikawa, and Takehiko Kitamori, "Implementation of a Nanochannel Open/Close Valve into a Glass Nanofluidic Device," *Microfluidics and Nanofluidics*, 24, 78(11pp), (2020)

Reviewed proceedings

(1) Hiroki Sano, Yutaka Kazoe, Kyojiro Morikawa, and Takehiko Kitamori, "FABRICATION OF A NANOSCALE CURVED STRUCTURE AND APPLICATION TO NANOCHANNEL OPEN/CLOSE VALVE," *The Proceedings of Conference μTAS 2021*, 1, 1399-1400 (2021)

(2) Hiroki Sano, Yutaka Kazoe, Kyojiro Morikawa, and Takehiko Kitamori, "INTEGRATION OF GLASS DEFORMATION NANOCHANNEL OPEN/CLOSE VALVES INTO A NANOFLUIDIC DEVICE AND FEMTO-LITER FLUID OPERATIONS," *The Proceedings of Conference μTAS 2020*, 1, 370-371 (2020)

Presentations

・Reviewed international conferences

(1) Hiroki Sano, Yutaka Kazoe, Kyojiro Morikawa, and Takehiko Kitamori, "FABRICATION OF A NANOSCALE CURVED STRUCTURE AND APPLICATION

TO NANOCHANNEL OPEN/CLOSE VALVE," *The 25th International Conference on Miniaturized Systems for Chemistry and Life Sciences (MicroTAS 2021)* (2021),online, Poster

(2) Hiroki Sano, Yutaka Kazoe, Kyojiro Morikawa, and Takehiko Kitamori, "INTEGRATION OF GLASS DEFORMATION NANOCHANNEL OPEN/CLOSE VALVES INTO A NANOFLUIDIC DEVICE AND FEMTO-LITER FLUID OPERATIONS," *The 24th International Conference on Miniaturized Systems for Chemistry and Life Sciences (MicroTAS 2020)* (2020), online, Poster

・Non-reviewed international conferences

(1) Hiroki Sano, Yutaka Kazoe, Kyojiro Morikawa, and Takehiko Kitamori, "Development of a nanochannel open/close valve utilizing glass deformation for biochemical analysis by nanofluidics," *The Intenational Chemical Congress of Pacific Basin Societies 2021 (PacifiChem 2021)* (2021), Online, Poster

(2) Hiroki Sano, Yutaka Kazoe, Kyojiro Morikawa, and Takehiko Kitamori, "Development of Nanochannel Open/Close Valve Utilizing Glass Deformation," *The 11th International Symposium on Microchemistry and Microsystems (ISMM 2019)* (2019), Yangling, China, Oral

(3) Hiroki Sano, Yutaka Kazoe, Kyojiro Morikawa, and Takehiko Kitamori, "Development of nanochannel open/close valve utilizing nanoscale glass deformation," *International Workshop on Advanced Nanomaterials and Nanodevices 2019* (2019), Shanghai, China, Poster

・Non-reviewed domestic conferences

(1) 佐野大樹，嘉副裕，森川響二朗，北森武彦,「ガラス変形とナノ空間曲面を利用した流路開閉バルブの開発」，化学とマイクロ・ナノシステム学会第 43 回研究会（2021），オンライン，ポスター

(2) 佐野大樹，嘉副裕，森川響二朗，北森武彦,「拡張ナノ流路開閉バルブの集積化によるフェムトリットル流体制御システムの開発」，化学とマイクロ・ナノシステム学会第 42 回研究会（2020），オンライン，ポスター

References

[1] Todd M. Squires and Stephen R. Quake. Microfluidics: Fluid physics at the nanoliter scale. *Reviews of modern physics*, Vol. 77, No. 3, pp. 977–1026, 2005.

[2] H. A. Stone, A. D. Stroock, and A. Ajdari. Engineering flows in small devices: Microfluidics toward a lab-on-a-chip. *Annual Review of Fluid Mechanics*, Vol. 36, pp. 381–411, 2004.

[3] Eric K. Sackmann, Anna L. Fulton, and David J. Beebe. The present and future role of microfluidics in biomedical research. *Nature*, Vol. 507, No. 7491, pp. 181–189, 2014.

[4] McCartney S. *ENIAC: The Triumphs and Tragedies of the World's First Computer*. Berkley Publishing Group, 2001.

[5] Stephen C. Terry, John H. Herman, and James B. Angell. A Gas Chromatographic Air Analyzer Fabricated on a Silicon Wafer. *IEEE Transactions on Electron Devices*, Vol. 26, No. 12, pp. 1880–1886, 1979.

[6] A Manz, Y Miyahara, J Miura, Y Watanabe, H Miyagi, and K Sat. Design of an Open-tubular Column Liquid Chromatograph Using Silicon Chip Technology. *Sensors and Actuators, B: Chemical*, pp. 249–255, 1990.

[7] H. M. Widmer A. Manz, N. Graber. Miniaturized Total Chemical Analysis Systems: a Novel Concept for Chemical Sensing. *Sensors and Actuators, B: Chemical*, pp. 244–248, 1990.

[8] Pierre Alain Auroux, Dimitri Iossifidis, Darwin R. Reyes, and Andreas Manz. Micro total analysis systems. 2. Analytical standard operations and applications. *Analytical Chemistry*, Vol. 74, No. 12, pp. 2637–2652, 2002.

[9] Darwin R Reyes, Dimitri Iossifidis, Pierre-alain Auroux, and Andreas Manz. Micro Total Analysis Systems . 1 . Introduction , Theory , and Technology. *Analytical Chemistry*, Vol. 74, No. 12, pp. 2623–2636, 2002.

[10] James L. Kinsey. LASER-INDUCED FLUORESCENCE. *Annual Review of Physical Chemistry*, Vol. 28, pp. 349–372, 1977.

[11] Alexander A. Oraevsky, Steven L. Jacques, and Frank K. Tittel. Measurement of tissue optical properties by time-resolved detection of laser-induced transient stress. *Applied Optics*, Vol. 36, No. 1, p. 402, 1997.

[12] Takehiko Kitamori, Manabu Tokeshi, Akihide Hibara, and Kiichi Sato. Thermal Lens Microscopy and Microchip Chemistry. *Analytical Chemistry*, Vol. 76, No. 3, 2004.

[13] R. C. C. Leite, S. P. S. Porto, and T. C. Damen. THE THERMAL LENS EFFECT AS A POWER - LIMITING DEVICE. *Applied Physics Letters*, Vol. 10, No. 3, pp. 100–101, 1967.

[14] Kiyoshi Sato, Hiroaki Kawanishi, Manabu Tokeshi, Takehiko Kitamori, and Tsuguo Sawada. Sub-zeptomole detection in a microfabricated glass channel by thermal-lens microscopy. *Analytical Sciences*, Vol. 15, No. 6, pp. 525–529, 1999.

[15] Kiyoshi Sato, Manabu Tokeshi, Takehiko Kitamori, and Tsuguo Sawada. Integration of flow injection analysis and zeptomole-level detection of the Fe(II)-o-phenanthroline complex. *Analytical Sciences*, Vol. 15, No. 7, pp. 641–645, 1999.

[16] Eiichiro Tamaki, Kiichi Sato, Manabu Tokeshi, Kae Sato, Makoto Aihara, and Takehiko Kitamori. Single-cell analysis by a scanning thermal lens microscope with a microchip: Direct monitoring of cytochrome c distribution during apoptosis process. *Analytical Chemistry*, Vol. 74, No. 7, pp. 1560–1564, 2002.

[17] Manabu Tokeshi, Tomoko Minagawa, Kenji Uchiyama, Akihide Hibara, Kiichi Sato, Hideaki Hisamoto, and Takehiko Kitamori. Continuous-flow chemical processing on a microchip by combining microunit operations and a multiphase flow network. *Analytical Chemistry*, Vol. 74, No. 7, pp. 1565–1571, 2002.

[18] David C. Duffy, J. Cooper McDonald, Olivier J.A. Schueller, and George M. Whitesides. Rapid prototyping of microfluidic systems in poly(dimethylsiloxane). *Analytical Chemistry*, Vol. 70, No. 23, pp. 4974–4984, 1998.

[19] S. R. Quake. From Micro- to Nanofabrication with Soft Materials. *Science*, Vol. 290, No. 5496, pp. 1536–1540, 2000.

[20] Rajendrani Mukhopadhyay. When PDMS isn't the Best. *Analytical Chemistry*, Vol. 79, No. 9, pp. 3248–3253, 2007.

[21] Jianhua Zhou, Hui Yan, Kangning Ren, Wen Dai, and Hongkai Wu. Convenient method for modifying poly(dimethylsiloxane) with poly(ethylene glycol) in microfluidics. *Analytical Chemistry*, Vol. 81, No. 16, pp. 6627–6632, 2009.

[22] Jung Uk Shim and Seth Fraden. Control of the phase behavior of aqueous solutions using microfluidics. *Proceedings of the 11th International Conference on Miniaturized Systems for Chemistry and Life Sciences, uTAS 2007*, Vol. 129, No. 7, pp. 370–372, 2007.

[23] Takehiko Tsukahara, Kazuma Mawatari, and Takehiko Kitamori. Integrated extended-nano chemical systems on a chip. *Chemical Society Reviews*, Vol. 39, No. 3, p. 1000, 2010.

[24] Kazuma Mawatari, Yutaka Kazoe, Hisashi Shimizu, Yuriy Pihosh, and Takehiko Kitamori. Extended-nanofluidics: Fundamental technologies, unique liquid properties, and application in chemical and bio analysis methods and devices. *Analytical Chemistry*, Vol. 86, No. 9, pp. 4068–4077, 2014.

[25] Kyojiro Morikawa, Yutaka Kazoe, Yuto Takagi, Yoshiyuki Tsuyama, Yuriy Pihosh, Takehiko Tsukahara, and Takehiko Kitamori. Advanced top-down fabrication for a fused silica nanofluidic device. *Micromachines*, Vol. 11, No. 11, nov 2020.

[26] Cees Dekker. Solid-state nanopores. *Nature nanotechnology*, Vol. 2, pp. 209–215, 2007.

[27] Eiichiro Tamaki, Akihide Hibara, Haeng Boo Kim, Manabu Tokeshi, and Takehiko Kitamori. Pressure-driven flow control system for nanofluidic chemical process. *Journal of Chromatography A*, Vol. 1137, No. 2, pp. 256–262, 2006.

[28] Hisashi Shimizu, Kazuma Mawatari, and Takehiko Kitamori. Sensitive determination of concentration of nonfluorescent species in an extended-nano channel by differential interference contrast thermal lens microscope. *Analytical Chemistry*, Vol. 82, No. 17, pp. 7479–7484, 2010.

[29] Hisashi Shimizu, Kazuma Mawatari, and Takehiko Kitamori. Femtoliter-scale separation and sensitive detection of nonfluorescent samples in an extended-nano fluidic device. *Analyst*, Vol. 139, No. 9, pp. 2154–2157, 2014.

[30] Lixiao Li, Yutaka Kazoe, Kazuma Mawatari, Yasuhiko Sugii, and Takehiko Kitamori. Viscosity and wetting property of water confined in extended nanospace simultaneously measured from highly-pressurized meniscus motion. *Journal of Physical Chemistry Letters*, Vol. 3, No. 17, pp. 2447–2452, sep 2012.

[31] Akihide Hibara, Takumi Saito, Haeng Boo Kim, Manabu Tokeshi, Takeshi Ooi, Masayuki Nakao, and Takehiko Kitamori. Nanochannels on a fused-silica microchip

and liquid properties investigation by time-resolved fluorescence measurements. *Analytical Chemistry*, Vol. 74, No. 24, pp. 6170–6176, 2002.

[32] Takehiko Tsukahara, Akihide Hibara, Yasuhisa Ikeda, and Takehiko Kitamori. NMR study of water molecules confined in extended nanospaces. *Angewandte Chemie - International Edition*, Vol. 46, No. 7, pp. 1180–1183, 2007.

[33] Takehiko Tsukahara, Wataru Mizutani, Kazuma Mawatari, and Takehiko Kitamori. NMR studies of structure and dynamics of liquid molecules confined in extended nanospaces. *Journal of Physical Chemistry B*, Vol. 113, No. 31, pp. 10808–10816, 2009.

[34] Ryo Ishibashi, Kazuma Mawatari, and Takehiko Kitamori. Highly efficient and ultra-small volume separation by pressure-driven liquid chromatography in extended nanochannels. *Small*, Vol. 8, No. 8, pp. 1237–1242, apr 2012.

[35] Ryo Ishibashi, Kazuma Mawatari, and Takehiko Kitamori. High resolution separation by pressure-driven liquid chromatography in meander extended nanochannels. *Journal of Chromatography A*, 2012.

[36] Kentaro Shirai, Kazuma Mawatari, and Takehiko Kitamori. Extended nanofluidic immunochemical reaction with femtoliter sample volumes. *Small*, 2014.

[37] Oliver Stegle, Sarah A. Teichmann, and John C. Marioni. Computational and analytical challenges in single-cell transcriptomics. *Nature Reviews Genetics*, Vol. 16, No. 3, pp. 133–145, 2015.

[38] John R.S. Newman, Sina Ghaemmaghami, Jan Ihmels, David K. Breslow, Matthew Noble, Joseph L. DeRisi, and Jonathan S. Weissman. Single-cell proteomic analysis of S. cerevisiae reveals the architecture of biological noise. *Nature*, Vol. 441, No. 7095, pp. 840–846, 2006.

[39] Alfredo J. Ibáñez, Stephan R. Fagerer, Anna Mareike Schmidt, Pawel L. Urban, Konstantins Jefimovs, Philipp Geiger, Reinhard Dechant, Matthias Heinemann, and Renato Zenobi. Mass spectrometry-based metabolomics of single yeast cells. *Proceedings of the National Academy of Sciences of the United States of America*, Vol. 110, No. 22, pp. 8790–8794, 2013.

[40] Tatsuro Nakao, Yutaka Kazoe, Kyojiro Morikawa, Ling Lin, Kazuma Mawatari, and Takehiko Kitamori. Femtoliter Volumetric Pipette and Flask Utilizing Nanofluidics. *Analyst*, Vol. 145, No. 7, pp. 2669–2675, apr 2020.

[41] Wenhua Zhang, Shuichao Lin, Chunming Wang, Jia Hu, Cong Li, Zhixia Zhuang, Yongliang Zhou, Richard A. Mathies, and Chaoyong James Yang. PMMA/PDMS valves and pumps for disposable microfluidics. *Lab on a Chip*, Vol. 9, No. 21, pp. 3088–3094, 2009.

[42] Yi Ning Yang, Suz Kai Hsiung, and Gwo Bin Lee. A pneumatic micropump incorporated with a normally closed valve capable of generating a high pumping rate and a high back pressure. *Microfluidics and Nanofluidics*, Vol. 6, No. 6, pp. 823–833, 2009.

[43] William H. Grover, Alison M. Skelley, Chung N. Liu, Eric T. Lagally, and Richard A. Mathies. Monolithic membrane valves and diaphragm pumps for practical large-scale integration into glass microfluidic devices. *Sensors and Actuators, B: Chemical*, 2003.

[44] Marc A. Unger, Hou-Pu Chou, Todd Thorsen, Axel Scherer, and Stephen R. Quake. Monolithic Microfabricated Valves and Pumps by Multilayer Soft Lithography. *Science*, Vol. 288, No. 5463, pp. 113–116, 2000.

[45] Stephen R. Quake Todd Thorsen Sebastian J. Maerkl. Microfluidic Large-Scale Integration. *Science*, Vol. 298, pp. 580–584, 2002.

[46] David J. Beebe, Jeffrey S. Moore, Joseph M. Bauer, Qing Yu, Robin H. Liu, Chelladurai Devadoss, and Byung-Ho Jo. Functional hydrogel structures for autonomous flow control inside microfluidic channels. *Nature*, Vol. 404, , 2000.

[47] Yingjie Liu, Cory B. Rauch, Randall L. Stevens, Ralf Lenigk, Jianing Yang, David B. Rhine, and Piotr Grodzinski. DNA amplification and hybridization assays in integrated plastic monolithic devices. *Analytical Chemistry*, Vol. 74, No. 13, pp. 3063–3070, 2002.

[48] E. T. Carlen and C. H. Mastrangelo. Paraffin actuated surface micromachined valves. *Proceedings of the IEEE Micro Electro Mechanical Systems (MEMS)*, pp. 381–385, 2000.

[49] Lena Klintberg, Mikael Karlsson, Lars Stenmark, Jan Åke Schweitz, and Greger Thornell. A large stroke, high force paraffin phase transition actuator. *Sensors and Actuators, A: Physical*, Vol. 96, No. 2-3, pp. 189–195, 2002.

[50] Lin Gui and Jing Liu. Ice valve for a mini/micro flow channel. *Journal of Micromechanics and Microengineering*, Vol. 14, No. 2, pp. 242–246, 2004.

[51] Yan Xu, Misato Shinomiya, and Atsushi Harada. Soft Matter-Regulated Active Nanovalves Locally Self-Assembled in Femtoliter Nanofluidic Channels. *Advanced Materials*, 2016.

[52] H. K. Ma, B. R. Hou, H. Y. Wu, C. Y. Lin, J. J. Gao, and M. C. Kou. Development and application of a diaphragm micro-pump with piezoelectric device. *Microsystem Technologies*, Vol. 14, No. 7, pp. 1001–1007, 2008.

[53] Junwu Kan, Kehong Tang, Guojun Liu, Guoren Zhu, and Chenghui Shao. Development of serial-connection piezoelectric pumps. *Sensors and Actuators, A: Physical*, Vol. 144, No. 2, pp. 321–327, 2008.

[54] Jangmi Woo, Dong Kee Sohn, and Han Seo Ko. Performance and flow analysis of small piezo pump. *Sensors and Actuators, A: Physical*, Vol. 301, p. 111766, 2020.

[55] Junwu Kan, Kehong Tang, Yu Ren, Guoren Zhu, and Peng Li. Study on a piezo-hydraulic pump for linear actuators. *Sensors and Actuators, A: Physical*, Vol. 149, No. 2, pp. 331–339, 2009.

[56] Xiaoqiang Wu, Lipeng He, Yi Hou, Xiaochao Tian, and Xilu Zhao. Advances in passive check valve piezoelectric pumps. *Sensors and Actuators, A: Physical*, Vol. 323, , jun 2021.

[57] M. Shen, C. Yamahata, and M. A.M. Gijs. A high-performance compact electromagnetic actuator for a PMMA ball-valve micropump. *Journal of Micromechanics and Microengineering*, Vol. 18, No. 2, 2008.

[58] D. Accoto, M. C. Carrozza, and P. Dario. Modelling of micropumps using unimorph piezoelectric actuator and ball valves. *Journal of Micromechanics and Microengineering*, Vol. 10, No. 2, pp. 277–281, 2000.

[59] H. K. Ma, R. H. Chen, and Y. H. Hsu. Development of a piezoelectric-driven miniature pump for biomedical applications. *Sensors and Actuators, A: Physical*, Vol. 234, pp. 23–33, 2015.

[60] Jing Shi Dong, Rui Gang Liu, Wei Shuai Liu, Quan Qu Chen, Yang Yang, Yue Wu, Zhi Gang Yang, and Bai Song Lin. Design of a piezoelectric pump with dual vibrators. *Sensors and Actuators, A: Physical*, Vol. 257, pp. 165–172, 2017.

[61] Ronghui Zhang, Feng You, Zhihan Lv, Zhaocheng He, Haiwei Wang, and Ling Huang. Development and characterization a single-active-chamber piezoelectric

membrane pump with multiple passive check valves. *Sensors (Switzerland)*, Vol. 16, No. 12, 2016.

[62] Erik Stemme and Göran Stemme. A valveless diffuser/nozzle-based fluid pump. *Sensors and Actuators: A. Physical*, Vol. 39, No. 2, pp. 159–167, 1993.

[63] Helene Andersson, Wouter van der Wijngaart, Peter Nilsson, Peter Enoksson, and Göran Stemme. A valve-less diffuser micropump for micro ¯ uidic analytical systems. *Sensors and Actuators, B: Chemical*, Vol. 72, pp. 259–265, 2001.

[64] Kazuma Mawatari, Shogo Kubota, Yan Xu, Craig Priest, Rossen Sedev, John Ralston, and Takehiko Kitamori. Femtoliter droplet handling in nanofluidic channels: A laplace nanovalve. *Analytical Chemistry*, 2012.

[65] Stephan P. Timoshenko and S. Woinowsky-Kreiger. *Theory of Plates and Shells*. McGRAW-HILL BOOK COMPANY, 1959.

[66] Rocscience. Factor of safety and probability of failure. Technical report.

[67] Yan Xu, Chenxi Wang, Lixiao Li, Nobuhiro Matsumoto, Kihoon Jang, Yiyang Dong, Kazuma Mawatari, Tadatomo Suga, and Takehiko Kitamori. Bonding of glass nanofluidic chips at room temperature by a one-step surface activation using an O2/CF4 plasma treatment. *Lab on a Chip*, Vol. 13, No. 6, p. 1048, 2013.

[68] Ciprian Iliescu. Wet Etching of Glass for MEMS Applications. *Romanian Journal of Information Science and Technology*, Vol. 9, No. 4, pp. 285–309, 2006.

[69] G. I. Parisi, S. E. Haszko, and G. A. Rozgonyi. Tapered Windows in SiO2: The Effect of NH 4 F : HF Dilution and Etching Temperature. *Journal of The Electrochemical Society*, Vol. 124, No. 6, pp. 917–921, 1977.

[70] S. Kal, S. Haldar, and S. K. Lahiri. Slope etching of silicon dioxide. *Microelectronics Reliability*, Vol. 30, No. 4, pp. 719–722, 1990.

[71] Nikola Pekas, Qing Zhang, Matthieu Nannini, and David Juncker. Wet-etching of structures with straight facets and adjustable taper into glass substrates. *Lab on a Chip*, Vol. 10, No. 4, pp. 494–498, 2010.

[72] Adela Ben-Yakar and Robert L. Byer. Femtosecond laser ablation properties of borosilicate glass. *Journal of Applied Physics*, Vol. 96, No. 9, pp. 5316–5323, 2004.

[73] Yasuyuki Akita, Takahiro Watanabe, Wakana Hara, Akifumi Matsuda, and Mamoru Yoshimoto. Atomically stepped glass surface formed by nanoimprint. *Japanese Journal of Applied Physics, Part 2: Letters*, Vol. 46, No. 12-16, pp. 2–5, 2007.

[74] Emmanuel Delamarche, André Bernard, Heinz Schmid, Alexander Bietsch, Bruno Michel, and Hans Biebuyck. Microfluidic networks for chemical patterning of substrates: Design and application to bioassays. *Journal of the American Chemical Society*, Vol. 120, No. 3, pp. 500–508, 1998.

[75] Ayokunle Olanrewaju, Maïwenn Beaugrand, Mohamed Yafia, and David Juncker. Capillary microfluidics in microchannels: From microfluidic networks to capillaric circuits. *Lab on a Chip*, Vol. 18, No. 16, pp. 2323–2347, 2018.

[76] D. Gowrisankar, K. Abbulu, O. Bala Souri, and K. Sujana. Validation and Calibration of Analytical Instruments. *Journal of Biomedical Science and Research*, Vol. 2, No. 2, pp. 89–99, 2010.

[77] Akihiko Ishida, Takahiro Yoshikawa, Masamichi Natsume, and Tamio Kamidate. Reversed-phase liquid chromatography on a microchip with sample injector and monolithic silica column. *Journal of Chromatography A*, Vol. 1132, No. 1-2, pp. 90–98, 2006.

[78] Xiu Li Wang, Ying Zhu, and Qun Fang. Valveless gated injection for microfluidic chip-based liquid chromatography system with polymer monolithic column. *Journal of Chromatography A*, Vol. 1246, pp. 123–128, 2012.

[79] Xiaoxia Bai, Hye Jin Lee, Joel S. Rossier, Frederic Reymond, Helwig Schafer, Michael Wossner, and Hubert H. Girault. Pressure pinched injection of nanolitre volumes in planar micro-analytical devices. *Lab on a Chip*, Vol. 2, No. 1, pp. 45–49, 2002.

[80] Lei Zhang, Xuefeng Yin, and Zhaolun Fang. Negative pressure pinched sample injection for microchip-based electrophoresis. *Lab on a Chip*, Vol. 6, No. 2, pp. 258–264, 2006.

[81] Zhiyong Wu, Henrik Jensen, Jean Gamby, Xiaoxia Bai, and Hubert H. Girault. A flexible sample introduction method for polymer microfluidic chips using a push/pull pressure pump. *Lab on a Chip*, Vol. 4, No. 5, pp. 512–515, 2004.

[82] Tatsuro Nakao, Yutaka Kazoe, Emi Mori, Kyojiro Morikawa, Takemichi Fukasawa, Ayumi Yoshizaki, and Takehiko Kitamori. Cytokine Analysis at Countable Number

of Molecules from Living Single Cell on Nanofluidic Device. *The Analyst*, Vol. 144, pp. 7200–7208, 2019.

[83] Koki Yamamoto, Kyojiro Morikawa, Hiroyuki Imanaka, Koreyoshi Imamura, and Takehiko Kitamori. Picoliter enzyme reactor on a nanofluidic device exceeding the bulk reaction rate. *Analyst*, Vol. 145, No. 17, pp. 5801–5807, 2020.

[84] Yuto Takagi, Yutaka Kazoe, and Takehiko Kitamori. Generation of femtoliter liquid droplets in gas phase by microfluidic droplet shooter. *Microfluidics and Nanofluidics*, Vol. 25, No. 9, pp. 1–8, 2021.

[85] Enrique I. Velazquez-Villarreal, Shamoni Maheshwari, Jon Sorenson, Ian T. Fiddes, Vijay Kumar, Yifeng Yin, Michelle G. Webb, Claudia Catalanotti, Mira Grigorova, Paul A. Edwards, John D. Carpten, and David W. Craig. Single-cell sequencing of genomic DNA resolves sub-clonal heterogeneity in a melanoma cell line. *Communications Biology*, Vol. 3, No. 1, pp. 1–8, 2020.

[86] Ying Zhu, Geremy Clair, William B. Chrisler, Yufeng Shen, Rui Zhao, Anil K. Shukla, Ronald J. Moore, Ravi S. Misra, Gloria S. Pryhuber, Richard D. Smith, Charles Ansong, and Ryan T. Kelly. Proteomic Analysis of Single Mammalian Cells Enabled by Microfluidic Nanodroplet Sample Preparation and Ultrasensitive NanoLC-MS. *Angewandte Chemie - International Edition*, Vol. 57, No. 38, pp. 12370–12374, 2018.

[87] Liwei Yang, Justin George, and Jun Wang. Deep Profiling of Cellular Heterogeneity by Emerging Single-Cell Proteomic Technologies. *Proteomics*, Vol. 20, No. 13, p. 24, 2020.

[88] Kyojiro Morikawa, Shu Matsuura, Yutaka Kazoe, Ayumi Yoshizaki, and Takehiko Kitamori. Cell Debris Filtering and Liquid Exchange Using Nanofludic. *Proceeding of MicroTAS*, Vol. 1, pp. 1409–1410, 2021.

[89] Kyojiro Morikawa, Kazuki Matsushita, and Takehiko Tsukahara. Rapid plasma etching for fabricating fused Silica Microchannels. *Analytical Sciences*, Vol. 33, No. 12, pp. 1453–1456, 2017.

Acknowledgments

I would like to express my deepest appreciation to Prof. Takehiko Kitamori for his guidance and supervision of my work and his sincere advice and criticism on my research. His lessons were not only helpful for improving my research but more fundamentally taught me how research should be promoted, how it should be presented and can make a greater impact on the audience, the importance of viewing problems from different perspectives and so on. I think such ideas will be important in any kind of work I will be engaged in and will be a treasure in my life. Besides his lessons in research, I have a lot of respect for his variety of hobbies (not only various but also deeply researched) such as music or outdoor activities, and having rare experiments in foreign countries. I would also like to keep that in mind since having such hobbies outside work would definitely broaden and enrich my life.

As the closest supervisor, I am deeply grateful to Prof. Yutaka Kazoe for his guidance and supervision of my work. He has been my supervisor for six years since I became a member of Kitamori group and has given me sincere advice and criticism since then. Although I could not improve my skills much and caused a lot of trouble until the end, I was always thankful to him for giving me constructive advice and encouragement. I am positive that I could not have accomplished my work without being under his teaching. Thank you again and I wish you continued success and prosperity and a happy home.

I would like to express my gratitude to Prof. Kyojiro Morikawa for his support on how to plan out experiments, especially when fabricating devices. His was also very helpful when writing papers or preparing for presentations.

I would like to thank Prof. Hisashi Shimizu for his support and advice on my work, particularly on setting up the thermal lens detection system. Although I knew almost nothing about the detection system works, his kind lecture on the working principle and how to adjust the system was essential for my final results.

I would like to thank Prof. Ryoichi Ohta for his warm support on my experiments. Thank you for accompanying me when my experiments took until late at night or even on holidays.

I would like to express my gratitude to Prof. Kazuma Mawatari for his useful advice

and criticism on my research. His advice on how to build a logic when preparing presentations, which I received when I was a master's student, left a great impression on me and I have kept the idea in mind since then.

I would like to express my sincere gratitude to Prof. Hiroyuki Noji, Prof. Ryo Miyake, Prof. Shoji Takeuchi, and Prof. Tetsu Tatsuma for their useful and helpful criticism and advice on my study.

Dr. Adelina Smirnova and Dr. Yu Sugimoto were very supportive as a member of the group and I would like to thank them for their cooperation and advice on my study. Although there were few opportunities for major discussions, their comments given from time to time were helpful not only for my experiments but also as an emotional support.

I would also like to express my gratitude to Ms. Yoshiko Ogawa and Ms. Aki Toyama for their support through administrative procedure in the laboratory and encouragement through daily conversation. I apologize for my delayed contacts of purchase orders and the processing after delivery.

I am deeply grateful to the staffs in Academic Consortium for Nano and Micro Fabrication of four universities. I have caused a lot of trouble not reserving the equipment beforehand, but thanks to your cooperation, the device fabrication process could be carried out without delay.

I would like to offer my special thanks to Mr. Tohru Ishizuya, who has greatly supported me on fabricating devices in the last year of my doctoral course. I will try to emulate the attitude that work must be done carefully and surely even if it takes time. Please take care of yourself and try not to work too hard.

Ms. Naoko Hirosawa has been greatly supportive for managing the consumables and tidying up the office and the laboratory. I was always able to work on my experiments comfortably thanks to her careful work.

I am also grateful to my ex-colleagues and seniors. Being the only student remaining in the laboratory, there were times I needed someone to talk to about my distresses. My ex-colleagues were kind enough to take the time to go out with me in such times and my seniors also kindly gave advice to me. Their support was undoubtfully a great mental support for me.

Finally, I would like to thank my family; my parents, my older brother, and my grandparents, for letting me to university for a total of nine years and supporting me in everyday life. An occasional discussion on my research at home, gave me fresh ideas and helped me straighten out my thoughts. Above all, their support in my daily life could not be thanked more and it would have been impossible for me to accomplish my doctoral course without it. I would like to make use of what I learned over the long long school/laboratory life and try hard to repay your support.

Hiroki Sano

December, 2021